Distribution Agreement

In presenting this thesis or dissertation as a partial fulfillment of the requirements for an advanced degree from Emory University, I hereby grant to Emory University and its agents the non-exclusive license to archive, make accessible, and display my thesis or dissertation in whole or in part in all forms of media, now or hereafter known, including display on the world wide web. I understand that I may select some access restrictions as part of the online submission of this thesis or dissertation. I retain all ownership rights to the copyright of the thesis or dissertation. I also retain the right to use in future works (such as articles or books) all or part of this thesis or dissertation.

Signature:

Tianyuan Zhang	Date

Developments of the projector configuration interaction method and the multireference driven similarity renormalization group

By

Tianyuan Zhang
Doctor of Philosophy

Chemistry

Dr. Francesco Evangelista, Ph.D
Advisor

Dr. Joel Bowman, Ph.D
Committee Member

Dr. James Kindt, Ph.D
Committee Member

Accepted:

Lisa A. Tedesco, Ph.D
Dean of the James T. Laney School of Graduate Studies

Date

Developments of the projector configuration interaction method and the multireference driven similarity renormalization group

By

Tianyuan Zhang
B.S., Nanjing University, 2014

Advisor: Dr. Francesco Evangelista, Ph.D

An abstract of
A dissertation submitted to the Faculty of the
James T. Laney School of Graduate Studies of Emory University
in partial fulfillment of the requirements for the degree of
Doctor of Philosophy
in Chemistry
2019

Abstract

Developments of the projector configuration interaction method and the multireference driven similarity renormalization group

By Tianyuan Zhang

In this dissertation, I have developed efficient methods for both static and dynamical correlation. For static correlation, we propose the projector configuration interaction (PCI) approach to solving the Schrödinger equation with a determinant coupling filtering scheme. In contrast to selected configuration interaction (SCI) methods, in which an important subset of determinants are selected and the Hamiltonian is diagonalized exactly, in PCI we filter the most important determinant couplings, and truncate the determinant space accordingly. The PCI approach realizes a deterministic version of the full configuration interaction quantum Monte Carlo (FCIQMC) method [Booth, G. H.; Thom, A. J. W.; Alavi, A. *J. Chem. Phys.* **2009**, *131*, 054106], where a trial vector is projected onto the ground state wave function with an optimal polynomial projection scheme. Important determinant couplings are selected by the path filtering algorithm integrated into the wave function projection. We show that PCI is able to compute more accurate wave function than general SCI methods with less theoretical computational cost, and chemical accuracy are usually achieved using only a small fraction of the determinants in full CI space. The other topic of this dissertation is the development of a low cost linear multireference driven similarity renormalization group with singles and doubles [MR-LDSRG(2)] method for dynamical correlation. The goal is achieved without compromising the accuracy of the original MR-LDSRG(2) method by using a combination of 1) a sequential unitary transformation, 2) density fitting (DF) of the two-electron integrals, and 3) the non-interacting virtual orbital (NIVO) operator approximation. The scaling of memory requirement is reduced, and the computation is also accelerated. We report improved MR-LDSRG(2) study on the cyclobutadiene automerization reaction using a quintuple-ζ basis set.

Developments of the projector configuration interaction method and the multireference driven similarity renormalization group

By

Tianyuan Zhang
B.S., Nanjing University, 2014

Advisor: Dr. Francesco Evangelista, Ph.D

A dissertation submitted to the Faculty of the
James T. Laney School of Graduate Studies of Emory University
in partial fulfillment of the requirements for the degree of
Doctor of Philosophy
in Chemistry
2019

Acknowledgement

Time flies. It is hard to believe that I have been living in Atlanta for five years. I can still remember clearly the sunny afternoon when Juncheng Yang picked me up from the Hartsfield–Jackson airport. I do want to thank him for his support in my early days in Atlanta without a car. Special thank to Bai Xue who suggested me to apply for the Ph.D. program at Emory University.

Most importantly, I want to thank my advisor Dr. Francesco Evangelista for accepting me to Emory University and his brilliant group, and for his tutorial during these years. The first time I met Francesco was the Skype interview in Jan. 2014. The interview was quite pleasant, and I got the offer on the Chinese New Year's Eve. Francesco is nice, talented and knowledgeable. He arranged my Ph.D. career carefully with delightful research projects and appropriate participating in conferences. He also revises my papers, talks, and posters patiently. I definitely learned a lot from him, and my skills improved significantly. For example, writing has always been a big problem for me as a straight F student in high school Chinese class. At the beginning of my graduate study, I just wished to get the science correct. I was always willing to spend time on coding and analysis, but I disliked writing. In research, my progress would be slowed down whenever there is a writing task. He patiently discusses writing skills with me, helped me improve my drafts. Now I feel much better when I need to write. I also would like to thank Dr. Joel Bowman and Dr. James Kindt for being on my committee. Their comments after every yearly report also helped me a lot on improving my scientific presentation skills.

I want to thank my parents and family members for their support these years. Their support encouraged me to do whatever I want to do. I want to thank my girlfriend Xueting Lin. Despite the distance and time gap, her accompany on Phone always makes me feel comfortable. I want to thank all of the Evangelista group members Dr. Chenyang Li, Dr. Prakash Verma, Jeff Schriber, Kevin Hannon, Chenxi Cai, Nan He, Shuhe Wang, Nick stair, Renke Huang, Xiaobai Li, and Junchu Zeng, thank friends in the Emerson computation center, and thank Psi4 developers. I enjoy the day-to-day chat with all of you!

I also want to thank all my friends here in Atlanta for every dinner, volleyball games, card games, and many other activities. Their supports and entertainments contribute to an important part of life when I am far from hometown.

Table of Contents

List of Figures

List of Tables

Chapter 1 Introduction and literature review

1.1 Introduction

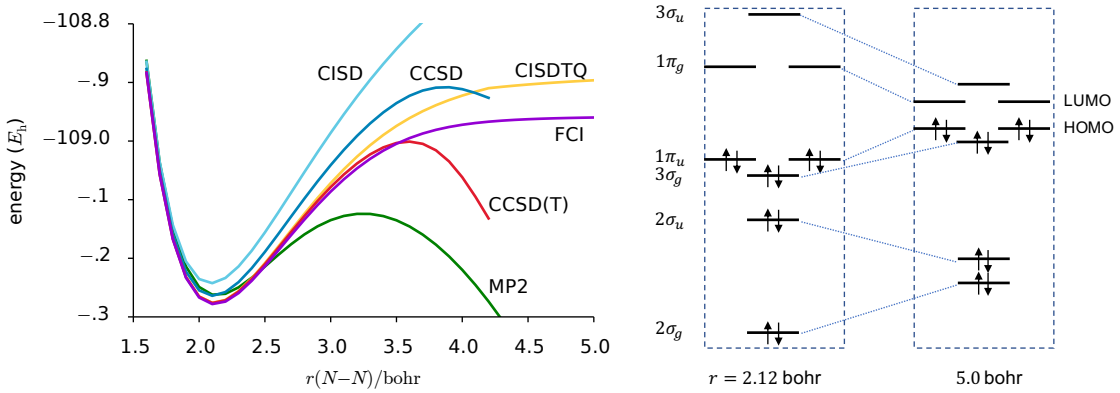

Figure 1.1 Left: The nitrogen (N_2) dissociation curve computed by full configuration interaction (FCI), Møller–Plesset second-order perturbation theory (MP2), configuration interaction methods (CISD, CISDTQ), and coupled cluster methods [CCSD, CCSD(T)]. All computations use cc-pVDZ basis set[1] and core 1s electrons are frozen doubly occupied. Right: A schematic diagram of molecular orbitals and energies in both equilibrium and stretched geometries.

Comparing the nitrogen dissociation curve computed by full configuration interaction (FCI) and other single-reference wave function methods, as in Figure 1.1, most of the single-reference wave function methods describe the curve around the equilibrium geometry correctly. However, truncated configuration interaction (CI) methods diverge when N_2 dissociates, while the Møller–Plesset second-order perturbation theory (MP2) and coupled cluster methods [CCSD, CCSD(T)] show strange local maximums. Further investigation shows that HOMO-LUMO gaps are dramatically different between equilibrium and stretched geometries. In the stretched N_2 where HOMO and LUMO are nearly degenerate, the Hartree–Fock reference determinant contribute only 9.8% to the FCI wave function in contrast to 87% in the equilibrium geometry. Thus, the stretched N_2 cannot be well approximated by a single Slater

determinant. Chemical systems like the stretched N_2 are called *strongly correlated systems*.

Electrons interact strongly in chemical systems where electronic configurations are nearly degenerate, such as bond breaking, transition metals, biradical systems, and excited states.[2–7] The near-degenerate states violate the basic assumption of single-reference quantum chemistry methods that the wave function can be approximated by a single Slater determinant. For example, consider a zeroth-order wave function Ψ_0 consisting of two degenerate determinants, a reference Φ and the doubly excited determinant $\Phi_{i\bar{i}}^{a\bar{a}}$, say

$$|\Psi_0\rangle = \frac{1}{\sqrt{2}}(|\Phi\rangle - |\Phi_{i\bar{i}}^{a\bar{a}}\rangle), \tag{1.1}$$

where i and a are occupied and virtual alpha spin orbitals, and $\bar{i}$ and $\bar{a}$ are corresponding occupied and virtual beta spin orbitals. In configuration interaction singles and doubles (CISD) method, important contributions from most singly and doubly excited determinants from $\Phi_{i\bar{i}}^{a\bar{a}}$ are missing because those are triple and quadruple excitations from the reference Φ. In Møller–Plesset second order perturbation theory, $\Phi_{i\bar{i}}^{a\bar{a}}$ causes an infinite "perturbation" to the reference for the energy denominator $\Delta = \epsilon_i + \epsilon_{\bar{i}} - \epsilon_a - \epsilon_{\bar{a}} \to 0$. In the coupled cluster singles and doubles (CCSD) method, even if we overpass the divergence problem, in principle the double excitation amplitude $t_{i\bar{i}}^{a\bar{a}} \approx -1$ by cluster analysis. Such a large amplitude will cause inaccurate disconnected triples and quadruples, and consequently ruin all other cluster amplitudes.

To accurately describe strongly correlated systems, the electron correlation effects are usually divided into static (strong) and dynamical (weak) correlations to treat separately.[8] Static correlation accounts for the strong mixing between near-degenerate electronic configurations, while dynamical correlation accounts for the repulsion between electrons in movement. Clearly, this division is arbitrary. In practice, scientists divide molecular orbitals into core (**C**), active (**A**) and virtual (**V**) spaces as shown

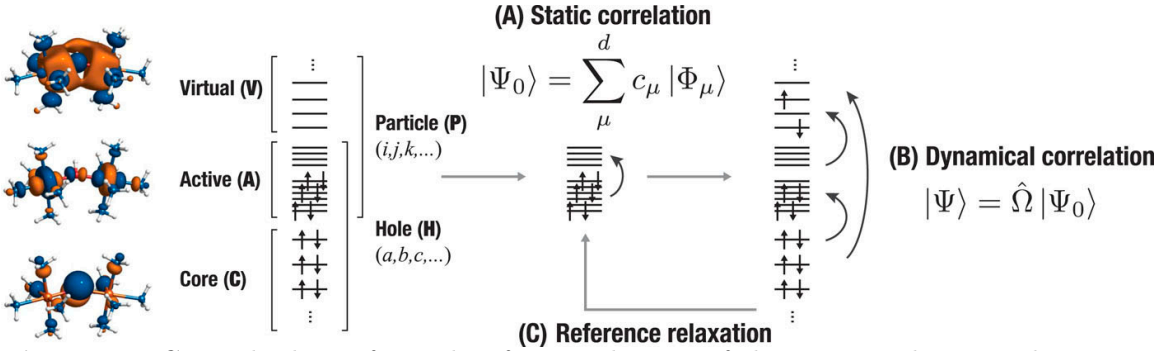

Figure 1.2 General scheme for multireference theories of electron correlation and partitioning of the orbital space into core, active, and virtual orbitals. (a) Static correlation effects are treated with a reference wave function (Ψ_0). (b) Dynamical correlation effects are introduced via a wave operator ($\hat{\Omega}$) acting on the reference. (c) Reference relaxation effects that couple static and dynamical correlations are introduced by diagonalizing an effective Hamiltonian.[1]

in Figure 1.2. The active space usually contain several molecular orbitals around the HOMO and LUMO and certain number of electrons (n_{act}). In second quantization, the determinants in the active space are

$$|\Phi_\mu\rangle = \underbrace{\hat{a}_u^\dagger \hat{a}_v^\dagger \cdots}_{n_{\text{act}}} \prod_{m}^{\mathbf{C}} \hat{a}_m^\dagger |\rangle \,, \tag{1.2}$$

where $|\rangle$ is the true vacuum and $\hat{a}_p^\dagger$ is a creation operator. The active space is usually treated with variations of configuration interaction (CI) methods[9] to describe the nature of static correlation with a multi-determinantal reference wave function. When all determinants in the active space are included in the CI computation, the result wave function is indicated with CAS(ne,ko), where CAS stands for complete active space, n is the number of electrons and k is the number of spatial orbitals in the active space. Unfortunately, the combinatorial growth of the number of determinants in the active space limits such references to around CAS(18e,18o), although CAS(22e,22o) computations have been recently computed on massively parallel architectures with more than 4,000 cores.[10]

On top of the reference wave function, in contrast to the methods for static cor-

[1] Repinted from Evangelista, F. A. Perspective: Multireference coupled cluster theories of dynamical electron correlation. *J. Chem. Phys.*, **2018**, *149*, 030901, with the permission of AIP Publishing.

relation where interactions between electron configurations are explicitly computed in the Hamiltonian and wave function, dynamical correlation is usually treated as a many-body expansion of interactions between molecular orbitals due to the enormous weak interactions. Candidate methods include multireference perturbation theory (MRPT),[11–16] multireference configuration interaction (MRCI),[17–21] multireference coupled cluster (MRCC)[22–37] methods and many other variants.[38–43] Good reviews of these methods can be found in Refs. 44, 45 and 46. Similar to the single-reference case, MRCC approaches and related variants are the most accurate. However, despite protracted efforts and progress, the applicability of MRCC has not reached the same level of MRPT or MRCI, due to the high computational cost. Meanwhile, MRCC methods suffer from the intruder-state problem,[46–52] and the multiple-parentage problem,[30,33,46,52–54] which will be discussed in detail in Sec. 1.6. Evangelista and co-workers[39–43,55] have recently proposed the multireference driven similarity renormalization group (MR-DSRG) to address both these technical issues in multireference theories. However, the applicability of the non-perturbative version [MR-LDSRG(2)][41] is usually limited to 250 correlated molecular orbitals due to the demand for computation resources.

In order for the static correlation to be coupled with the dynamical correlation effects, we iterate the two types of treatement where a new set of coefficients c_μ for the CI expansion in the active space is computed with dynamical correlation dressed Hamiltonian. This iteration process is called *reference relaxation*. The combination of accurate static and dynamical correlation methods can provide computation results agree well with experiments. The purpose of this dissertation is to propose efficient methods for both static and dynamical correlation. Specifically, we developed the projector configuration interaction (PCI) method for efficient static correlation treatment and reduced the computational cost of the MR-LDSRG(2) method to compute dynamical correlation in larger strongly correlated systems. In this introduction, I will

first overview methods for static correlation, then focus on the formalism of selected CI algorithms. What follows is an analysis of MRCC methods and an introduction to DSRG methods.

1.2 Sparsity in the full configuration interaction Hamiltonian

In the Born–Oppenheimer approximation and second quantization, the electronic Hamiltonian on a basis of one-particle spin orbitals $\{\phi^p, p = 1, 2, \ldots, 2k\}$ is

$$\hat{H} = \sum_{pq} h_p^q \hat{a}_p^\dagger \hat{a}_q + \frac{1}{4} \sum_{pqrs} v_{rs}^{pq} \hat{a}_p^\dagger \hat{a}_q^\dagger \hat{a}_s \hat{a}_r, \tag{1.3}$$

where p, q, r and s are indices of spin orbitals, $\hat{a}^\dagger$ and $\hat{a}$ are creation and annihilation operators, $h_p^q = \langle \phi_p | \hat{h} | \phi^q \rangle$ and $v_{rs}^{pq} = \langle \phi_p \phi_q \| \phi^r \phi^s \rangle$ are the one-electron and anti-symmetrized two-electron integrals, respectively.

Configuration interaction methods represent wave function as linear combination of determinants in a primary active space P,

$$|\Psi_0\rangle = \sum_{\Phi_I \in P} C_I \, |\Phi_I\rangle \,, \tag{1.4}$$

where $|\Phi_I\rangle$ are Slater determinants in the active space and C_I are the corresponding coefficients. The coefficients are obtained by computing the eigenvector of the Hamiltonian matrix $\mathbf{H}$, where matrix elements are given by

$$H_{IJ} = \langle \Phi_I | \hat{H} | \Phi_J \rangle \,, \ \Phi_I, \Phi_J \in P. \tag{1.5}$$

According to the definition of $\hat{H}$ and the Slater's rules, $H_{IJ} = 0$ if Φ_I and Φ_J are differed by more than two spin orbitals.

Common methods to compute a CAS reference wave function are complete active space configuration interaction (CASCI) or complete active space self-consistent field (CASSCF).[56] Both methods are effectively full configuration interaction (FCI) in the

active space with or without orbital optimization, where the number of determinants in CAS(ne,ko) is $\binom{k}{n/2}^2$ (for a closed shell system). In principle, FCI exactly diagonalizes the Hilbert space and provides accurate wave function for any quantum many-body system. However, as Hilbert space grows combinatorially with respect to the number of electrons and molecular orbitals, it is prohibitively expensive even for moderate size chemical systems.[57]

A general approach to reducing the cost of FCI is to exploit the sparsity of the FCI Hamiltonian. The sparsity is reflected in many aspects:

1. A majority of Hamiltonian matrix elements are zero or small, due to Slater rule or sometimes orbital locality;

2. Most CI wave function determinant coefficients are small due to large energy difference or small coupling to the target state;

3. Tensor rank is not full if the Hamiltonian matrix or the coefficient vector is appropriately factorized.

Three major categories of methods have been developed that take advantage of the sparsity: factorization, importance selection, and stochastic sampling.

The density matrix renormalization group (DMRG) is a successful example of methods factorizing the FCI wave function.[58–64] The formalism factorizes the coefficient tensor to be a product of matrix product state (MPS) tensors and truncate the connection between adjacent tensors to a finite number. However, because the MPS factorization is one-dimensional, it is computationally advantageous only for quasi-1D systems. At the same time, its convergence is sensitive to the ordering of molecular orbitals.[59,65,66]

In this dissertation, we focus on more generally applicable methods. We will first overview the selected CI methods in the next section, then discuss a Monte-Carlo method that samples the Hamiltonian in Sec. 1.5.

1.3 Selected configuration interaction methods

Selected CI methods seek to select an important subset of determinants (S) of diagonalizable size out of the $\binom{k}{n/2}^2$ determinants. The naïve way of including single and double excitations from the Hartree–Fock configuration is denoted as CISD. However, missing important higher excitation determinants can result in a noticeable error, especially in strongly correlated systems. In the early developments of selected CI methods, Davidson and co-workers[67] selected the most important 1000 configurations according to their second-order perturbation energies. In the MRD-CI developed by Buenker and Peyerimhoff,[68–70] configurations sorted by the expected energy lowering are truncated by a threshold T, where the FCI energy is estimated by extrapolating $T \to 0$.

Instead of second-order perturbation energy, Malrieu and co-workers proposed the CIPSI method in which important determinants are selected by the perturbative estimation of their coefficients.[71–75] More importantly, CIPSI established the general iterative scheme of selected CI methods:

1. Choose an initial determinant space $[S^{(1)}]$. It may contain only the SCF determinant.

2. At the k-th iteration, diagonalize the Hamiltonian $\mathbf{H}$ restricted in determinant space $S^{(k)}$ to obtain the corresponding wave function,

$$|\Psi^{(k)}\rangle = \sum_{\Phi_J \in S^{(k)}} C_J^{(k)} |\Phi_J\rangle ; \tag{1.6}$$

3. Estimate the importance of determinants $\Phi_I \notin S^{(k)}$ that are connected to determinants in $S^{(k)}$ by some *criteria*;

4. Select the most important connected determinants with a *threshold*, then gather those with $S^{(k)}$ to form a new determinant space $S^{(k+1)}$;

5. Iterate steps (2) to (4) until converge.

Obviously, the degrees of freedom in the selected CI framework are the criteria and threshold, the combination of which determines the accuracy and efficiency of a selected CI method. Criteria and thresholds of representative selected CI methods are listed in Table 1.1. More recent developments include other variations which are usually more sophisticated[76–85] or adapted and applied in multireference CI methods,[19,86–88] but the basic selected CI idea is similar.

Among the listed methods, the adaptive CI (ACI) by Schriber and Evangelista[95,96] is distinguished by its accuracy. The energy lowering criteria in ACI is one of the most accurate estimations for the importance of determinants. Meanwhile, the cumulative selection criteria and thresholds guarantee the result energy error to FCI is on the order of the user-specified threshold σ, which also result in small parallelism errors. In contrast, Heat-bath CI (HCI) by Holmes and co-workers[97–99] utilizes an easy to compute selection criterion. Although it sacrifices the accuracy of targeting important determinants, the computational efficiency is maximized.

1.4 Cost in exact diagonalization of Hamiltonian

In general selected CI algorithm, step 2 requires diagonalization of the Hamiltonian in the subset $S^{(k)}$. The standard approach to diagonalize a Hamiltonian is the Davidson–Liu algorithm,[100,101] as described in Algorithm 1.

In the algorithm, the most time consuming step is computing the sigma vectors in Eqs. (1.8) and (1.10),

$$\sigma = \mathbf{Hb}, \tag{1.11}$$

[2] Adapted from Sherrill, C. D.; Schaefer, H. F., The Configuration Interaction Method: Advances in Highly Correlated Approaches. *Adv. Quant. Chem.*, **1999**, *34*, 143–269, Copyright 1999, with permission from Elsevier.

Table 1.1 Selection criteria and thresholds of representative selected CI methods. $\Psi^{(k)}$ is the wave function at the k-th iteration, $E_\Psi^{(k)} = \langle\Psi^{(k)}|\hat{H}|\Psi^{(k)}\rangle$. Φ_J and Φ_I represent determinants in and out of $S^{(k)}$ ($\Phi_J \in S^{(k)}$, $\Phi_I \notin S^{(k)}$), where $S^{(k)}$ is the subset of the primary determinant space P at the k-th iteration. $E_I = \langle\Phi_I|\hat{H}|\Phi_I\rangle$, $H_{IJ} = \langle\Phi_I|\hat{H}|\Phi_J\rangle$, and C_J is the coefficient of Φ_J at the k-th iteration. $E_0 = \langle\Phi_0|\hat{H}|\Phi_0\rangle$ is the energy of the reference determinant energy. All other quantities in this table are the criterion and threshold in each method.

Method	Importance estimate	Threshold
CIPSI[71]	$C_I^{(1)} = \frac{\langle\Phi_I\|\hat{H}\|\Psi^{(k)}\rangle}{E_\Psi^{(k)} - E_I}$	$\lvert C_I^{(1)}\rvert \geq \eta$
CI+PT[89]	$\epsilon_I^{(2)} = \frac{\lvert\langle\Phi_I\|\hat{H}\|\Psi^{(k)}\rangle\rvert^2}{E_\Psi^{(k)} - E_I}$	$\lvert\epsilon_I^{(2)}\rvert \geq T$
MCCI[90–92]	C_I from diagonalizing $\mathbf{H}^{(k)}$ [a]	$\lvert C_I\rvert > c_{\min}$ [a]
ΛCI[93]	$\Delta E = E_I - E_0$	$\Delta E \leq \lambda$
ASCI[94]	$A_I = \frac{\sum_{J\neq I}^{core} H_{IJ}C_J}{E_I - E_\Psi^{(k)}}$ [b]	fixed $S^{(k)}$ size [b]
ACI[95,96]	$\epsilon_I = \frac{E_I - E_\Psi^{(k)}}{2} - \sqrt{\frac{(E_I - E_\Psi^{(k)})^2}{4} + \lvert\langle\Phi_I\|\hat{H}\|\Psi^{(k)}\rangle\rvert^2}$	$\sum_{\Phi_I \in F^{(k)}\setminus Q^{(k)}} \lvert\epsilon_I\rvert \leq \sigma$ [c]
HCI[97–99]	$f_{\mathrm{HCI}}(\Phi_I) = \max_J(\lvert H_{IJ}C_J\rvert)$	$f_{\mathrm{HCI}}(\Phi_I) \geq \epsilon_1$

[a] In MCCI, the Hamiltonian $\mathbf{H}^{(k)}$ is constructed in a Monte-Carlo sampled determinant space. See Ref. 92 for detail.

[b] In ASCI, the determinant space is splitted into *core* and *target*, only *core* contributions are summed up to compute A_I. Core and target spaces contain fixed number of determinants selected by A_I value. See Ref. 94 for detail.

[c] In ACI, determinant space $F^{(k)}$ contains all $\Phi_I \notin S^{(k)}$, and $Q^{(k)}$ is a subset of $F^{(k)}$ containing candidate determinants to merge with $S^{(k)}$. Selecting determinants with the largest $|\epsilon_I|$ values so that the accumulated energy lowering of discarded determinants does not exceed the threshold σ. See Ref. 95 for detail.

or explicitly for all determinant $\Phi_J \in S^{(k)}$,

$$\sigma_J = \sum_{\Phi_K \in S^{(k)}} H_{JK} b_K, \tag{1.12}$$

where each matrix element H_{JK} is a determinant coupling Φ_K to Φ_J. According to Slater's rules, the number of non-trivial coupling in $\mathbf{H}$ is of $\mathcal{O}(N_{\mathrm{det}} o^2 v^2)$, where N_{det} is the number of determinants in space $S^{(k)}$, o and v are the number of occupied and virtual spin orbitals. This scaling is also the scaling of computational cost because each

Algorithm 1 The Davidson–Liu iterative method for the lowest few eigenvectors and eigenvalues of real symmetric matrices.[2]

1: Select a set of L orthonormal guess vectors, at least one for each root desired, and place in the set $\{\mathbf{b}_i\}$.
2: Use a standard diagonalization method to solve the $L \times L$ eigenvalue problem

$$\mathbf{G}\alpha^k = \lambda^k \alpha^k, k = 1, 2, ..., M \tag{1.7}$$

where

$$G_{ij} = (\mathbf{b}_i, \mathbf{H}\mathbf{b}_j) = (\mathbf{b}_i, \sigma_j), 1 \leq i, j \leq L \tag{1.8}$$

and M is the number of roots of interest.
3: Form the correction vectors $\{\delta^k\}, k = 1, 2, ..., M$, defined as

$$\delta_I^k = (\lambda^k - H_{II})^{-1} r_I^k, I = 1, 2, ..., N \tag{1.9}$$

where

$$\mathbf{r}^k = \sum_{i=1}^{L} \alpha_i^k (\mathbf{H} - \lambda^k)\mathbf{b}_i \tag{1.10}$$

and N is the number of determinants.
4: Normalize $\{\delta^k\}$.
5: Schmidt orthonormalize δ^1 against the set $\{\mathbf{b}_i\}$ and append the result to $\{\mathbf{b}_i\}$. Repeat this process for each of the other $M-1$ correction vectors, neglecting those whose Schmidt orthonormalized norm is less than some threshold $T \approx 10^{-3}$. This results in the addition of m new $\mathbf{b}$ vectors, whith $1 \leq m \leq M$.
6: Increase L by m and return to step 2.

sigma build step loops over all the non-trivial couplings. Computing sigma vector with intermediate residue lists requires $\mathcal{O}(N_{\text{det}} o^2)$ memory for an efficient implementation[102] for . These costs, currently limit the size of selected determinant space to around 10^7 determinants.

1.5 Full configuration interaction quantum Monte Carlo

Monte-Carlo algorithm is a major branch of stochastic methods[103] that usually require only limited resources. In contrast to selected CI methods where all the couplings need to be evaluated, the full configuration interaction quantum Monte Carlo

(FCIQMC) method samples these couplings by a walker spawning dynamics.[104–109] Many FCIQMC computations on strongly correlated system have been reported in the last decade.[110–115]

This method applies the linearized imaginary-time projector to an initial guess of the wave function,

$$|\Psi\rangle = \lim_{\beta\to\infty} \exp\left(-\beta(\hat{H} - E_0)\right)|\Omega\rangle \approx \lim_{k\to\infty}\left(1 - \tau(\hat{H} - E_0)\right)^k |\Omega\rangle\,, \tag{1.13}$$

where $|\Psi\rangle$ and $|\Omega\rangle$ are the result and initial guess of the wave function, β is the imaginary time scale, E_0 is the ground state energy, and τ is an imaginary time step. In the FCIQMC method, at each propagation step, the coefficient C_J of determinant Φ_J is proportional to the number of walkers on it (N_J),

$$C_J \propto N_J. \tag{1.14}$$

According to the walker spawning algorithm described in Ref. 104, for each walker α, the Hamiltonian can be written as:

$$\widetilde{H}^{(k,\alpha)} = \{\widetilde{H}_{IJ}^{(k,\alpha)}\} = \begin{cases} \frac{H_{IJ}}{p_{\text{gen}}(I|J)} & \text{if } \alpha \text{ is on } \Phi_J \text{ and choose to spawn on } \Phi_I, \\ H_{JJ} & \text{if } \alpha \text{ is on } \Phi_J \text{ and } I = J, \\ 0 & \text{otherwise,} \end{cases} \tag{1.15}$$

where $p_{\text{gen}}(I|J)$ is the probability that determinant Φ_I is randomly selected out of all the determinants coupled with Φ_J, and only one spawning target is selected at each step k. Obviously, there are only two non-zero matrix elements in $\widetilde{H}^{(k,\alpha)}$: one for diagonal contribution, the other for sampling the determinant coupling. The overall sampled Hamiltonian at k-th imaginary-time propagation step is

$$\widetilde{H}^{(k)} = \sum_{\alpha}^{N_w^{(k)}} \widetilde{H}^{(k,\alpha)}, \tag{1.16}$$

where $N_w^{(k)}$ is the total number of walkers at step k. In this way, the Hamiltonian $\hat{H}$ is sampled to be $\widetilde{H}^{(k)}$ by the walker spawning process, where only $N_w^{(k)}$ off-diagonal matrix elements (determinant couplings) need to be evaluated. The computational

cost is thus proportional to the $N_w^{(k)}$, which can be much smaller than the cost of exact diagonalization.

However, the result lacks an accurately represented wave function, and large numbers of walkers and iterations are required to overcome the "sign problem" and decrease the statistical errors in the result. Besides, the linearized imaginary-time projector in the FCIQMC converges slowly, in that a small imaginary-time step is required to control the energy fluctuation.

Inspired by FCIQMC, we proposed the projector CI (PCI) method. It can be interpreted as a deterministic alternative to the FCIQMC, with two major modifications: 1) The stochastic propagation is replaced by a deterministic path-filtering projection scheme. 2) The imaginary-time propagation is replaced by much faster projection schemes. PCI may also be understood as an improved selected CI method, where the exact diagonalization of the subset Hamiltonian is replaced with diagonalizing a Hamiltonian with only the most important determinant couplings. The PCI algorithm and performance will be discussed in these two different flavors in Chapters 2 and 3.

1.6 Problems in multireference coupled cluster methods

Now we switch to introduce main dynamical correlation methods. In single-reference coupled cluster (SRCC), the exact ground state wave function is written as

$$|\Psi\rangle = e^{\hat{T}} |\Phi_0\rangle , \tag{1.17}$$

where Φ_0 is a reference Slater determinant, and $\hat{T}$ is the cluster operator containing up to n-body operators,

$$\hat{T} = \sum_{k=1}^{n} \hat{T}_k, \tag{1.18}$$

where n is the number of electrons and $\hat{T}_k$ contains operators that excite k electrons from the occupied to virtual orbitals in Φ_0,

$$\hat{T}_k = \frac{1}{(k!)^2} \sum_{ij\cdots}^{\text{occ}} \sum_{ab\cdots}^{\text{vir}} t_{ab\cdots}^{ij\cdots} \hat{a}_{ij\ldots}^{ab\ldots}, \tag{1.19}$$

where $t_{ij\ldots}^{ab\cdots}$ are the cluster amplitudes, and for convenience we introduce the compact notation $\hat{a}_{ij\ldots}^{ab\ldots} = \underbrace{\hat{a}_a^\dagger \hat{a}_b^\dagger \cdots \hat{a}_j \hat{a}_i}_{k \text{ excitations}}$.

Plugging in this wave function ansatz into the Schrödinger equation gives:

$$\hat{H} e^{\hat{T}} |\Phi_0\rangle = E e^{\hat{T}} |\Phi_0\rangle , \tag{1.20}$$

where E is the ground state energy. We can left-multiply $e^{-\hat{T}}$ to cancel the cluster operator on the right hand side,

$$e^{-\hat{T}} \hat{H} e^{\hat{T}} |\Phi_0\rangle = E |\Phi_0\rangle , \tag{1.21}$$

where we define $e^{-\hat{T}} \hat{H} e^{\hat{T}}$ to be the transformed Hamiltonian $\bar{H}$. Employing the Baker-Campbell-Hausdorff expansion we can write $\bar{H}$ as:

$$\begin{aligned} \bar{H} = e^{-\hat{T}} \hat{H} e^{\hat{T}} =& \hat{H} + [\hat{H}, \hat{T}] \\ &+ \frac{1}{2!} \left[[\hat{H}, \hat{T}], \hat{T} \right] \\ &+ \frac{1}{3!} \left[\left[[\hat{H}, \hat{T}], \hat{T} \right], \hat{T} \right] \\ &+ \frac{1}{4!} \left[\left[\left[[\hat{H}, \hat{T}], \hat{T} \right], \hat{T} \right], \hat{T} \right] . \end{aligned} \tag{1.22}$$

This expansion terminates at the forth-order commutator because $\hat{H}$ is a two-body operator and $\hat{T}$ is a pure excitation operator.

Since determinants are orthonormalized, when we left project an arbitrary determinant on to Eq. (1.21), we get

$$\langle \Phi | \bar{H} | \Phi \rangle = E \tag{1.23}$$

or

$$\langle \Phi_{ij\ldots}^{ab\ldots} | \bar{H} | \Phi \rangle = 0, \tag{1.24}$$

where $\Phi_{ij\ldots}^{ab\cdots}$ represents a determinant generated from reference determinant by exciting electrons from spin orbitals $i, j, \ldots$ to $a, b, \ldots$. Obviously, for a truncated cluster operator $\hat{T}$, we can always have an identical number of non-trivial equations by Eq. (1.24) to solve the amplitudes, and compute the energy by Eq. (1.23). Note that the amplitudes obtained in the truncated CC methods are different from those in the full CC method because amplitudes for different excitation order are coupled in Eq. (1.22) and therefore in Eq. (1.24).

The multireference coupled cluster formalism is not as straightforward as the single-reference case. Two major branches of MRCC schemes are the internally contracted MRCC (ic-MRCC)[30,34,35,116–118] ansatz where

$$|\Psi_{\mathrm{ic}}\rangle = e^{\hat{T}} |\Psi_0\rangle = e^{\hat{T}} \sum_{\mu} |\Phi_\mu\rangle C_\mu, \tag{1.25}$$

and the Jeziorski–Monkhorst (JM) MRCC[23,30,31,33,119–121] ansatz where

$$|\Psi_{\mathrm{JM}}\rangle = \sum_{\mu} e^{\hat{T}^\mu} |\Phi_\mu\rangle C_\mu. \tag{1.26}$$

We have defined P space to contain determinants in the reference wave function. Here we define Q space to contain determinants excited from P but not in P. The conditions to solve cluster amplitudes can be derived according to the Schrödinger's equation, or explicitly $QH^{\mathrm{eff}}P = 0$. In SRCC, $QH^{\mathrm{eff}}P = 0$ yields the same conditions as Eq. (1.24), for $P = \{\Phi_0\}$, $H^{\mathrm{eff}} = \bar{H}$ and $Q = \{\Phi_{ij\ldots}^{ab\cdots}\}$, where the numbers of unknowns and equations are identical. However, this good trait does not hold in either JM-MRCC or ic-MRCC schemes, which is called the *multiple-parentage problem*. This problem originates from the fact that multiple determinants in the P space may be excited to the same determinant in the Q space, as shown in Figure 1.3. In the JM, although the effective Hamiltonian is not obvious, we directly satisfy the Schrödinger equation,

$$\hat{H} \sum_{\mu} e^{\hat{T}^\mu} |\Phi_\mu\rangle C_\mu = E \sum_{\mu} e^{\hat{T}^\mu} |\Phi_\mu\rangle C_\mu. \tag{1.27}$$

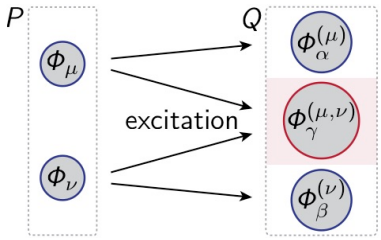

Figure 1.3 In multireference coupled cluster theories, each reference (P space) determinant are excited to multiple determinants in the Q space. However, for determinant Φ_γ in the Q space, it can be from both the excitation of Φ_μ and Φ_ν (parents) in P.

Due to the multiple-parentage problem, the number of determinants in $\sum_\mu e^{\hat{T}^\mu} |\Phi_\mu\rangle C_\mu$ is less than the number of $(t^\mu)^{ij\cdots}_{ab\cdots}$ amplitudes. In other words, the number of determinants in $|\Psi_{\mathrm{JM}}\rangle$ as the result of $\hat{H} |\Psi_{\mathrm{JM}}\rangle = E |\Psi_{\mathrm{JM}}\rangle$ cannot provide sufficient conditions to solve for the $(t^\mu)^{ij\cdots}_{ab\cdots}$ amplitudes.

In the internally contracted scheme,

$$H^{\mathrm{eff}} = e^{-\hat{T}} \hat{H} e^{\hat{T}}. \tag{1.28}$$

Due to the multiple-parentage problem, H^{eff} operator generates linear-dependent excitations of the reference wave function. Consequently, the number of conditions in $QH^{\mathrm{eff}}P = 0$ are also not sufficient for the number of unknowns in $\hat{T}$.

Although the multiple-parentage problem can be solved in some formalisms,[24,27,28] these methods also suffer from numerical instabilities related to the intruder-state problem in MRPT.[46–52] In perturbation theories, the denominator is computed by the difference of orbital energies. The determinants in the Q space that are near-degenerate to those in the P space contribute to small denominators, which causes "spikes" on the potential energy surface as shown in Figure 1.4. In nonperturbative cases, the effect is indirect, but intruder causes numerical instabilities in solving the amplitudes from the nonlinear equations. In practice, the intruder-state problem is due to the fact that

$$QH^{\mathrm{eff}}P = 0 \tag{1.29}$$

has to be satisfied by all the hole to particle excitation, as shown in Figure 1.5 (a)

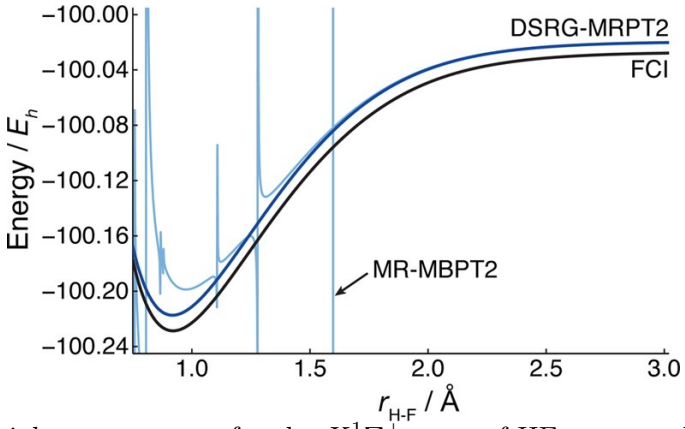

Figure 1.4 Potential energy curves for the $X^1\Sigma^+$ state of HF computed using various methods and the cc-pVDZ basis set. All multireference perturbation theories employed a CASSCF(2e,2o) reference. The fluorine 1s orbital was excluded from the correlation treatment. DSRG-MRPT2 employed a flow parameter of $s = 0.5E_{\mathrm{h}}^{-2}$, and the MR-MBPT2 curve is identical to the curve of DSRG-MRPT2 ($s \to \infty$).[3]

and (b).

1.7 Driven similarity renormalization group methods

In order to address these technical issues in multireference theories, our group recently developed the multireference driven similarity renormalization group (MR-DSRG).[39–43,55] The idea originated from renormalization techniques created in quantum field theory to deal with infinite quantities. In the similarity renormalization group (SRG) method by Wegner[122] and Głazek and Wilson,[123] a continuous unitary similarity transformation is performed on the Hamiltonian,

$$\hat{H} \to \hat{H}(s) = \hat{U}(s)\hat{H}\hat{U}^\dagger(s), s \in [0, \infty), \tag{1.30}$$

where s is a time-like flow parameter, $\hat{U}(s)$ is an unitary operator such that the transformation satisfies the boundary conditions $\hat{H}(s = 0) = \hat{H}$ and the *off-diagonal* couplings $\hat{H}_{\mathrm{od}}(s = \infty) = 0$. Off-diagonal couplings are elements of $\hat{H}$ that couple hole and particle orbitals represented by excitation $[\bar{H}^{ij\cdots}_{ab\cdots}(s)\{\hat{a}^{ab\cdots}_{ij\cdots}\}]$ and de-excitation

[3] Adapted with permission from Li, C.; Evangelista, F. A., Multireference Driven Similarity Renormalization Group: A Second-Order Perturbative Analysis. *J. Chem. Theory Comput.*, **2015**, *11*, 2097–2108. Copyright 2015 American Chemical Society.

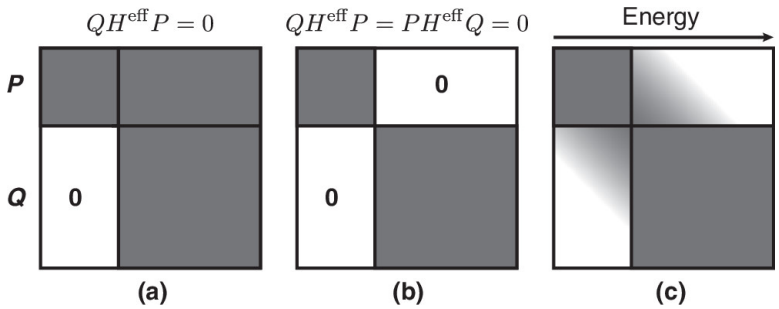

Figure 1.5 Matrix representation of the similarity-transformed Hamiltonian. (a) and (b) illustrate the decoupling of the P and Q spaces in coupled cluster theory and its unitary variant, respectively. (c) Decoupling of states with large energy difference achieved by the similarity renormalization group approach.[4]

$[\bar{H}^{ab\cdots}_{ij\cdots}(s)\{\hat{a}^{ij\cdots}_{ab\cdots}\}]$ operators, where $ij\cdots \in \mathbf{H}$ and $ab\cdots \in \mathbf{P}$, operators $\{\hat{a}^{ab\cdots}_{ij\cdots}\}$ are normal-ordered with respect to the reference Fermi vacuum, where **H** and **P** are spaces containing the hole and particle orbitals, respectively.

The goal of this transformation is to gradually bring the Hamiltonian to a block-diagonal form, $\hat{H}_{\text{od}} = 0$. If we order the indices of Hamiltonian by energy, in the middle of the SRG transformation as shown in Figure 1.5 (c), most of the couplings with large orbital energy differences between P and Q spaces are decoupled, but those with small differences are left approximately unchanged. Since these couplings are the cause of the intruder-state problem, the danger zone of intruder states is avoided. We call this behavior of SRG the *separation of energy scales*.

Obviously, the form of $\hat{U}(s)$ is *a priori* unknown. In driven similarity renormalization group (DSRG), $\hat{U}^\dagger(s)$ is rewritten in an exponential form,

$$\hat{U}^\dagger(s) = e^{\hat{A}(s)}, \tag{1.31}$$

where $\hat{A}(s)$ is an s-dependent anti-Hermitian operator. Then the DSRG transformed Hamiltonian $\bar{H}(s)$ is given by

$$\bar{H}(s) = e^{-\hat{A}(s)}\hat{H}e^{\hat{A}(s)}. \tag{1.32}$$

[4] Reprinted from Evangelista, F. A., A driven similarity renormalization group approach to quantum many-body problems. *J. Chem. Phys.*, *141*, 054109, with the permission of AIP Publishing.

This formula is similar to the unitary coupled cluster (uCC) ansatz.[37,124–130] We can write $\hat{A}(s)$ as many-body expansion in terms of the s-dependent standard cluster operator $\hat{T}(s)$,

$$\hat{A}(s) = \sum_{k=1}^{n} \hat{A}_k(s), \tag{1.33}$$

$$\hat{A}_k(s) = \hat{T}_k(s) - \hat{T}_k^\dagger(s), \tag{1.34}$$

and

$$\hat{T}_k = \frac{1}{(k!)^2} \sum_{ij\cdots}^{\text{occ}} \sum_{ab\cdots}^{\text{vir}} t_{ab\cdots}^{ij\cdots}(s) \{\hat{a}_{ij\cdots}^{ab\cdots}\}, \tag{1.35}$$

where $t_{ab\cdots}^{ij\cdots}(s)$ are s-dependent cluster amplitudes.

Detailed explanation of how to determine the cluster amplitudes in DSRG can be found in Chapter 4 and Refs. 39 and 41. In brief, to simulate the separation of energy scales behavior in SRG, we require the off-diagonal part of the transformed Hamiltonian $\bar{H}_{\text{od}}(s)$ to equal a *source operator* $\hat{R}(s)$,

$$\bar{H}_{\text{od}}(s) = \hat{R}(s). \tag{1.36}$$

The role of the source operator in the DSRG flow equation is to drive the off-diagonal elements of $\bar{H}(s)$ to zero. This goal can be achieved by an appropriate parameterization of $\hat{R}(s)$.[39] The source operator $\hat{R}(s)$ is many-body operator analogous to $\hat{A}(s)$, whose k-body component is defined as

$$\hat{R}_k(s) = \frac{1}{(k!)^2} \sum_{ij\cdots}^{\text{occ}} \sum_{ab\cdots}^{\text{vir}} r_{ab\cdots}^{ij\cdots}(s) \{\hat{a}_{ij\cdots}^{ab\cdots}\} + \text{h.c.} \tag{1.37}$$

where "h.c." stands for the Hermitian conjugate of the first term and the indices of $r_{ab\cdots}^{ij\cdots}(s)$ exclude internal (de)excitations. By applying the *many-body conditions* in Eq. (1.36), we have equal number of conditions and parameters. The intruder state problem is also alleviated by selecting an appropriate value of s that recover most of the electron correlation, but do not decouple the problematic excitations.

However, contrary to Eq. (1.22) in the traditional single-reference coupled cluster (CC) theory, the DSRG unitary formalism leads to a non-terminating expression for the similarity transformed Hamiltonian and require truncating the Baker–Campbell–Hausdorff (BCH) expansion.[125,127,129] As such, approximations to the BCH formula must be introduced to achieve computationally viable approach.

In the previous work in our group, we introduced the linearized MR-DSRG truncated to two-body operators [MR-LDSRG(2)],[41] where we adopt the recursive single commutator (RSC) approximation proposed originally by Yanai and Chan in canonical transformation theory,[38]

$$\bar{H}_{0,1,2}(s) \approx \hat{H} + \sum_{k=1}^{\infty} \frac{1}{k!} \underbrace{[\cdots[[\hat{H}, \hat{A}_1(s) + \hat{A}_2(s)]_{1,2}, \hat{A}_1(s) + \hat{A}_2(s)]_{1,2}, \cdots]_{0,1,2}}_{k \text{ nested commutators}}, \quad (1.38)$$

where the subscripts $1, 2$ indicate that the commutator is truncated to contain only one- and two-body contributions. In the RSC scheme, every single commutator in the BCH expansion is approximated with at most two-body operators, for which closed form can be easily derived. The nested commutator can thus be evaluated using a recurrence relation based on the truncated single commutator. A preliminary benchmark shows that the MR-LDSRG(2) method yields superior accuracy than CCSD around equilibrium geometries and the accuracy persists across the entire potential energy curves, especially for single-bond breaking processes.[55]

The time of computing one truncated single commutator scales as $\mathcal{O}(N^2 N_{\mathbf{V}}^2 N_{\mathbf{C}}^2)$ where $N_{\mathbf{C}}$, $N_{\mathbf{V}}$, and N are the numbers of core, virtual, and total orbitals, respectively. This asymptotic cost is similar to that of CC with singles and doubles (CCSD) $[\mathcal{O}(N_{\mathbf{V}}^4 N_{\mathbf{C}}^2)]$. However, the actual total time is much longer than CCSD, because unlike in CCSD, the expansion in Eq. (1.38) does not terminate. Moreover, the $\mathcal{O}(N^4)$ memory requirement in MR-LDSRG(2) prevents application on systems with more than 250 correlated molecular orbitals. We will detail how to reduce both the computational time and memory cost of MR-LDSRG(2) in Chapter 4.

1.8 Prospectus

In Chapter 2 we describe the projector configuration interaction (PCI) method based on path filtering and polynomial projection. This method is a deterministic version of full configuration interaction quantum Monte Carlo (FCIQMC). We modified the stochastic walker spawning algorithm in FCIQMC to a deterministic path-filtering scheme. Then the imaginary-time propagation is accelerated by a Chebyshev polynomial projector. Chapter 3 reports improvements based on the original PCI method in the previous chapter. The accuracy was improved by modifying the approximated Hamiltonian to be Hermitian, and we implemented a more efficient projector based on the Davidson–Liu algorithm. We also showed the connection between PCI and the Heat-bath selected CI method, and why PCI is theoretically more efficient than selected CI methods. We switch gear in Chapter 4 to describe an efficient alternative to the MR-LDSRG(2) method. In this chapter, we introduce a sequential transformation ansatz to simplify the MR-LDSRG(2) formalism and apply density fitting and the non-interacting virtual orbital (NIVO) approximations to reduce both the memory requirement and total computational time.

Bibliography

[1] Dunning Jr, T. H. *J. Chem. Phys.* **1989**, *90*, 1007–1018.

[2] Zaanen, J.; Sawatzky, G. A.; Allen, J. W. *Phys. Rev. Lett.* **1985**, *55*, 418–421.

[3] Maynau, D.; Evangelisti, S.; Guihéry, N.; Calzado, C. J.; Malrieu, J.-P. *J. Chem. Phys.* **2002**, *116*, 10060–10010.

[4] Whitman, D. W.; Carpenter, B. K. *J. Am. Chem. Soc.* **1982**, *104*, 6473–6474.

[5] Wu, H.; Wang, L.-S. *J. Phys. Chem. A* **1998**, *102*, 9129–9135.

[6] Li, X.; Paldus, J. *Chem. Phys. Lett.* **2006**, *431*, 179–184.

[7] González, L.; Escudero, D.; Andrés, L. S. *ChemPhysChem* **2012**, *13*, 28–51.

[8] Mok, D. K. W.; Neumann, R.; Handy, N. C. *J. Phys. Chem.* **1996**, *100*, 6225–6230.

[9] Sherrill, C. D.; Schaefer, H. F. *Adv. Quant. Chem.* **1999**, *34*, 143–269.

[10] Vogiatzis, K. D.; Ma, D.; Olsen, J.; Gagliardi, L.; de Jong, W. A. *J. Chem. Phys.* **2017**, *147*, 184111.

[11] (a) Andersson, K.; Malmqvist, P. A.; Roos, B. O.; Sadlej, A. J.; Wolinski, K. *J. Phys. Chem.* **1990**, *94*, 5483–5488; (b) Andersson, K.; Malmqvist, P.-Å.; Roos, B. O. *J. Chem. Phys.* **1998**, *96*, 1218–1226.

[12] Hirao, K. *Chem. Phys. Lett.* **1992**, *190*, 374–380.

[13] Nakano, H. *J. Chem. Phys.* **1993**, *99*, 7983–7992.

[14] Werner, H.-J. *Mol. Phys.* **1996**, *89*, 645–661.

[15] Mahapatra, U. S.; Datta, B.; Mukherjee, D. *J. Phys. Chem. A* **1999**, *103*, 1822–1830.

[16] (a) Angeli, C.; Cimiraglia, R.; Evangelisti, S.; Leininger, T.; Malrieu, J. P. *J. Chem. Phys.* **2001**, *114*, 10252–10264; (b) Angeli, C.; Pastore, M.; Cimiraglia, R. *Theor. Chem. Acc.* **2007**, *117*, 743–754.

[17] Liu, B. *J. Chem. Phys.* **1973**, *58*, 1925–1937.

[18] (a) Werner, H.-J.; Knowles, P. J. *J. Chem. Phys.* **1988**, *89*, 5803–5814; (b) Knowles, P. J.; Werner, H.-J. *Chem. Phys. Lett.* **1988**, *145*, 514–522.

[19] (a) Hanrath, M.; Engels, B. *Chem. Phys.* **1997**, *225*, 197–202; (b) Engels, B.; Hanrath, M.; Lennartz, C. *Comput. Chem.* **2001**, *25*, 15–38.

[20] Szalay, P. G.; Müller, T.; Gidofalvi, G.; Lischka, H.; Shepard, R. *Chem. Rev.* **2012**, *112*, 108–181.

[21] Sivalingam, K.; Krupicka, M.; Auer, A. A.; Neese, F. *J. Chem. Phys.* **2016**, *145*, 054104.

[22] Čížek, J. *Adv. Chem. Phys.* **1969**, *14*, 35–89.

[23] Jeziorski, B.; Monkhorst, H. J. *Phys. Rev. A* **1981**, *24*, 1668–1681.

[24] Haque, M. A.; Mukherjee, D. *J. Chem. Phys.* **1984**, *80*, 5058–5069.

[25] Stolarczyk, L. Z.; Monkhorst, H. J. *Phys. Rev. A* **1985**, *32*, 725–742.

[26] Malrieu, J. P.; Durand, P.; Daudey, J. P. *J. Phys. A: Math. Gen.* **1985**, *18*, 809–826.

[27] Lindgren, I.; Mukherjee, D. *Phys. Rep.* **1987**, *151*, 93–127.

[28] (a) Piecuch, P.; Paldus, J. *Theoret. Chim. Acta* **1992**, *83*, 69–103; (b) Paldus, J.; Piecuch, P.; Pylypow, L.; Jeziorski, B. *Phys. Rev. A* **1993**, *47*, 2738–2782; (c) Piecuch, P.; Paldus, J. *J. Chem. Phys.* **1994**, *101*, 5875–5890.

[29] Mášik, J.; Hubač, I. *Adv. Quant. Chem.* **1998**, *31*, 75–104.

[30] Mahapatra, U. S.; Datta, B.; Bandyopadhyay, B.; Mukherjee, D. *Adv. Quant. Chem.* **1998**, *30*, 163–193.

[31] (a) Mahapatra, U. S.; Datta, B.; Mukherjee, D. *Mol. Phys.* **1998**, *94*, 157–171; (b) Mahapatra, U. S.; Datta, B.; Mukherjee, D. *J. Chem. Phys.* **1999**, *110*, 6171–6188.

[32] Li, S. *J. Chem. Phys.* **2004**, *120*, 5017–5026.

[33] Hanrath, M. *J. Chem. Phys.* **2005**, *123*, 084102.

[34] Evangelista, F. A.; Gauss, J. *J. Chem. Phys.* **2011**, *134*, 114102.

[35] Hanauer, M.; Köhn, A. *J. Chem. Phys.* **2011**, *134*, 204111.

[36] Datta, D.; Kong, L.; Nooijen, M. *J. Chem. Phys.* **2011**, *134*, 214116.

[37] Chen, Z.; Hoffmann, M. R. *J. Chem. Phys.* **2012**, *137*, 014108.

[38] (a) Yanai, T.; Chan, G. K.-L. *J. Chem. Phys.* **2006**, *124*, 194106; (b) Yanai, T.; Chan, G. K.-L. *J. Chem. Phys.* **2007**, *127*, 104107.

[39] Evangelista, F. A. *J. Chem. Phys.* **2014**, *141*, 054109.

[40] Li, C.; Evangelista, F. A. *J. Chem. Theory Comput.* **2015**, *11*, 2097–2108.

[41] (a) Li, C.; Evangelista, F. A. *J. Chem. Phys.* **2016**, *144*, 164114; (b) Li, C.; Evangelista, F. A. *J. Chem. Phys.* **2018**, *148*, 079903.

[42] Li, C.; Evangelista, F. A. *J. Chem. Phys.* **2018**, *148*, 124106.

[43] Li, C.; Evangelista, F. A. *Annu. Rev. Phys. Chem.* **2019**, *70*, 275–303.

[44] Chaudhuri, R. K.; Freed, K. F.; Hose, G.; Piecuch, P.; Kowalski, K.; Włoch, M.; Chattopadhyay, S.; Mukherjee, D.; Rolik, Z.; Szabados, Á.; Tóth, G.; Surján, P. R. *J. Chem. Phys.* **2005**, *122*, 134105.

[45] Hoffmann, M. R.; Datta, D.; Das, S.; Mukherjee, D.; Szabados, Á.; Rolik, Z.; Surján, P. R. *J. Chem. Phys.* **2009**, *131*, 204104.

[46] Lyakh, D. I.; Musiał, M.; Lotrich, V. F.; Bartlett, R. J. *Chem. Rev.* **2012**, *112*, 182–243.

[47] (a) Schucan, T. H.; Weidenmüller, H. A. *Ann. Phys.* **1972**, *73*, 108–135; (b) Schucan, T. H.; Weidenmüller, H. A. *Ann. Phys.* **1973**, *76*, 483–509.

[48] Salomonson, S.; Lindgren, I.; Mårtensson, A.-M. *Phys. Scr.* **1980**, *21*, 351–356.

[49] Evangelisti, S.; Daudey, J. P.; Malrieu, J. P. **1987**, *35*, 4930–4941.

[50] Zarrabian, S.; Laidig, W. D.; Bartlett, R. J. *Phys. Rev. A* **1990**, *41*, 4711–4720.

[51] (a) Kowalski, K.; Piecuch, P. *Phys. Rev. A* **2000**, *61*, 052506; (b) Kowalski, K.; Piecuch, P. *Int. J. Quantum Chem.* **2000**, *80*, 757–781.

[52] Evangelista, F. A. *J. Chem. Phys.* **2018**, *149*, 030901.

[53] Meller, J.; Malrieu, J. P.; Caballol, R. *J. Chem. Phys.* **1996**, *104*, 4068–4076.

[54] Köhn, A.; Hanauer, M.; Mück, L. A.; Jagau, T. C.; Gauss, J. *WIREs: Comput. Mol. Sci.* **2013**, *3*, 176–197.

[55] (a) Li, C.; Evangelista, F. A. *J. Chem. Phys.* **2017**, *146*, 124132; (b) Li, C.; Evangelista, F. A. *J. Chem. Phys.* **2018**, *148*, 079902.

[56] Roos, B. O.; Taylor, P. R.; Siegbahn, P. E. M. *Chem. Phys.* **1980**, *48*, 157–173.

[57] Rossi, E.; Bendazzoli, G. L.; Evangelisti, S.; Maynau, D. *Chem. Phys. Lett.* **1999**, *310*, 530–536.

[58] (a) White, S. R. *Phys. Rev. Lett.* **1992**, *69*, 2863–2866; (b) White, S. R.; Martin, R. L. *J. Chem. Phys.* **1999**, *110*, 4127–4130.

[59] (a) Chan, G. K.-L.; Head-Gordon, M. *J. Chem. Phys.* **2002**, *116*, 4462–4476; (b) Chan, G. K.-L.; Kállay, M.; Gauss, J. *J. Chem. Phys.* **2004**, *121*, 6110–6117.

[60] Booth, G. H.; Chan, G. K.-L. *J. Chem. Phys.* **2012**, *137*, 191102–191105.

[61] Mizukami, W.; Kurashige, Y.; Yanai, T. *J. Chem. Theory Comput.* **2012**, *9*, 401–407.

[62] (a) Kurashige, Y.; Yanai, T. *J. Chem. Phys.* **2009**, *130*, 234114; (b) Kurashige, Y.; Chan, G. K.-L.; Yanai, T. *Nat Chem* **2013**, *5*, 660–666; (c) Kurashige, Y.; Yanai, T. *Bull. Chem. Soc. Jpn.* **2014**, *87*, 1071–1073.

[63] (a) Wouters, S.; Nakatani, N.; Van Neck, D.; Chan, G. K.-L. *Phys. Rev. B* **2013**, *88*, 075122; (b) Wouters, S.; Bogaerts, T.; Van Der Voort, P.; Van Speybroeck, V.; Van Neck, D. *J. Chem. Phys.* **2014**, *140*, 241103; (c) Wouters, S.; Poelmans, W.; De Baerdemacker, S.; Ayers, P. W.; Van Neck, D. *Comput. Phys. Commun.* **2015**, *191*, 235–237.

[64] Olivares-Amaya, R.; Hu, W.; Nakatani, N.; Sharma, S.; Yang, J.; Chan, G. K.-L. *J. Chem. Phys.* **2015**, *142*, 034102.

[65] Rissler, J.; Noack, R. M.; White, S. R. *Chem. Phys.* **2006**, *323*, 519–531.

[66] Moritz, G.; Hess, B. A.; Reiher, M. *J. Chem. Phys.* **2005**, *122*, 024107.

[67] Bender, C. F.; Davidson, E. R. *Phys. Rev.* **1969**, *183*, 23–30.

[68] Buenker, R. J.; Peyerimhoff, S. D. *Theoret. Chim. Acta* **1974**, *35*, 33–58.

[69] Buenker, R. J.; Peyerimhoff, S. D. *Theoret. Chim. Acta* **1975**, *39*, 217–228.

[70] Burton, P. G.; Buenker, R. J.; Bruna, P. J.; Peyerimhoff, S. D. *Chem. Phys. Lett.* **1983**, *95*, 379–385.

[71] Huron, B.; Malrieu, J. P.; Rancurel, P. *J. Chem. Phys.* **2003**, *58*, 5745–5759.

[72] Evangelisti, S.; Daudey, J.-P.; Malrieu, J.-P. *Chem. Phys.* **1983**, *75*, 91–102.

[73] (a) Angeli, C.; Cimiraglia, R.; Persico, M.; Toniolo, A. *Theor. Chem. Acc.* **1997**, *98*, 57–63; (b) Angeli, C.; Persico, M. *Theor. Chem. Acc.* **1997**, *98*, 117–128; (c) Angeli, C.; Cimiraglia, R.; Persico, M. *Theor. Chem. Acc.* **1998**, *100*, 324–328.

[74] Cimiraglia, R. *J. Chem. Phys.* **1985**, *83*, 1746–1749.

[75] Giner, E.; Scemama, A.; Caffarel, M. *J. Chem. Phys.* **2015**, *142*, 044115.

[76] (a) Knowles, P. J.; Handy, N. C. *Comput. Phys. Commun.* **1989**, *54*, 75–83; (b) Knowles, P. J.; Handy, N. C. *J. Chem. Phys.* **1989**, *91*, 2396–2394.

[77] Meller, J.; Heully, J. L.; Malrieu, J. P. *Chem. Phys. Lett.* **1994**, *218*, 276–282.

[78] Sambataro, M.; Gambacurta, D.; Lo Monaco, L. *Phys. Rev. B* **2011**, *83*, 045102.

[79] Bytautas, L.; Ruedenberg, K. *Chem. Phys.* **2009**, *356*, 64–75.

[80] Ivanic, J.; Ruedenberg, K. *Theor. Chem. Acc.* **2001**, *106*, 339–351.

[81] Miralles, J.; Castell, O.; Caballol, R.; Malrieu, J.-P. *Chem. Phys.* **1993**, *172*, 33–43.

[82] Cave, R. J.; Xantheas, S. S.; Feller, D. *Theoret. Chim. Acta* **1992**, *83*, 31–55.

[83] Mitrushenkov, A. O.; Dmitriev, Y. Y. **1995**, *235*, 410–413.

[84] Bunge, C. F. *J. Chem. Phys.* **2006**, *125*, 014107.

[85] Knowles, P. J. *Mol. Phys.* **2015**, *113*, 1655–1660.

[86] Ben Amor, N.; Bessac, F.; Hoyau, S.; Maynau, D. *J. Chem. Phys.* **2011**, *135*, 014101.

[87] Bories, B.; Maynau, D.; Bonnet, M.-L. *J. Comput. Chem.* **2006**, *28*, 632–643.

[88] Neese, F. *J. Chem. Phys.* **2003**, *119*, 9428–9443.

[89] Harrison, R. J. *J. Chem. Phys.* **1991**, *94*, 5021–5031.

[90] Greer, J. C. *J. Chem. Phys.* **1995**, *103*, 1821–1828.

[91] Greer, J. C. *J. Comput. Phys.* **1998**, *146*, 181–202.

[92] Győrffy, W.; Bartlett, R. J.; Greer, J. C. *J. Chem. Phys.* **2008**, *129*, 064103.

[93] Evangelista, F. A. *J. Chem. Phys.* **2014**, *140*, 124114.

[94] Tubman, N. M.; Lee, J.; Takeshita, T. Y.; Head-Gordon, M.; Whaley, K. B. *J. Chem. Phys.* **2016**, *145*, 044112.

[95] Schriber, J. B.; Evangelista, F. A. *J. Chem. Phys.* **2016**, *144*, 161106.

[96] Schriber, J. B.; Evangelista, F. A. *J. Chem. Theory Comput.* **2017**, *13*, 5354–5366.

[97] Holmes, A. A.; Tubman, N. M.; Umrigar, C. J. *J. Chem. Theory Comput.* **2016**, *12*, 3674–3680.

[98] Sharma, S.; Holmes, A. A.; Jeanmairet, G.; Alavi, A.; Umrigar, C. J. *J. Chem. Theory Comput.* **2017**, *13*, 1595–1604.

[99] Smith, J. E. T.; Mussard, B.; Holmes, A. A.; Sharma, S. *J. Chem. Theory Comput.* **2017**, *13*, 5468–5478.

[100] Davidson, E. R. *J. Comput. Phys.* **1975**, *17*, 87–94.

[101] Liu, B. *Technical Report LBL-8158* **1978**, Lawrence Berkeley Laboratory, University of California, Berkeley.

[102] Stampfuß, P.; Wenzel, W. *J. Chem. Phys.* **2005**, *122*, 024110–024116.

[103] Tempo, R.; Ishii, H. *Eur. J. Control* **2007**, *13*, 189–203.

[104] Booth, G. H.; Thom, A. J. W.; Alavi, A. *J. Chem. Phys.* **2009**, *131*, 054106–054110.

[105] Cleland, D.; Booth, G. H.; Alavi, A. *J. Chem. Phys.* **2010**, *132*, 041103–041104.

[106] Thomas, R. E.; Sun, Q.; Alavi, A.; Booth, G. H. *J. Chem. Theory Comput.* **2015**, *11*, 5316–5325.

[107] Ten-no, S. L. *J. Chem. Phys.* **2017**, *147*, 244107.

[108] Blunt, N. S. *J. Chem. Phys.* **2018**, *148*, 221101.

[109] Neufeld, V. A.; Thom, A. J. W. *J. Chem. Theory Comput.* **2018**,

[110] (a) Booth, G. H.; Cleland, D.; Thom, A. J. W.; Alavi, A. *J. Chem. Phys.* **2011**, *135*, 084104–084115; (b) Cleland, D. M.; Booth, G. H.; Alavi, A. *J. Chem. Phys.* **2011**, *134*, 024112–024119; (c) Cleland, D.; Booth, G. H.; Overy, C.; Alavi, A. *J. Chem. Theory Comput.* **2012**, *8*, 4138–4152.

[111] Thomas, R. E.; Overy, C.; Booth, G. H.; Alavi, A. *J. Chem. Theory Comput.* **2014**, *10*, 1915–1922.

[112] Booth, G. H.; Smart, S. D.; Alavi, A. *Mol. Phys.* **2014**, *112*, 1855–1869.

[113] Thomas, R. E.; Booth, G. H.; Alavi, A. *Phys. Rev. Lett.* **2015**, *114*, 033001.

[114] Petruzielo, F. R.; Holmes, A. A.; Changlani, H. J.; Nightingale, M. P.; Umrigar, C. J. *Phys. Rev. Lett.* **2012**, *109*, 230201–230205.

[115] Blunt, N. S.; Smart, S. D.; Kersten, J. A. F.; Spencer, J. S.; Booth, G. H.; Alavi, A. *J. Chem. Phys.* **2015**, *142*, 184107–184110.

[116] Evangelista, F. A.; Hanauer, M.; Köhn, A.; Gauss, J. *J. Chem. Phys.* **2012**, *136*, 204108.

[117] Hanauer, M.; Köhn, A. *J. Chem. Phys.* **2012**, *137*, 131103.

[118] Sinha, D.; Maitra, R.; Mukherjee, D. *Comput. Theor. Chem.* **2013**, *1003*, 62–70.

[119] Mášik, J.; Hubač, I.; Mach, P. *J. Chem. Phys.* **1998**, *108*, 6571–6579.

[120] Pittner, J.; Nachtigall, P.; Čársky, P.; Mášik, J.; Hubač, I. *J. Chem. Phys.* **1999**, *110*, 10275–10282.

[121] Kong, L. *Int. J. Quantum Chem.* **2009**, *109*, 441–447.

[122] Wegner, F. *Ann. Phys.* **1994**, *506*, 77–91.

[123] (a) Głazek, S. D.; Wilson, K. G. *Phys. Rev. D* **1993**, *48*, 5863–5872; (b) Głazek, S. D.; Wilson, K. G. *Phys. Rev. D* **1994**, *49*, 4214–4218.

[124] Hoffmann, M. R.; Simons, J. *J. Chem. Phys.* **1988**, *88*, 993–1002.

[125] Bartlett, R. J.; Kucharski, S. A.; Noga, J. **1989**, *155*, 133–140.

[126] Watts, J. D.; Trucks, G. W.; Bartlett, R. J. *Chem. Phys. Lett.* **1989**, *157*, 359–366.

[127] Kutzelnigg, W. *Theoret. Chim. Acta* **1991**, *80*, 349–386.

[128] Mertins, F.; Schirmer, J. *Phys. Rev. A* **1996**, *53*, 2140–2152.

[129] Taube, A. G.; Bartlett, R. J. *Int. J. Quantum Chem.* **2006**, *106*, 3393–3401.

[130] Harsha, G.; Shiozaki, T.; Scuseria, G. E. *J. Chem. Phys.* **2018**, *148*, 044107.

Chapter 2 A deterministic projector configuration interaction approach for the ground state of quantum many-body systems

Chapter Abstract

In this work we propose a novel approach to solve the Schrödinger equation which combines projection onto the ground state with a path-filtering truncation scheme. The resulting projector configuration interaction (PCI) approach realizes a deterministic version of the full configuration interaction quantum Monte Carlo (FCIQMC) method [Booth, G. H.; Thom, A. J. W.; Alavi, A. *J. Chem. Phys.* **2009**, *131*, 054106]. To improve upon the linearized imaginary-time propagator, we develop an optimal projector scheme based on an exponential Chebyshev expansion in the limit of an infinite imaginary time step. After writing the exact projector as a path integral in determinant space, we introduce a path filtering procedure that truncates the size of the determinantal basis and approximates the Hamiltonian. The path filtering procedure is controlled by one real threshold that determines the accuracy of the PCI energy and is not biased towards any determinant. Therefore, the PCI approach can equally well describe static and dynamic electron correlation. This point is illustrated in benchmark computation on N_2 at both equilibrium and stretched geometries. In both cases, the PCI achieves chemical accuracy with wave functions that contain less than 0.5% of the full CI space. We also report computations on the ground state of C_2 with up to quaduple-ζ basis sets and wave functions as large as 200 million determinants, which allow a direct comparison of the PCI, FCIQMC, and density matrix renormalization group (DMRG) methods. The size of the PCI wave function grows

modestly with the number of unoccupied orbitals and its accuracy may be tuned to match that of FCIQMC and DMRG.

2.1 Introduction

The full configuration interaction (FCI) approach provides the exact solution to the electronic Schrödinger equation within a finite one-particle basis set.[1] However, since the number of FCI wave function parameters grows rapidly with system size, this approach is only feasible for few electrons distributed in a small number of orbitals.[2] Contrary to what is suggested by this observation, a large body of evidence has been amassed that shows that the information content of *molecular* wave functions is just a small fraction of the size of the FCI basis.[3] For example, for wave functions dominated by one Slater determinant, truncated coupled cluster theory can recover a large fraction of the dynamical correlation energy at a cost that is polynomial in the number of electrons.[4] However, in the case of strongly correlated electrons, the problem of finding general polynomial-scaling wave function methods is still open.[5,6]

Several strategies have been suggested to overcome the exponential cost of FCI and FCI performed in a complete active space (CASCI), including selected CI approaches that truncate FCI space,[7–21] tensor factorization,[22–39] alternative configuration interaction and coupled cluster methods,[40–43] symmetry breaking and restoration,[44–46] and Monte-Carlo methods.[47–64] Recently, Monte-Carlo methods that stochastically sample the wave function in the space of Slater determinants have received wide attention. The Monte-Carlo CI method (MCCI) randomly samples interacting spin projected Slater determinants.[47–52] MCCI may be viewed as a stochastic version of selected CI since at each iteration the energy is obtained by diagonalizing the Hamiltonian is a subset of the FCI space.[7–10] Another stochastic method is the auxiliary-field QMC (AFQMC) approach.[53–55,57] AFQMC uses a projector formalism to stochastically sample the wave function in a basis of non-orthogonal Slater determinants.

Deterministic analogs of the AFQMC approach have also been developed, including the path-integral renormalization group method[65,66] and the non-orthogonal multi-component adaptive greedy iterative compression approach of McClean and Aspuru-Guzik.[67]

An alternative to the MCCI and AFQMC methods is the FCI Quantum Monte-Carlo (FCIQMC) method developed by Alavi and co-workers.[58–64] FCIQMC is a projector Monte-Carlo method that samples the imaginary-time propagator in a space of orthogonal Slater determinants. By working in a basis of Slater determinants, FCIQMC can more easily account for the annihilation of walkers of different sign. This feature ameliorates the sign problem, but a large number of walkers are necessary to accurately sample the FCI space of determinants. The initiator approximation[59] reduces the number of walkers required in FCIQMC and increases the sign coherence of the sampling. Furthermore, a semi-stochastic version of FCIQMC (SFCIQMC) was later introduced,[68–70] which shows that treating part of the imaginary-time projection deterministically accelerates convergence and reduces statistical uncertainty.

The improvements to the performance of FCIQMC brought by treating part of determinant space deterministically raises the interesting question of whether a fully deterministic projector method might be even more advantageous. As pointed out by Tubman and co-workers,[71] the stochastic dynamics of FCIQMC reinterpreted in a deterministic way corresponds to a truncation criterion for selected CI. In this work, we demonstrate an alternative route to create a deterministic analog of FCIQMC. An important feature of our new method is the use of a projection scheme that simultaneously selects an optimal CI space and approximately diagonalizes the Hamiltonian. The resulting computational method is named projector configuration interaction (PCI). The PCI approach automatically identifies the most important determinants that contribute to the ground state wave function, therefore, it can treat both dynamic and static electron correlation.

The PCI methods presents two major differences with respect to FCIQMC. As in other projector Monte-Carlo methods, FCIQMC relies on a linearized approximation to the imaginary-time projector obtained by Taylor expansion. One of the major drawbacks of this approximation is that a small time step is required to guarantee convergence to the ground state, the length of which is bound by the inverse spectral radius of the Hamiltonian. Following the work of Kosloff and Tal-Ezer,[72] we overcome this limitation by using a Chebyshev expansion of the exponential projector.[73–77] In particular, we consider the *wall*-Chebyshev projector, which is derived from the Chebyshev representation of the imaginary-time propagator in the limit of an infinite time step. In this respect, our goal is analogous to that of the t expansion method, in which the $t \to \infty$ limit of the imaginary-time propagator is expressed using Padé approximants.[78] The wall-Chebyshev generator is shown to be equivalent to a power method with alternating shifts, and it is more efficient than the corresponding Taylor and Chebyshev expansions of the exponential projector. We also address the issue of replacing Monte-Carlo sampling with a deterministic truncation of the determinant space. Since projection onto the ground state may be viewed as a path-integral scheme, we apply the idea of path filtering[79–82] in order to truncate CI space and control accuracy. In the PCI, path filtering is applied to screen excited determinants generated by projection onto the ground state. Path filtering is controlled by one threshold parameter, and as a consequence, the PCI forms a family of one-parameter theories that are systematically improvable and equivalent to FCI when path filtering is suppressed.

The paper is organized in the following way. In section 2, we introduce the formalism of ground state projection, Chebyshev fitting of the imaginary-time propagator, and path filtering. Section 3 details the PCI algorithm and our implementation and analyzes the sources of error in the PCI approach. In section 4 we demonstrate the ability of PCI to adapt to various regimes of electron correlation by applying it to

the dissociation of N_2. In the same section, we study the scaling of the PCI cost with respect to basis set size and the size consistency error introduced by the path-filtering approximation.

2.2 Theory

2.2.1 General formalism of ground state projection

Given the Hamiltonian operator $\hat{H}$, we write its eigenvalues and eigenfunctions as E_i and Ψ_i, respectively. Within a finite computational basis, the Hamiltonian is assumed to have N eigenfunctions, and its spectral radius (R) is defined as the difference between the largest (E_{N-1}) and smallest (E_0) eigenvalues divided by two:

$$R = \frac{E_{N-1} - E_0}{2} \tag{2.1}$$

The goal of projector CI (PCI) is to obtain the ground state wave function Ψ_0 starting from a trial wave function Ω via a projector operator $\hat{P}_0$:

$$|\Psi_0\rangle = N_P \hat{P}_0 |\Omega\rangle \tag{2.2}$$

The only assumption concerning the trial wave function is that its overlap with the exact ground state is not zero, that is $\langle\Omega|\Psi_0\rangle \neq 0$. In Eq. (3.16), N_P is a normalization factor introduced to guarantee that $\langle\Psi_0|\Psi_0\rangle = 1$ and the projector operator $\hat{P}_0$ is assumed to be idempotent ($\hat{P}_0^2 = \hat{P}_0$).

We restrict our discussion to a class of projectors that can be written as the infinite product:

$$\hat{P}_0 = \lim_{n\to\infty} g^n(\hat{H}) \tag{2.3}$$

where $g(\cdot)$ is the *generator of the projector* $\hat{P}_0$ (also abbreviated as *generator* in the following). The projector generator is assumed to be a real function $g : \mathbb{R} \to \mathbb{R}$ extended to the domain of Hermitian operators. Given a generic state vector $|\Omega\rangle$, it

may be decomposed as a sum over the eigenfunctions of the Hamiltonian as:

$$|\Omega\rangle = \sum_i c_i |\Psi_i\rangle \tag{2.4}$$

so that the action of the projector generator $g(\hat{H})$ onto $|\Omega\rangle$ may be written out:

$$g(\hat{H})|\Omega\rangle = \sum_i c_i g(\hat{H})|\Psi_i\rangle = \sum_i g(E_i)c_i|\Psi_i\rangle \tag{2.5}$$

Thus, the application of a generator onto a trial state vector leads to a new state vector in which the coefficient that multiplies each $|\Psi_i\rangle$ is scaled by a factor $g(E_i)$, where E_i is the eigenvalue corresponding to $|\Psi_i\rangle$.

For an appropriately chosen generator, the repeated application of $g(\hat{H})$ may be used to project out the contribution of excited states to a given trial wave function. A necessary condition for the generator to project a state onto Ψ_0 is to satisfy the inequality:

$$|g(E_0)| > |g(x)| \quad \forall x \in (E_0, E_{N-1}] \tag{2.6}$$

so that the relative weight of the excited states is reduced by a factor $q_i = g(E_i)/g(E_0)$:

$$g(\hat{H})|\Omega\rangle = c_0|\Psi_0\rangle + \sum_{i=1}^{N-1} q_i c_i |\Psi_i\rangle \quad |q_i| < 1 \tag{2.7}$$

where without loss of generality, we have assumed that $g(x)$ is scaled so that $g(E_0) = 1$. In practical applications, the range of $\hat{H}$ is unknown, but as discussed in section 2.3, one may obtain upper bounds of E_0 and E_{N-1} (here denoted $\tilde{E}_0$ and $\tilde{E}_{N-1}$). In this case, it is convenient to work with generators that decrease monotonically in the left-neighborhood of $\tilde{E}_0$, that is for any two points $x, y \in [E_0, \tilde{E}_0]$:

$$|g(x)| > |g(y)| \text{ if } x < y \tag{2.8}$$

When the monotonicity condition expressed by Eq. (2.8) is satisfied, the projector is guaranteed to converge to the ground state even if E_0 and E_{N-1} are approximated with their respective upper bound estimates. Therefore, in the following discussion we do not distinguish $\tilde{E}_0$ from E_0.

2.2.2 Rate of convergence of generators.

The repeated application of the generator onto a trial wave function $\Omega^{(0)}$ generates a sequence of vectors:

$$|\Omega^{(n)}\rangle = N_P^{(n)} g^n(\hat{H}) \, |\Omega^{(0)}\rangle \tag{2.9}$$

where $N_P^{(n)}$ is a normalization factor for the wave function at step n. In the limit of n that goes to infinity $\Omega^{(n)}$ converges to the exact ground state:

$$|\Psi_0\rangle = \lim_{n\to\infty} |\Omega^{(n)}\rangle \tag{2.10}$$

The asymptotic rate of convergence of this sequence is defined as:

$$\mu = \lim_{n\to\infty} \frac{\|\Omega^{(n+1)} - \Psi_0\|}{\|\Omega^{(n)} - \Psi_0\|} = \max_i |q_i| \tag{2.11}$$

and is determined by the excited state Ψ_i for which the ratio $q_i = g(E_i)/g(E_0)$ has the largest absolute value [see Eq. (2.7)].

When the rate of convergence is controlled by the first excited state, that is $\mu = |q_1|$, and the energy difference $E_1 - E_0$ is small compared to the spectral radius, then we can approximate μ as:

$$\mu = \left| \frac{g(E_1)}{g(E_0)} \right| \approx |1 + g'(E_0) \cdot (E_1 - E_0)| \tag{2.12}$$

where $g'(E_0)$ is the first derivative of $g(x)$ at E_0. Hence, we can define the convergence factor γ for $g(x)$ as

$$\gamma = -g'(E_0) \tag{2.13}$$

It is possible to show that the number of times one must apply $g(\hat{H})$ to a trial wave function in order to achieve a certain level of accuracy is inversely proportional to γ. Therefore, the convergence factor provides a quantitative estimate of the numerical efficiency of a generator. Generators with large convergence factors are in general preferable as they are expected to reduce the computational cost of the PCI. The parameters that enter the definition of all the generators discussed in this work and their corresponding convergence factor are summarized in Table 2.1.

Table 2.1 Comparison of different projector generators. The form of the projector generator $[g(x)]$ and convergence factor (γ) is given as a function of the time step (τ), the spectral radius of the Hamiltonian (R), and the order of the polynomial expansion (m).

Generator	Parameters $g(x)$		Convergence factor (γ)
Exponential	τ	$e^{-\tau(x-E_0)}$	τ
Linear	τ	$1-\tau(x-E_0)$	$\tau < \frac{1}{R}$ *
Exp-Taylor	τ,m	$\sum_{k=0}^{m} \frac{1}{k!}(-\tau)^k(x-E_0)^k$	$\tau < \frac{m+1}{2R}$ **
Exp-Chebyshev	τ,R,m	$C_m(\tau R)\sum_{k=0}^{m}(2-\delta_{k0})I_k(\tau R)T_k\left(-\frac{x-E_0-R}{R}\right)$	$\frac{\sum_{k=1}^{m} 2I_k(\tau R)k^2}{R\sum_{k=0}^{m}(2-\delta_{k0})I_k(\tau R)} < \frac{m(m+1)}{3R}$
Wall-Chebyshev	R,m	$\frac{1}{2m+1}\sum_{k=0}^{m}(2-\delta_{k0})T_k\left(-\frac{x-E_0-R}{R}\right)$	$\frac{m(m+1)}{3R}$

* In order to converge onto the ground state wave function, the time step must satisfy the condition: $\tau < \frac{1}{R}$.

** In order to converge onto the ground state wave function, the time step must satisfy the condition: $|\sum_{k=0}^{m} \frac{1}{k!}(-\tau)^k(2R)^k| < 1$. From this expression one may derive the upper bound: $\tau < \frac{m+1}{2R}$.

2.2.3 Taylor and Chebyshev expansions of the imaginary-time propagator

The projector generator corresponding to the imaginary-time propagator, $\lim_{\beta\to\infty} e^{-\beta(\hat{H}-E_0)}$, is the exponential generator (g_{exp}), defined as:

$$g_{\text{exp}}(x) = e^{-\tau(x-E_0)} \tag{2.14}$$

This generator satisfies both conditions Eqs. (2.6) and (2.8). Nevertheless, it is not expressed as a polynomial of the Hamiltonian and therefore, to make its evaluation computationally viable it must be approximated with a polynomial expansion. To evaluate the projector based on the exponential generator [Eq. (2.14)] it is necessary to expand $g_{\text{exp}}(x)$ into a polynomial series.

An m-th order Taylor expansion of $g_{\text{exp}}(x)$ centered around E_0 yields the generator:

$$g_{\text{expTaylor}}(x) = \sum_{k=0}^{m} \frac{1}{k!}(-\tau)^k(x-E_0)^k \tag{2.15}$$

which has convergence factor $\gamma_{\text{expTaylor}} = \tau$ independent of the truncation order m. Consequently, there is not gain in efficiency when $g_{\text{expTaylor}}(x)$ is expanded beyond

$m = 1$. More importantly, the Taylor expansion is only accurate near E_0, and since the error grows as a power of $\tau(x - E_0)$, a very small value of τ may be required to satisfy the necessary condition for the convergence of the projector [see Eq. (2.6)].

Note, that the first-order Taylor expansion of the exponential:

$$g_{\text{linear}}(x) = 1 - \tau(x - E_0) = -\tau(x - s) \tag{2.16}$$

is equivalent to a power method with shift $s = E_0 + \frac{1}{\tau}$. In order to converge to the ground state wave function, the shift must be chosen to satisfy $s > R$. The corresponding convergence factor is bound by the inverse of the spectral range of the Hamiltonian:

$$\gamma_{\text{linear}} = \tau < \frac{1}{R} \tag{2.17}$$

An alternative approximation of the exponential with better error control is an expansion in terms of Chebyshev polynomials (for example, see Refs. 72 and 77). Following Kosloff and Tal-Ezer,[72] we write the m-th order Chebyshev polynomial fitting of the exponential generator as:

$$g_{\text{expCh}}(x) = C_m(\tau R) \sum_{k=0}^{m} (2 - \delta_{k0}) I_k(\tau R) T_k \left(-\frac{x - E_0 - R}{R} \right) \tag{2.18}$$

where $C_m(\tau R) = 1/\left(\sum_{k=0}^{m}(2 - \delta_{k0}) I_k(\tau R)\right)$ is a scaling factor that guarantees $g_{\text{expCh}}(E_0) = 1$, δ_{k0} is a Kronecker delta, I_k is the k-th modified Bessel function of the first kind, and T_k is the k-th order Chebyshev polynomial.

Figure 2.1A shows first- and second-order Taylor and Chebyshev expansions of the exponential evaluated for $\tau = 2\ E_{\text{h}}^{-1}$ in the range $[-1, 1]\ E_{\text{h}}$. This plot illustrates the points made above: i) the Taylor expansion of the exponential is accurate only near the expansion point (in this case $E_0 = -1\ E_{\text{h}}$) and ii) the Chebyshev expansion is well behaved on the entire range. Figure 2.1B shows the Chebyshev expansion for the same range but with $\tau = 10\ E_{\text{h}}^{-1}$. In this case the fitting error is larger and the convergence of the Chebyshev expansion with respect to the order m is slower than

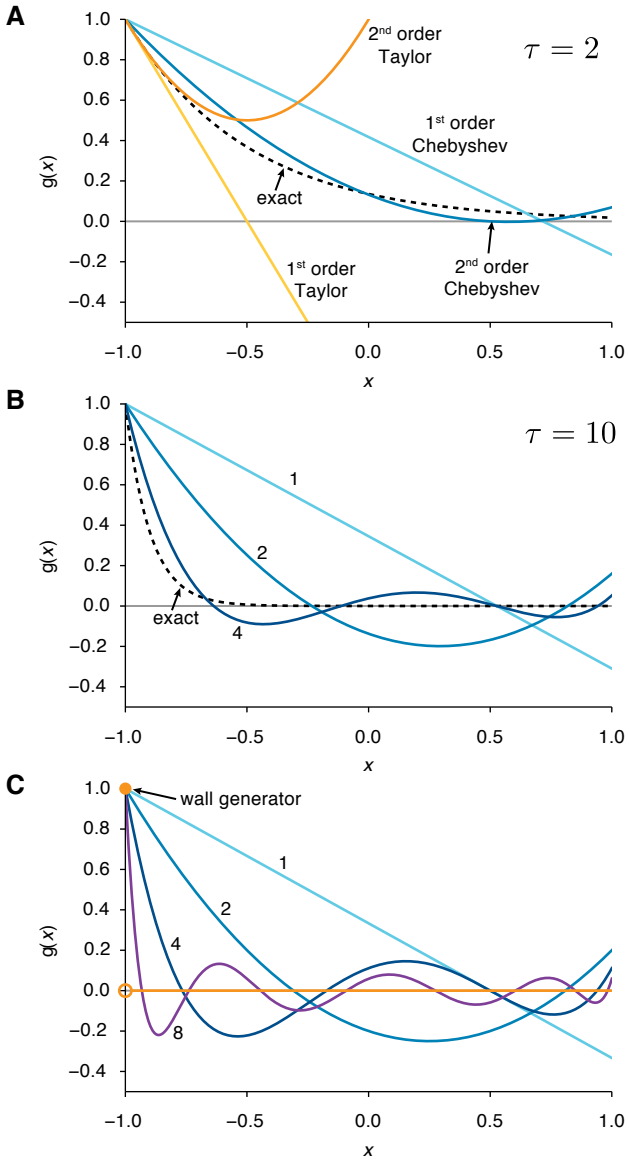

Figure 2.1 Polynomial approximations of the exponential generator [Eq. (2.14)] and the $\tau \to \infty$ limit of the exponential generator (wall generator) [Eq. (2.20)] plotted in the range $[-1, 1]$ E_h. (A) Taylor and Chebyshev approximation of the exponential generator for $\tau = 2$ E_h^{-1} at order 1 and 2. (B) Chebyshev approximation of the exponential generator for $\tau = 10$ E_h^{-1} at order 1, 2, and 4. (C) Chebyshev approximation of the wall generator at order 1, 2, 4, and 8.

the case $\tau = 2\ E_{\mathrm{h}}^{-1}$. Nevertheless, even though the Chebyshev expansion for $\tau = 10\ E_{\mathrm{h}}^{-1}$ does not accurately match the exponential function, it is still a valid projector generator since it satisfies Eqs. (2.6) and (2.8).

2.2.4 An improved generator: the wall generator and its Chebyshev expansion.

In the previous subsection we discussed how to improve the accuracy of the Taylor expansion of the exponential generator via Chebyshev fitting. Ideally, the best projector generator is the the *wall* function, defined as:

$$g_{\mathrm{wall}}(x) = \begin{cases} 0 \text{ for } x > E_0 \\ 1 \text{ for } x = E_0 \\ \infty \text{ for } x < E_0 \end{cases} \tag{2.19}$$

This generator may be viewed as the $\tau \to \infty$ limit of the exponential generator:

$$g_{\mathrm{wall}}(x) = \lim_{\tau\to\infty} e^{-\tau(x-E_0)} \tag{2.20}$$

Despite the fact that neither definitions of $g_{\mathrm{wall}}(x)$ are computationally viable, we can still approximate the wall generator using a Chebyshev expansion, by taking the $\tau \to \infty$ limit of the m-th order exponential Chebyshev generator:

$$\begin{aligned} g_{\mathrm{wallCh}}(x) =& \lim_{\tau\to\infty} g_{\mathrm{expCh}}(x) \\ =& \frac{1}{2m+1} \sum_{k=0}^{m} (2-\delta_{k0}) T_k\left(-\frac{x-E_0-R}{R}\right) \end{aligned} \tag{2.21}$$

where we used the fact that $\lim_{\tau\to\infty} I_{k+1}(\tau R)/I_k(\tau R) = 1$.[83] Note that this polynomial is a special case of the Chebyshev expansion of the delta distribution with the origin translated to the lower bound of the fitting range.[73–76]

The wall-Chebyshev generators of order 1, 2, 4, and 8 are plotted in Figure 2.1C. An important property of the wall-Chebyshev generator is that for values of x less than E_0 these functions are monotonic and diverge when $x \to -\infty$. Therefore they satisfy Eq. (2.8) and are able to converge onto the ground state even when the range of $\hat{H}$ is not known precisely.

The Chebyshev expansion of the wall generator may shown to converge with factor

$$\gamma_{\text{wallCh}} = \frac{m(m+1)}{3R} \tag{2.22}$$

which is the largest one among all the polynomial generators discussed in this work. It is important to note that although we can design generators with even larger convergence factors, an efficient generator must also efficiently suppress high energy excited states. For example, the Chebyshev generator, defined as $g_{\text{Ch}}(x) = T_k\left(-\frac{x-E_0-R}{R}\right)$ gives $\gamma_{\text{Ch}} = \frac{m^2}{R}$, which is larger than the convergence factor of the generators discussed previously. However, the convergence of the projector generated by $g_{\text{Ch}}(x)$ is slow because the coefficients of high energy excited states are not efficiently reduced.

In each projection generation step, an m-th order wall-Chebyshev generator involves the application of the Hamiltonian m times, therefore, it has a cost that is m times that of the linear generator (power method). Consequently, the theoretical relative acceleration with respect to the most efficient linear generator ($\tau_{\text{linear}} = 1/R$) is:

$$\frac{\gamma_{\text{wallCh}}}{m\gamma_{\text{linear}}} = \frac{m+1}{3} \tag{2.23}$$

For instance, an 8^{th}-order wall-Chebyshev generator has a computational cost that is a third of the linear generator with the largest allowed value of τ $(1/R)$.

An important property of the m-th order $g_{\text{wallCh}}(x)$ generator is that it has m distinct real roots in the range (E_0, E_{N-1}). Therefore, it can be decomposed as a product of m linear generators with real shifts:

$$g_{\text{wallCh}}(x) = \prod_{i=1}^{m} \frac{x - s_i}{E_0 - s_i} \tag{2.24}$$

where the shifts s_i are the zeros of $g_{\text{wallCh}}(x)$. It is easy to show that the zeros of $g_{\text{wallCh}}(x)$ can be expressed in closed form as:

$$s_i = E_0 + R\left(1 - \cos\frac{i}{m+\frac{1}{2}}\pi\right) \tag{2.25}$$

Eq. (2.24) allows us to implement the wall generator as a product of linear generators applied successively onto a state vector. Hence, the projector associated with the wall generator may be interpreted as an optimized power method that uses a sequence of energy shifts. Besides its high efficiency, there are two other advantages of the wall-Chebyshev generator: i) Only two vectors (previous and current) need to be stored during the calculation, in contrast to three vectors necessary for the exp-Chebyshev generator (previous, current and accumulator) and ii) the wall-Chebyshev generator is numerically more stable than the exp-Chebyshev generator since for $\tau \to \infty$ the numerical evaluation of Bessel functions introduces numerical errors.

2.2.5 Determinant selection via path filtering.

The projector CI discussed in Section 2.2.1 provides an alternative approach to finding the exact ground state. In this section we show how to combine this methods with path filtering to generate an approach that diagonalizes the Hamiltonian in an optimal subset of FCI space. We discuss path filtering only for the case of the linear generator and report details for higher-order polynomial generators in appendix 2.A.

Consider a normalized trial state $\Omega^{(n)}$ that approximates the exact ground state in the subset $S^{(n)}$ of FCI space:

$$|\Omega^{(n)}\rangle = \sum_{\Phi_J \in S^{(n)}} C_J^{(n)} |\Phi_J\rangle \tag{2.26}$$

where $C_J^{(n)}$ is the coefficient of determinant $|\Phi_J\rangle$ at the n-th step. The action of the linear generator onto $\Omega^{(n)}$ leads to a new state $\tilde{\Omega}^{(n+1)}$:

$$g_{\text{linear}}(\hat{H}) |\Omega^{(n)}\rangle = |\tilde{\Omega}^{(n+1)}\rangle = \sum_I \tilde{C}_I^{(n+1)} |\Phi_I\rangle \tag{2.27}$$

where, in general, the vector of coefficients $\tilde{C}_I^{(n+1)}$ is not normalized. The coefficients of $\tilde{C}_I^{(n+1)}$ may be expressed as a sum over *spawning amplitudes*, $A_{IJ}^{(n+1)}$:

$$\begin{aligned} \tilde{C}_I^{(n+1)} &= \langle \Phi_I | \, 1 - \tau(\hat{H} - E_0) \, |\Omega^{(n)}\rangle \\ &= \tau \sum_{\Phi_J \in S^{(n)}} A_{IJ}^{(n+1)} \end{aligned} \tag{2.28}$$

where $A_{IJ}^{(n+1)}$ is defined as:

$$A_{IJ}^{(n+1)} = \frac{1}{\tau} \langle \Phi_I | \, 1 - \tau(\hat{H} - E_0) \, | \Phi_J \rangle \, C_J^{(n)} \tag{2.29}$$

The spawning amplitude has the units of a rate and represents the contribution of the Φ_J component of $\Omega^{(n)}$ that "flows" to the coefficient of Φ_I for state $\tilde{\Omega}^{(n+1)}$.

The repeated application of the generator onto a trial function generates paths in FCI space that may be filtered (approximated) by applying a threshold to the spawning amplitude. To this end we introduce a *spawning threshold* η and truncate the off-diagonal spawning amplitude as:

$$A_{IJ}^{(n)}(\eta) = \begin{cases} A_{II}^{(n)} & \text{if } I = J \\ A_{IJ}^{(n)} \Theta(|A_{IJ}^{(n)}| - \eta) & \text{if } I \neq J \end{cases} \tag{2.30}$$

where $\Theta(x)$ is the Heaviside step function. Consequently, the PCI update equations for the wave function coefficients are:

$$\tilde{C}_I^{(n+1)} = \tau \sum_{\Phi_J \in S^{(n)}} A_{IJ}^{(n+1)}(\eta) \tag{2.31}$$

and the determinant set at step $n+1$ includes only those elements of the FCI space that may be reached from $S^{(n)}$ via non-zero amplitudes:

$$S^{(n+1)} = \{\Phi_I : \exists \Phi_J \in S^{(n)}, A_{IJ}^{(n+1)}(\eta) \neq 0\} \tag{2.32}$$

In other words, a determinant is included in $S^{(n+1)}$ when there is at least one spawning amplitude that is larger than the spawning threshold. Note that this selection criterion is analogous to the one used in heat-bath CI (HCI).[84,85] In the HCI method, a determinant Φ_I is selected if there is at least one significant spawning amplitude that connects it to a determinant contained in the trial wave function, that is, if it meets the condition $\max_J |\langle \Psi_I | \hat{H} | \Phi_J \rangle C_J| = \max_J |A_{IJ}^{(n+1)}| > \epsilon_1$, where ϵ_1 is a parameter equivalent to η. Since path filtering allows spawning to new determinants Φ_I if there are one or more paths for which $|A_{IJ}^{(n+1)}| > \eta$, this condition is equivalent to the one used in HCI. In contrast, most selected CI approaches estimate the importance of a

determinant either using a second-order correction to the energy or the first-order amplitude corresponding to Φ_I. The major difference between the first-order amplitude and path filtering criteria is that the former also includes a denominator given by the difference between the energy of the sampled determinant and the current wave function. However, as shown in Ref. 85, while the numerator of the first-order amplitude varies over several orders of magnitude, the denominator spans a much smaller range and therefore it plays a minor role in the selection. Therefore, we expect that for appropriately chosen thresholds, path filtering will yield truncated FCI spaces that are close to those obtained from conventional selected CI approaches and HCI.

In order to further reduce the computation cost, the so-called initiator approximation[59] is introduced in FCIQMC, which imposes a screening of the determinants that may be spawned. Translated in the language of the PCI approach, the initiator approximation is equivalent to a path-filtering procedure in which the screening is done according to the absolute value of a determinant coefficient $[C_I^{(n)}]$. Thus, the initiator approximation considers only the importance of the parent determinant, while as already mentioned selection performed by the PCI considers both the importance of parent determinants and the coupling between parent and spawned determinants.

2.2.6 Sources of errors in the PCI method

When compared to FCI, the PCI method introduces two types of error. The first, the truncation error, is connected to the use of a subset of the full Hilbert space of determinants, and also affects selected CI methods. Note that the truncation error does not affect methods like FCIQMC, which in principle can sample the entire Hilbert space. The second type of error, the path filtering error, arises from approximating the action of the generator onto a state vector via Eqs. (2.30) and (3.25). The path filtering error may be viewed as arising from the diagonalization of an approximate

Hamiltonian ($\tilde{H}$), which results from the path filtering procedure:

$$\tilde{H}_{IJ}^{(n)} = \begin{cases} H_{IJ} & \text{if } A_{IJ}^{(n)}(\eta) \neq 0 \\ 0 & \text{if } A_{IJ}^{(n)}(\eta) = 0 \end{cases} \tag{2.33}$$

Obviously, $\tilde{H}^{(n)}$ depends on the current wave function, and it is not guaranteed to be symmetric since in general $A_{IJ}^{(n)}(\eta) \neq A_{JI}^{(n)}(\eta)$. In the PCI, the path filtering error arises from the fact that the wave function coefficient vector is the right eigenvector of $\tilde{H}^{(n)}$, which differs from the eigenvector of the full Hamiltonian in the subset $S^{(n)}$. Note, that the initiator approximation used in the FCIQMC approach is a form of path filtering, and consequently, it introduces a source of error analogous to the path-filtering error.

2.3 Implementation

2.3.1 The PCI algorithm

The determinant selection procedure implemented via path filtering may be combined with the repeated application of the generator to obtain an approximate representation of the ground state wave function. In the case of the linear generator the resulting PCI algorithm consists of the following steps:

1. Trial wave function generation. The PCI procedure starts by selecting a trial wave function $\Omega^{(0)}$ to which corresponds the determinant space $S^{(0)}$. Although a convenient choice for the initial trial wave function $\Omega^{(0)}$ is the Hartree–Fock determinant Φ_{HF}, a CI with selected single and doubles out of Φ_{HF} yields faster convergence to the ground state.

2. Range estimation. The expectation value of the Hamiltonian with respect to the initial guess, $\langle\Omega^{(0)}|\,\hat{H}\,|\Omega^{(0)}\rangle$ is used to estimate an upper bound to the ground state energy E_0. To estimate an upper bound to the energy of the highest excited state E_{N-1}, we employ Gershgorin's circle theorem. Accordingly, we

approximate the upper bound to the eigenvalues of $\hat{H}$ as the sum of the diagonal element with the highest energy ($\langle\Phi_{N-1}|\,\hat{H}\,|\Phi_{N-1}\rangle$) plus the sum of the absolute values of the off-diagonal matrix elements that couple $|\Phi_{N-1}\rangle$ to other determinants:

$$\tilde{E}_{N-1} = \langle\Phi_{N-1}|\,\hat{H}\,|\Phi_{N-1}\rangle + \sum_{I}^{N-2} |\,\langle\Phi_{N-1}|\,\hat{H}\,|\Phi_I\rangle\,| \tag{2.34}$$

This estimate is not guaranteed to be a strict upper bound to E_{N-1} since it is possible that other Gershgorin circles might enclose energy ranges higher than the value of Eq. (2.34).

3. Propagation step. At step n, for each determinant $\Phi_J \in S^{(n)}$ loop over all the singly and doubly excited determinants Φ_I:

$$\Phi_I \in \{\hat{a}^a\hat{a}_i\Phi_J, \hat{a}^a\hat{a}^b\hat{a}_j\hat{a}_i\Phi_J\} \tag{2.35}$$

where the indices i, j (a, b) label occupied (virtual) orbitals of Φ_J. For each determinant Φ_I, compute the thresholded spawning amplitude $[A_{IJ}^{(n+1)}(\eta)]$ according to Eq. (2.30) and add it to the wave function coefficient $\tilde{C}_I^{(n)}$:

$$\tilde{C}_I^{(n+1)} \leftarrow \tilde{C}_I^{(n+1)} + A_{IJ}^{(n+1)}(\eta) \tag{2.36}$$

Since the propagation step can be performed independently for each of the determinant in $S^{(n)}$, this section of the PCI algorithm may be easily parallelized by distributing the evaluation of $\tilde{C}_I^{(n+1)}$ over multiple threads/instances.

4. Normalization. The wave function at step $n+1$ is normalized according to

$$C_I^{(n+1)} = \frac{\tilde{C}_I^{(n+1)}}{\|\tilde{C}^{(n+1)}\|_2} \quad \forall\Phi_I \in S^{(n+1)} \tag{2.37}$$

where $\|\tilde{C}^{(n+1)}\|_2$ is the 2-norm of the vector $\tilde{C}^{(n+1)}$.

5. Energy evaluation. The updated wave function coefficients are used to estimate the energy using two approaches. The first is the variational estimator $[E_{\text{var}}^{(n)}]$, which is given by the expectation value of the PCI wave function:

$$E_{\text{var}}^{(n)} = \langle \Omega^{(n)} | \hat{H} | \Omega^{(n)} \rangle = \sum_{IJ} C_I^{(n)} H_{IJ} C_J^{(n)} \tag{2.38}$$

The evaluation of E_{var} scales as $O^2V^2N_{\text{det}}$, where N_{det} is the number of determinants in $S^{(n)}$, therefore it has a computational cost comparable to that of applying $\hat{H}$ without path filtering. Nevertheless, E_{var} is an upper bound to the exact ground state energy and the error is quadratic in the error of the wave function. To speed up the evaluation of E_{var} during the iterative procedure we apply numerical screening to the vector $C_I^{(n)}$.

We also compute the energy via the projective estimator $[E_{\text{proj}}^{(n)}]$, defined as:

$$E_{\text{proj}}^{(n)}(J) = H_{JJ} + \sum_{I(\neq J)} H_{IJ} \frac{C_I^{(n)}}{C_J^{(n)}} \tag{2.39}$$

where $H_{IJ} = \langle \Phi_J | \hat{H} | \Phi_I \rangle$ and Φ_J is chosen to be the determinant with the largest contribution to the wave function, that is, $J = \arg\max_I |C_I^{(n)}|$. E_{proj} may be evaluate with a cost proportional to O^2V^2, where O and V are the number of occupied and virtual orbitals, respectively. However, the projective estimator is not variational and its error is linear in the wave function error. Consequently, the projective estimator is only used to monitor the convergence of the PCI algorithm.

6. Convergence check. Evaluate the approximate energy gradient:

$$\delta E^{(n+1)} = \frac{1}{\gamma}(E^{(n+1)} - E^{(n)}), \tag{2.40}$$

where γ is the convergence factor of the projector generator. If $|\delta E^{(n+1)}|$ is larger then the convergence threshold increase n by one and go to Step 2. Otherwise, the computation is converged and the final variational energy is evaluated including all contributions from the truncated CI space $S^{(n+1)}$.

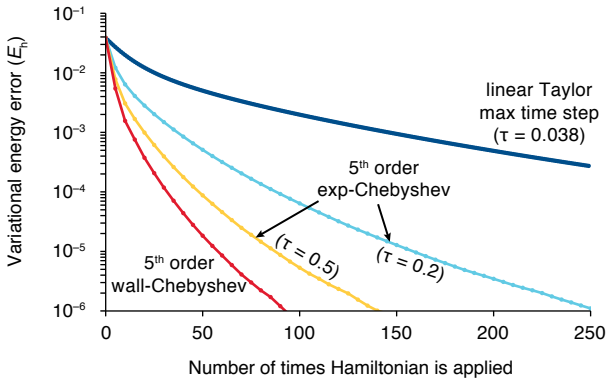

Figure 2.2 Ground state of N_2 at the equilibrium geometry ($r = 2.118$ bohr) computed with the PCI using a spawning threshold $\eta = 1 \times 10^{-5}$ and various projector generators. Difference between the variational energy at a given iteration and the converged energy as a function of the number of times the Hamiltonian is applied. All computations used canonical Hartree–Fock orbitals and the cc-pVDZ basis set. The 1s-like orbitals of nitrogen were excluded from computations of the correlation energy.

The PCI algorithm is implemented in FORTE, a suite of multireference electronic structure methods[86] written as a plugin to the open-source quantum chemistry package PSI4.[87]

2.4 Results

Unless otherwise noted, all the PCI calculations are performed with the 5$^{\text{th}}$-order wall-Chebyshev generator. PCI results obtained with a spawning threshold equal to η are labeled as PCI(η). Preliminary computations showed that the variational estimator [Eq. (2.38)] yields energy errors that are consistently one order of magnitude smaller than those from than the projective estimator [Eq. (2.39)]. Consequently, all results presented in this work are based on the variational energy estimator.

2.4.1 N_2

To investigate the properties of the PCI approach we report computations of the ground state energy of the nitrogen molecule using the cc-pVDZ basis set[88] and freezing the 1s core orbitals. We discuss both the equilibrium ($r = 2.118$ bohr) and

Table 2.2 Comparison of the ground state energy of N_2 computed with the PCI and several wave function approaches using the cc-pVDZ basis at equilibrium and stretched bond lengths (r=2.118 and 4.2 bohr). ΔE is the energy error with respect to FCI computed with the variational estimate. N_{par} is the number of variational parameters, with values in parentheses indicating the number of perturbative parameters. NPE is the non-parallelism error defined by the difference of energy errors between stretched and equilibrium geometries. All PCI computations use canonical restricted Hartree–Fock orbitals. The nitrogen 1s-like orbitals were frozen in all computations of the correlation energies.

Method	$r = 2.118$ bohr		$r = 4.2$ bohr		NPE/mE_{h}
	N_{par}	$\Delta E/E_{\text{h}}$	N_{par}	$\Delta E/E_{\text{h}}$	
MP2	(2,090)	1.56×10^{-2}	(2,090)	-3.07×10^{-1}	−322.275
CISD	2,090	3.65×10^{-2}	2,090	2.64×10^{-1}	227.215
CISDT	60,842	2.59×10^{-2}	60,842	2.41×10^{-1}	215.173
CISDTQ	969,718	2.31×10^{-3}	969,718	5.72×10^{-2}	54.855
CCSD	2,090	1.45×10^{-2}	2,090	4.07×10^{-2}	26.234
CCSD(T)	(58,752)	1.87×10^{-3}	(58,752)	-1.65×10^{-1}	−166.876
MRCISD[a]	···	6.64×10^{-3}	···	6.91×10^{-3}	0.259
MRCCSD[a]	···	1.52×10^{-3}	···	2.25×10^{-3}	0.732
PCI(1×10^{-3})	12,393	2.45×10^{-2}	30,379	2.63×10^{-2}	1.816
PCI(1×10^{-4})	292,858	4.87×10^{-3}	573,665	1.06×10^{-2}	5.709
PCI(5×10^{-5})	532,728	3.08×10^{-3}	1,108,882	6.03×10^{-3}	2.952
PCI(2×10^{-5})	1,264,528	1.57×10^{-3}	2,628,056	2.25×10^{-3}	0.682
PCI(1×10^{-5})	2,703,218	8.76×10^{-4}	4,630,411	9.69×10^{-4}	0.093
PCI(1×10^{-6})	22,855,011	7.30×10^{-5}	32,900,610	8.82×10^{-5}	0.015
PCI(1×10^{-3})+diag[b]	12,393	1.32×10^{-2}	30,379	1.55×10^{-2}	2.276
PCI(1×10^{-4})+diag[b]	292,858	1.51×10^{-3}	573,665	2.68×10^{-3}	1.171
PCI(1×10^{-5})+diag[b]	2,703,218	1.68×10^{-4}	4,630,411	1.82×10^{-4}	0.014
PCI(1×10^{-6})+diag[b]	22,855,011	8.39×10^{-6}	32,900,610	9.12×10^{-6}	0.001
FCI	540,924,024		540,924,024		

[a] MRCISD and MRCCSD data based on a CASSCF($6e$,$6o$) reference wave function were taken from Ref. 25.

[b] The PCI+diag energies are computed by diagonalizing the Hamiltonian in the space of determinants obtained from a converged PCI computation.

stretched ($r = 4.2$ bohr) geometries of N_2.

Figure 3.3 illustrates the difference in efficiency between various generator at the equilibrium geometry. To facilitate the comparison among the various generators, we plot the energy error with respect to the number of times $\hat{H}$ is applied to a state

vector using a spawning threshold equal to 10^{-5}. For the linear generator we select $\tau = 1/R = 0.038\ E_\mathrm{h}^{-1}$, the largest value of τ compatible with the spectral range of $\hat{H}$ [see Eq. (2.17)]. As illustrated in Figure 3.3, the linear generator shows very slow convergence. After 250 steps, the total error is still larger than $10^{-4}\ E_\mathrm{h}$. Projectors based on the exp-Chebyshev generators allow to use larger values of τ and converge more readily. For example, with $\tau = 0.5\ E_\mathrm{h}^{-1}$, the fifth-order exp-Chebyshev projector requires 150 applications of $\hat{H}$ to achieve an error less than $10^{-6}\ E_\mathrm{h}$. The fifth-order wall-Chebyshev generator (which correspond to the limit $\tau \to \infty$) is more efficient than the exp-Chebyshev generators as it can achieve the same level of accuracy with less than 100 applications of $\hat{H}$.

Next, we study the accuracy of the PCI as a function of the spawning threshold (η) and compare it to a selection of single-reference and multireference methods. Table 2.2 reports a comparison of the total error with respect to FCI for the variational energy estimator [Eq. (2.38)]. Additionally, Table 2.2 reports energies for N_2 computed using second-order Møller–Plessett (MP2) perturbation theory, truncated CI with up to quadruple excitations (CISD–CISDTQ), coupled cluster with singles and doubles (CCSD), CCSD with perturbative triples corrections [CCSD(T)], uncontracted multireference CISD (MRCISD), and multireference CCSD (MRCCSD) based on a CASSCF(6e,6o) reference.[25]

From Table 2.2 it can be seen that since the PCI wave function is not biased towards a reference determinant, it can efficiently capture both static and dynamic electron correlation and provide an accurate description of N_2 at both equilibrium and stretched geometries. For example, even with a large spawning threshold ($\eta = 1{\times}10^{-3}$) the PCI yields a non-parallelism error (NPE, defined as the difference in energy error between the equilibrium and stretched geometries) that is of the order of a few mE_h. In contrast, single-reference approaches give NPEs that range from -322 to $+227$ mE_h.

The accuracy of the PCI is effectively tuned by the spawning threshold and can be chosen to match or go beyond that of MRCI and MRCC. For example, for $\eta = 2\times10^{-5}$, the NPE is equal to 0.37 kcal mol^{-1}, which is within chemical accuracy (defined as an error less than 1 kcal mol^{-1}). At the equilibrium geometry the PCI wave function has 1,264,528 determinants, with the Hartree–Fock determinant having a coefficient equal to 0.94. At the stretched geometry, when the coefficient of the Hartree–Fock determinant is only 0.46, this number increases to 2,628,056 determinants to accommodate the multideterminantal character of the wave function. Note that at both geometries the PCI(2×10^{-5}) wave function uses less than 0.5% of the FCI space determinants.

In order to illustrate the importance of the truncation and path-filtering errors, in Table 2.2 we report energies obtained by diagonalizing the Hamiltonian in the PCI determinant space (indicates as PCI+diag). These energies are more accurate than the corresponding PCI values. For example, with $\eta = 1\times10^{-4}$, the NPE for the PCI and PCI+diag are 5.7 and 1.2 mE_h, respectively. The difference between the energy from FCI and PCI+diag represents the truncation error, while the gap between the PCI and PCI+diag energies is the path-filtering error. For large spawning thresholds (e.g. $\eta = 1\times10^{-3}$) the truncation and path-filtering errors contribute equally to the total error. However, as the spawning threshold decreases, path-filtering becomes the dominant source of error. For example, when the spawning threshold is equal to 1×10^{-6}, the path-filtering error contributes to 90% of the total error. In this case, the diagonalization of the PCI space yields energies within 10 μE_h from FCI values, while the nonparallelism error is about 1 μE_h.

To give an idea of the computational cost of the PCI, we note that the N_2 computations at equilibrium geometry with $\eta = 10^{-6}$ ran in 3 hours on 16 threads on a single node (on two Intel Xeon E5-2650 v2 processors) and took 16 iterations to finish. The corresponding computation at the stretched geometry ran in 44 hours

and took 127 iterations. In this example the the wave function contains 33 million determinants and convergence is slowed by the small energy gap between the ground and first excited state.

2.4.2 C_2

To study the performance of PCI on larger basis sets we computed the ground state energy of C_2 at the equilibrium geometry using basis sets that range from double- to quadruple-ζ quality. Table 2.3 collects PCI results obtained using MP2 natural orbitals, together with truncated configuration interaction, coupled cluster, DMRG, and i-FCIQMC results. When possible, computations were reported for the first three basis sets of the cc-pVXZ series (X=D,T,Q, also abbreviated as XZ in the following discussion).[88,92] For the TZ and QZ basis sets the FCI energy cannot be computed, and we take DMRG results from Ref. 31 as a reference. PCI(η) energies are extrapolated to zero spawning threshold by fitting results with $\eta = 1\times10^{-5}$, 5×10^{-6}, and 1×10^{-6} to a quadratic function.

Table 2.3 illustrates how the PCI energy may be systematically converged to the reference FCI/DMRG energy with control over the absolute energy error. For example, with a spawning threshold equal to 10^{-5}, for all basis sets the PCI energy is within 1.3 mE_h from the DMRG energy. While with a spawning threshold equal to 10^{-6}, the error is further reduced to less than 0.2 mE_h in all cases.

When compared to other methods, the cheapest PCI calculations ($\eta = 10^{-4}$) shown in Tab. 2.3 are found to be already more accurate than truncated CI methods up to quadruple excitation and CCSD. Moreover, the PCI selects the most important determinants efficiently and therefore shows a more favorable accuracy/(number of parameters) ratio. For example, the cc-pVQZ PCI($\eta = 10^{-4}$) wave function has about one million determinants, but yields an energy that is more accurate than that of CISDT (3 million determinants) and CISDTQ (200 million determinants). We

Table 2.3 Comparison of the ground state energy of C_2 calculated with the PCI and several wave function approaches using the cc-pVXZ basis set (X = D,T,Q). All PCI computations use MP2 natural orbitals. The carbon 1s-like orbitals were frozen in all calculations. N_{par} indicates the number of variational parameters, with values in parentheses indicating perturbative parameters. All results are shifted by +75 E_{h}.

Method	cc-pVDZ (8e, 26o)		cc-pVTZ (8e, 58o)		cc-pVQZ (8e, 108o)	
	$(E+75)/E_{\text{h}}$	N_{par}	$(E+75)/E_{\text{h}}$	N_{par}	$(E+75)/E_{\text{h}}$	N_{par}
MP2	−0.697 678	(1.43×10^3)	−0.756 562	(8.35×10^3)	−0.777 234	(3.05×10^4)
CISD	−0.663 765	1.43×10^3	−0.711 300	8.35×10^3	−0.726 551	3.05×10^4
CISDT	−0.682 929	3.34×10^4	−0.733 939	4.96×10^5	−0.749 947	3.55×10^6
CISDTQ	−0.721 845	4.11×10^5	−0.777 182	1.51×10^7	−0.794 504	2.09×10^8
CCSD	−0.699 132	1.43×10^3	−0.749 551	8.35×10^3	−0.765 696	3.05×10^4
CCSD(T)	−0.726 697	(3.20×10^4)	−0.783 070	(4.88×10^5)	−0.800 807	(3.52×10^6)
PCI(1×10^{-4})	−0.725 914	1.58×10^5	−0.779 959	5.67×10^5	−0.796 216	1.00×10^6
PCI(5×10^{-5})	−0.727 131	3.09×10^5	−0.781 984	1.27×10^6	−0.798 720	2.40×10^6
PCI(1×10^{-5})	−0.728 292	1.22×10^6	−0.784 133	7.45×10^6	−0.801 450	1.67×10^7
PCI(5×10^{-6})	−0.728 439	2.03×10^6	−0.784 561	1.50×10^7	−0.801 973	3.65×10^7
PCI(1×10^{-6})	−0.728 541	5.56×10^6	−0.784 961	6.79×10^7	−0.802 513	1.99×10^8
PCI(extrapol.)[a]	−0.728 565		−0.785 069		−0.802 665	
DMRG[b,c]	−0.728 556	5.2×10^5	−0.785 054	1.2×10^7	−0.802 671	7.0×10^7
DMRG[d]	···	···	···	···	−0.802 69	···
i-FCIQMC[e,f]	−0.728 7(8)	4.2×10^6	−0.784 9(3)	6.3×10^6	−0.802 5(1)	3.0×10^7
i-SFCIQMC[g,f]	···	···	···	···	−0.802 575	1.6×10^7
FCI[h]	−0.728 556	2.79×10^7	···	2.25×10^{10}	···	3.59×10^{12}

[a] Extrapolated PCI values obtained from a quadratic fitting of the results with $\eta = 10^{-5}$, 5×10^{-6}, and 10^{-6}.

[b] DMRG data taken from Ref. 31. Based on the genetic algorithm ordering and accurate to better than 0.01 mE_{h}.

[c] DMRG number of variational parameters were kindly provided by Guo and Chan[89] for computations with 946, 3234, and 6738 renormalized states using the DZ, TZ, and QZ basis sets, respectively.

[d] DMRG data taken from Ref. 90. Based on the genetic algorithm ordering and accurate to better than 0.01 mE_{h}.

[e] Initiator FCIQMC (i-FCIQMC) data taken from Ref. 60.

[f] For i-FCIQMC and i-SFCIQMC the column labeled N_{par} reports the total number of walkers.

[g] Initiator semi-stochastic FCIQMC (i-SFCIQMC) data taken from Ref. 91.

[h] The number of FCI determinants for the triple- and quadruple-ζ basis sets was estimated as $\binom{N_{\text{orb}}}{N_{\text{el}}/2}^2/N_{\text{irrep}}$, where N_{orb}, N_{el}, and N_{irrep} are the number of orbitals, electrons, and irreps, respectively.

note that PCI results surpass the accuracy of the CCSD(T) method with a spawning threshold of 1×10^{-5}.

The PCI shows a favorable scaling with respect to the size of basis set. When

the basis set is enlarged from DZ to QZ, the number of orbitals involved in calculation grow from 26 to 108 and the corresponding FCI space increased ca. 10^5 folds. The corresponding growth of PCI determinants with respect to the number of virtual orbitals (n_{virt}) is found to be linear, with increase of only 14 and 36 times when $\eta = 1\times10^{-5}$ and 1×10^{-6}, respectively. In comparison, truncated CI and CC schemes scale as n_{virt}^2, n_{virt}^3, and n_{virt}^4 for the SD, SDT, and SDTQ truncation schemes, respectively. Consequently, the cost of these computations grows by a factor 21, 106, and 509 when going from the DZ to the QZ basis set. FCIQMC also shows very good scaling with respect to virtual orbitals, with an increase of only about 7 times the number of walkers. In the case of DMRG, assuming that the number of renormalized states (M) required to obtain a given level of accuracy scales as $n_{\mathrm{occ}}n_{\mathrm{vir}}$,[31] then the number of variational parameters scales as $n_{\mathrm{orb}}M^2 \approx n_{\mathrm{vir}}^3$.

We would like to point out that the QZ PCI calculation with spawning threshold 1×10^{-6} (200 million determinants) ran on a single node. This computation is two orders of magnitude larger than the largest selected CI calculations reported in the literature (4 million determinants),[93] which was performed with a parallel algorithm on a distributed memory architecture with 32–256 nodes. As a comparison, typical FCIQMC computations may employ up to 2–7 billion walkers.[58]

2.4.3 Size consistency and molecular orbital comparison

Lastly, we investigate the degree to which the PCI wave function lacks size consistency, and how different type of molecular orbitals affect its performance. In our tests we have considered a monomer consisting of Be and He separated by 2.5 Å. In one set of computations two monomers are arranged in a $D_{\infty\mathrm{h}}$ geometry, so that the orbitals are delocalized over the two fragments. Starting from the $D_{\infty\mathrm{h}}$ geometry, we obtained a $C_{\infty\mathrm{v}}$ structure in which the Be–He distances of the monomers are shortened and lengthened by $\pm10^{-5}$ Å, respectively. This geometric change leads to

Table 2.4 Analysis of the size consistency error (ΔE) of truncated CI methods and the PCI for the $(\text{Be–He})_2$ system. All results used the cc-pVDZ and STO-3G basis sets for Be and He, respectively. The Be–He bond distance in the monomer is equal to 2.5 Å. The column labeled N_{det} reports the size of each CI space.

	Be–He ($6e$,$15o$)		He–Be $\cdots$ Be–He ($12e$,$30o$)		
Method	Energy/E_{h}	N_{det}	Energy/E_{h}	N_{det}	ΔE/mE_{h}
RHF	−17.374 136	1	−34.748 272	1	0.000
FCI	−17.420 556	51,853	−34.841 113	4.41×10^{10}	0.000
CISD	−17.420 420	523	−34.833 525	4,405	7.316
CISDT	−17.420 484	4,257	−34.833 664	170,685	7.305
CISDTQ	−17.420 556	17,973	−34.841 084	3,833,121	0.029
		Delocalized canonical Hartree–Fock orbitals			
PCI(1×10^{-4})	−17.420 537	1,424	−34.840 544	34,164	0.529
PCI(1×10^{-5})	−17.420 556	5,311	−34.841 066	255,342	0.045
PCI(1×10^{-6})	−17.420 556	15,465	−34.841 108	1,558,745	0.005
		Delocalized MP2 natural orbitals			
PCI(1×10^{-4})	−17.420 547	1,138	−34.840 924	23,979	0.169
PCI(1×10^{-5})	−17.420 556	5,077	−34.841 088	163,469	0.024
PCI(1×10^{-6})	−17.420 556	14,801	−34.841 110	1,185,988	0.002
		Localized canonical Hartree–Fock orbitals			
PCI(1×10^{-4})	−17.420 537	1,424	−34.840 981	9,746	0.092
PCI(1×10^{-5})	−17.420 556	5,311	−34.841 104	60,740	0.007
PCI(1×10^{-6})	−17.420 556	15,465	−34.841 112	337,662	0.001
		Localized MP2 natural orbitals			
PCI(1×10^{-4})	−17.420 547	1,138	−34.841 064	5,910	0.029
PCI(1×10^{-5})	−17.420 556	5,077	−34.841 109	41,580	0.003
PCI(1×10^{-6})	−17.420 556	14,801	−34.841 113	247,364	0.000

localization of the molecular orbitals on one of the two monomers. For both localized and delocalized molecular orbitals we considered canonical Hartree–Fock orbitals and MP2 natural orbitals.

Table 2.4 reports the size consistency error (ΔE) for a pair of noninteracting Be–He units as a function of the spawning threshold, where ΔE is defined as the energy difference between a non-interacting dimer (Be–He$\cdots$Be–He) and twice the energy of

the monomer (Be–He):

$$\Delta E = E(\text{Be–He}\cdots\text{Be–He}) - 2E(\text{Be–He}). \tag{2.41}$$

As expected, the PCI energy is not size consistent, but a comparison with truncated CI methods shows that the corresponding error is significantly smaller in the case of PCI and can be effectively controlled via the spawning threshold. In comparison to CISDTQ, which requires 3,833,121 determinants for the dimer computation, the PCI(10^{-6}) with canonical orbitals requires only 1,558,745 determinants and leads to a size consistency error that is six times smaller. When delocalized orbitals are used, going from canonical Hartree–Fock orbitals to MP2 natural orbitals leads to a reduction of the size consistency error of the PCI by a factor of ca. two. At the same time, the use of MP2 natural orbitals also slightly reduces the number of determinants.

Upon localization of the orbitals we observe a significant reduction of the size consistency error and wave function size. For example, localization of the canonical Hartree–Fock orbitals reduces the PCI(10^{-6}) size consistency error and number of determinants by a factor of five. The best performance is obtained by combining localization with MP2 natural orbitals. In this case the overall size of the PCI wave function is reduced by a factor of 6 and the size consistency error is less than 0.001 mE_h. This comparison shows that the use of optimized orbitals can significantly reduce the computational cost of the PCI and the magnitude of the size consistency error.

2.5 Summary and conclusions

In this paper, we introduced a general projector diagonalization approach and combined it with path filtering to create a novel projector configuration interaction (PCI) method. Given an operator (matrix) $\hat{H}$, the projector diagonalization method

seeks to obtain one of the eigenvectors of $\hat{H}$ via repeated application of the projector generator $g(\hat{H})$ onto a trial vector. The projector generator is a matrix function designed to amplify the coefficient of one of the eigenvectors. The focus of this work is on polynomial projector generators derived from the imaginary-time propagator, which project the trial wave function onto the ground electronic state. To improve the performance of a Taylor expansion of the imaginary-time propagator, we discuss its approximation in terms of Chebyshev polynomials, and propose a new generator (wall-Chebyshev) with superior convergence properties.

The PCI optimization process is formulated in terms of a dynamics in which each application of the projector generator is equivalent to a spawning process. In this process, each determinant spawns singly and doubly excited determinants with a given spawning amplitude. In order to truncate the determinant space explored by the PCI algorithm, we consider a path filtering approach in which spawning amplitudes are truncated according to a user-provided *spawning threshold* (η). Path filtering applied at each step of the projector diagonalization controls the size of the PCI wave function and the accuracy of the energy by selecting important determinants that contribute the most to a given eigenstate. In this respect, the PCI method is similar to selected CI, with the important difference that the former also approximates the diagonalization process to increase computational efficiency.

Since the PCI is not biased towards any reference determinants, it can describe dynamic and static electron correlation equally well. This point is illustrated with computations of the energy of N_2 at equilibrium and stretched geometries. As shown in Table 2.2, the PCI($\eta = 2 \times 10^{-5}$) can predict the energy difference between these two geometries with a non-parallelism error equal to 0.682 mE_h (0.43 kcal mol^{-1}) using only a small fraction of the Hilbert space of determinants (less than 0.5%). Additionally, we compare PCI with DMRG and FCIQMC using the carbon dimer as a challenging benchmark. With a spawning threshold equal to 10^{-6}, the PCI can

match the accuracy of FCIQMC results, while PCI extrapolated to the limit $\eta \to 0$ yields total energies that are within 0.01 mE_h of DMRG reference data. We have also analyzed the extent of size consistency errors in PCI computations. This error is effectively controlled by the spawning threshold and may be further reduced by using a localized basis.

One of the interesting features of the PCI algorithm is that it can be expressed as a series of update steps in which spawning amplitudes for different determinants can be computed independently with no communication. Moreover, the linear and wall-Chebyshev generators only require storage of two vectors of the size of the CI space. These two features make the PCI amenable to computations with large CI spaces containing 10^7–10^8 determinants. A parallel implementation of the PCI for distributed-memory machines would allow to further increase the size of the CI space. Both the PCI and FCIQMC use a sparse representation of the FCI wave function and present similar challenges when implemented on distributed memory architectures. Therefore, the recent successful implementation of a parallel FCIQMC code[64] suggests that it should be possible to also produce an efficient parallel implementation of the PCI.

Currently, the PCI algorithm has been formulated to optimize the ground state. However, several strategies may be explored to extend the PCI to electronic excited states. One possibility is a state-specific approach in which excited states are optimized individually, while maintaining orthogonality with lower energy states. An alternative is a multistate version of the PCI in which several states are optimized simultaneously.[94] Since the convergence of the PCI depends on ratio of the first excitation energy and the spectral radius, $(E_1 - E_0)/R$, a multistate version of the PCI would also be helpful to speed up convergence to the ground state in cases when this ratio is small. Another interesting venue to explore is to use the PCI approach to target the density matrix at finite temperatures[95,96] or to compute approximate

spectral densities of systems with a dense manifold of low-energy electronic states.[97]

Appendices

2.A Path filtering for polynomial generators

In this appendix we report a generalization of the path filtering approach for polynomial generators $g(x)$ of order m that have m real roots $(s_i, i = 1, \ldots, m)$. In this case, $g(x)$ can be written as:

$$g(x) = \prod_{i=1}^{m} \frac{x - s_i}{E_0 - s_i} \tag{2.A.1}$$

and $g(\hat{H})\,|\Omega^{(n)}\rangle$ may be computed by repeated application of a linear generator with modified shift to which path filtering is applied in all intermediate steps. It it important to point out that the path-filtering algorithm presented here gives results that are consistent with those of the algorithm outlined in the paper, which applies only to linear generators.

For convenience, we start by defining a series of normalized trial wave functions

$$|\Omega^{(n+1,i)}\rangle = \sum_{I \in S^{(n,i)}} C_I^{(n+1,i)}\,|\Phi_I\rangle \tag{2.A.2}$$

expanded over the space $S^{(n,i)}$. The coefficient vector for $i = 0$ is given by:

$$C_I^{(n+1,0)} = C_I^{(n)} \tag{2.A.3}$$

and spans the space $S^{(n+1,0)} = S^{(n)}$.

The coefficients $C_I^{(n+1,i)}$ for $i > 0$ are obtained from the unnormalized wave function coefficients $[\tilde{C}_I^{(n+1,i)}]$:

$$C_I^{(n+1,i)} = \frac{\tilde{C}_I^{(n+1,i)}}{\|\tilde{C}^{(n+1,i)}\|_2} \tag{2.A.4}$$

which are obtained as the sum:

$$\tilde{C}_I^{(n+1,i)} = \sum_{\Phi_J \in S^{(n+1,i)}} A_{IJ}^{(n+1,i)}(\eta) \tag{2.A.5}$$

The path-filtered spawning amplitudes $[A_{IJ}^{(n,i)}(\eta)]$ that enter into Eq. (2.A.5) are obtained from the untruncated amplitudes $[A_{IJ}^{(n,i)}]$:

$$A_{IJ}^{(n,i)} = \langle \Phi_I | \, \hat{H} - s_i \, | \Phi_J \rangle \, C_J^{(n,i-1)} \tag{2.A.6}$$

and truncated according to:

$$A_{IJ}^{(n,i)}(\eta) = \begin{cases} A_{II}^{(n,i)} & \text{if } I = J \\ A_{IJ}^{(n,i)} \Theta(|A_{IJ}^{(n,i)}| - \eta) & \text{if } I \neq J \end{cases} \tag{2.A.7}$$

The normalized coefficients are evaluated recursively for $i = 1, 2, \ldots, m$ following Eqs. (2.A.4)–(2.A.7). Finally, the coefficients for the updated wave function are given by:

$$C_I^{(n+1)} = C_I^{(n+1,m)}. \tag{2.A.8}$$

Note that to evaluate the application of factorizable generators with real zeros onto a trial vector requires storage of two vectors. Thus, require the same amount of memory as the linear projector.

Acknowledgments

The authors are grateful to Philip Shushkov and Michele Benzi for valuable discussions concerning the theory of projectors. The authors would also like to thank Sheng Guo and Garnet Chan for providing the number of wave function parameters for the DMRG computations on the carbon dimer.

This work was supported by start-up funds provided by Emory University.

Bibliography

[1] Sherrill, C. D.; Schaefer III, H. F. *Adv. Quant. Chem.* **1999**, *34*, 143–269.

[2] Rossi, E.; Bendazzoli, G. L.; Evangelisti, S.; Maynau, D. *Chem. Phys. Lett.* **1999**, *310*, 530–536.

[3] Knowles, P. J.; Handy, N. C. *J. Chem. Phys.* **1989**, *91*, 2396–2398.

[4] Bartlett, R. J.; Musiał, M. *Rev. Mod. Phys.* **2007**, *79*, 291.

[5] Bartlett, R. J. *Annu. Rev. Phys. Chem.* **1981**, *32*, 359–401.

[6] Dagotto, E. *Science* **2005**, *309*, 257–262.

[7] Buenker, R. J.; Peyerimhoff, S. D. *Theor. Chim. Acta* **1974**, *35*, 33–58.

[8] Buenker, R. J.; Peyerimhoff, S. D. *Theor. Chim. Acta* **1975**, *39*, 217–228.

[9] Huron, B.; Malrieu, J. P.; Rancurel, P. *J. Chem. Phys.* **1973**, *58*, 5745–5759.

[10] Evangelisti, S.; Daudey, J.-P.; Malrieu, J.-P. *Chem. Phys.* **1983**, *75*, 91–102.

[11] Meller, J.; Heully, J.; Malrieu, J. *Chem. Phys. Lett.* **1994**, *218*, 276–282.

[12] Bender, C. F.; Davidson, E. R. *Phys. Rev.* **1969**, *183*, 23.

[13] Langhoff, S. R.; Elbert, S. T.; Davidson, E. R. *Int. J. Quant. Chem.* **1973**, *7*, 999–1019.

[14] Angeli, C.; Cimiraglia, R.; Persico, M.; Toniolo, A. *Theor. Chem. Acc.* **1997**, *98*, 57–63.

[15] Angeli, C.; Persico, M. *Theor. Chem. Acc.* **1997**, *98*, 117–128.

[16] Angeli, C.; Cimiraglia, R.; Persico, M. *Theor. Chem. Acc.* **1998**, *100*, 324–328.

[17] Olsen, J.; Roos, B. O.; Jørgensen, P.; Jensen, H. J. A. *J. Chem. Phys.* **1988**, *89*, 2185–2192.

[18] Ivanic, J. *J. Chem. Phys.* **2003**, *119*, 9364.

[19] Ma, D.; Li Manni, G.; Gagliardi, L. *J. Chem. Phys.* **2011**, *135*, 044128.

[20] Li Manni, G.; Ma, D.; Aquilante, F.; Olsen, J.; Gagliardi, L. *J. Chem. Theory Comput.* **2013**, *9*, 3375–3384.

[21] Schriber, J. B.; Evangelista, F. A. *J. Chem. Phys.* **2016**, *144*, 161106.

[22] White, S. R. *Phys. Rev. Lett.* **1992**, *69*, 2863.

[23] White, S. R.; Martin, R. L. *J. Chem. Phys.* **1999**, *110*, 4127–4130.

[24] Chan, G. K.-L.; Head-Gordon, M. *J. Chem. Phys.* **2002**, *116*, 4462–4476.

[25] Chan, G. K.-L.; Kállay, M.; Gauss, J. *J. Chem. Phys.* **2004**, *121*, 6110–6.

[26] Kurashige, Y.; Yanai, T. *J. Chem. Phys.* **2009**, *130*, 234114.

[27] Mizukami, W.; Kurashige, Y.; Yanai, T. *J. Chem. Theory Comput.* **2012**, *9*, 401–407.

[28] Kurashige, Y.; Yanai, T. *Bull. Chem. Soc. Japan* **2014**, *87*, 1071–1073.

[29] Kurashige, Y.; Chan, G. K.-L.; Yanai, T. *Nature Chem.* **2013**, *5*, 660–666.

[30] Booth, G. H.; Chan, G. K.-L. *J. Chem. Phys.* **2012**, *137*, 191102.

[31] Olivares-Amaya, R.; Hu, W.; Nakatani, N.; Sharma, S.; Yang, J.; Chan, G. K. *J. Chem. Phys.* **2015**, *142*, 034102.

[32] Vidal, G. *Phys. Rev. Lett.* **2007**, *99*, 220405.

[33] Nakatani, N.; Chan, G. K.-L. *J. Chem. Phys.* **2013**, *138*, 134113.

[34] Nakano, H.; Hirao, K. *Chem. Phys. Lett.* **2000**, *317*, 90–96.

[35] Parker, S. M.; Seideman, T.; Ratner, M. A.; Shiozaki, T. *J. Chem. Phys.* **2013**, *139*, 021108.

[36] Parker, S. M.; Shiozaki, T. *J. Chem. Phys.* **2014**, *141*, 211102.

[37] Murg, V.; Verstraete, F.; Schneider, R.; Nagy, P. R.; Legeza, Ö. *J. Chem. Theory Comput.* **2015**,

[38] Szalay, S.; Pfeffer, M.; Murg, V.; Barcza, G.; Verstraete, F.; Schneider, R.; Legeza, Ö. *Int. J. Quantum Chem.* **2015**, *115*, 1342–1391.

[39] Böhm, K.-H.; Auer, A. A.; Espig, M. *J. Chem. Phys.* **2016**, *144*, 244102.

[40] Mayhall, N. J.; Horn, P. R.; Sundstrom, E. J.; Head-Gordon, M. *Phys. Chem. Chem. Phys.* **2014**, *16*, 22694–22705.

[41] Small, D. W.; Lawler, K. V.; Head-Gordon, M. *J. Chem. Theory Comput.* **2014**, *10*, 2027–2040.

[42] Stein, T.; Henderson, T. M.; Scuseria, G. E. *J. Chem. Phys.* **2014**, *140*, 214113.

[43] Bulik, I. W.; Henderson, T. M.; Scuseria, G. E. *J. Chem. Theory Comput.* **2015**, *11*, 3171–3179.

[44] Tsuchimochi, T.; Scuseria, G. E. *J. Chem. Phys.* **2009**, *131*, 121102.

[45] Jiménez-Hoyos, C. A.; Henderson, T. M.; Tsuchimochi, T.; Scuseria, G. E. *J. Chem. Phys.* **2012**, *136*, 164109.

[46] Rodríguez-Guzmán, R.; Jiménez-Hoyos, C. A.; Schutski, R.; Scuseria, G. E. *Phys. Rev. B* **2013**, *87*, 235129.

[47] Greer, J. C. *J. Chem. Phys.* **1995**, *103*, 1821.

[48] Greer, J. C. *J. Comput. Phys.* **1998**, *146*, 181–202.

[49] Coe, J.; Murphy, P.; Paterson, M. *Chem. Phys. Lett.* **2014**, *604*, 46–52.

[50] Coe, J. P.; Paterson, M. J. *J. Chem. Phys.* **2013**, *139*, 154103.

[51] Coe, J.; Paterson, M. *J. Chem. Phys.* **2012**, *137*, 204108.

[52] Gyorffy, W.; Bartlett, R. J.; Greer, J. C. *J. Chem. Phys.* **2008**, *129*, 064103.

[53] Sugiyama, G.; Koonin, S. *Ann. Phys.* **1986**, *168*, 1–26.

[54] Honma, M.; Mizusaki, T.; Otsuka, T. *Phys. Rev. Lett.* **1995**, *75*, 1284.

[55] Al-Saidi, W.; Zhang, S.; Krakauer, H. *J. Chem. Phys.* **2006**, *124*, 224101.

[56] Ohtsuka, Y.; Nagase, S. *Chem. Phys. Lett.* **2008**, *463*, 431–434.

[57] Shi, H.; Zhang, S. *Phys. Rev. B* **2013**, *88*, 125132.

[58] Booth, G. H.; Thom, A. J. W.; Alavi, A. *J. Chem. Phys.* **2009**, *131*, 054106.

[59] Cleland, D.; Booth, G. H.; Alavi, A. *J. Chem. Phys.* **2010**, *132*, 041103.

[60] Booth, G. H.; Cleland, D.; Thom, A. J. W.; Alavi, A. *J. Chem. Phys.* **2011**, *135*, 084104.

[61] Cleland, D. M.; Booth, G. H.; Alavi, A. *J. Chem. Phys.* **2011**, *134*, 024112.

[62] Cleland, D.; Booth, G. H.; Overy, C.; Alavi, A. *J. Chem. Theory Comput.* **2012**, *8*, 4138–4152.

[63] Thomas, R. E.; Overy, C.; Booth, G. H.; Alavi, A. *J. Chem. Theory Comput.* **2014**, *10*, 1915–1922.

[64] Booth, G. H.; Smart, S. D.; Alavi, A. *Mol. Phys.* **2014**, *112*, 1855–1869.

[65] Imada, M.; Kashima, T. *J. Phys. Soc. Jpn.* **2000**, *69*, 2723–2726.

[66] Imai, Y.; Otsuka, Y.; Imada, M. *J. Phys. Condens. Matter* **2007**, *19*, 365230.

[67] McClean, J. R.; Aspuru-Guzik, A. *RSC Adv.* **2015**, *5*, 102277–102283.

[68] Petruzielo, F.; Holmes, A.; Changlani, H. J.; Nightingale, M.; Umrigar, C. *Phys. Rev. Lett.* **2012**, *109*, 230201.

[69] Blunt, N. S.; Smart, S. D.; Kersten, J. A.; Spencer, J. S.; Booth, G. H.; Alavi, A. *J. Chem. Phys.* **2015**, *142*, 184107.

[70] Umrigar, C. *J. Chem. Phys.* **2015**, *143*, 164105.

[71] Tubman, N. M.; Lee, J.; Takeshita, T. Y.; Head-Gordon, M.; Whaley, K. B. *arXiv:1603.02686* **2016**,

[72] Kosloff, R.; Tal-Ezer, H. *Chem. Phys. Lett.* **1986**, *127*, 223–230.

[73] Zhu, W.; Huang, Y.; Kouri, D.; Chandler, C.; Hoffman, D. K. *Chem. Phys. Lett.* **1994**, *217*, 73–79.

[74] Kouri, D. J.; Zhu, W.; Parker, G. A.; Hoffman, D. K. *Chem. Phys. Lett.* **1995**, *238*, 395–403.

[75] Parker, G. A.; Zhu, W.; Huang, Y.; Hoffman, D. K.; Kouri, D. J. *Comput. Phys. Commun.* **1996**, *96*, 27–35.

[76] Chen, R.; Guo, H. *Comput. Phys. Commun.* **1999**, *119*, 19–31.

[77] Boyd, J. P. *Chebyshev and Fourier spectral methods*; Dover Publications, Inc.: Mineola, New York, USA, 2001.

[78] Horn, D.; Weinstein, M. *Phys. Rev. D* **1984**, *30*, 1256.

[79] Sim, E.; Makri, N. *Comput. Phys. Commun.* **1997**, *99*, 335–354.

[80] Sim, E.; Makri, N. *J. Phys. Chem. B* **1997**, *101*, 5446–5458.

[81] Makri, N. *Annu. Rev. Phys. Chem.* **1999**, *50*, 167–191.

[82] Lambert, R.; Makri, N. *J. Chem. Phys.* **2012**, *137*, 22A553.

[83] Amos, D. E. *Math. Comp.* **1974**, *28*, 239–251.

[84] Holmes, A. A.; Changlani, H. J.; Umrigar, C. J. *J. Chem. Theory Comput.* **2016**, *12*, 1561–71.

[85] Holmes, A. A.; Tubman, N. M.; Umrigar, C. J. *J. Chem. Theory Comput.* **2016,** DOI: 10.1021/acs.jctc.6b00407,

[86] Forte, a suite of quantum chemistry methods for strongly correlated electrons. For current version see https://github.com/evangelistalab/forte, 2016.

[87] Turney, J. M. et al. *WIREs: Comput. Mol. Sci.* **2012**, *2*, 556–565.

[88] Dunning, T. H. *J. Chem. Phys.* **1989**, *90*, 1007.

[89] Guo, S.; Chan, G. K.-L. (personal communication, 2016).

[90] Sharma, S. *J. Chem. Phys.* **2015**, *142*, 024107.

[91] Blunt, N. S.; Smart, S. D.; Booth, G. H.; Alavi, A. *J. Chem. Phys.* **2015**, *143*, 134117.

[92] Kendall, R. A.; Dunning Jr, T. H.; Harrison, R. J. *J. Chem. Phys.* **1992**, *96*, 6796–6806.

[93] Stampfuss, P.; Wenzel, W. *J. Chem. Phys.* **2005**, *122*, 024110.

[94] Ten-no, S. *J. Chem. Phys.* **2013**, *138*, 164126.

[95] Blunt, N. S.; Rogers, T. W.; Spencer, J. S.; Foulkes, W. M. C. *Phys. Rev. B* **2014**, *89*, 245124.

[96] Malone, F. D.; Blunt, N. S.; Shepherd, J. J.; Lee, D. K. K.; Spencer, J. S.; Foulkes, W. M. C. *J. Chem. Phys.* **2015**, *143*, 044116.

[97] Lin, L.; Saad, Y.; Yang, C. *SIAM Rev.* **2016**, *58*, 34–65.

Chapter 3 Hermitian projected configuration interaction method: Filtering the most important determinant couplings

Chapter Abstract

The projector configuration interaction (PCI) method has been recently proposed as a robust and deterministic alternative to stochastic full configuration interaction (FCI) methods for application to strongly correlated electrons [T. Zhang and F. A. Evangelista, *J. Chem. Theory Comput.* **12**, 4326 (2016)]. However, the current polynomial projection scheme is not optimal. In order to obtain more accurate results, we propose an Hermitian version of the PCI. Meanwhile, the convergence is accelerated by combining the PCI path filtering with the Davidson–Liu method. With these improvements, the PCI non-parallelism error is halved and three times faster convergence to the ground state is observed for the N_2 dissociation potential energy curve. We also discuss the connection between heat-bath CI and PCI methods, and demonstrate that PCI is able to compute more accurate wave function with significantly lower computational cost. In computing the ground state energy of Cr_2, we achieved a result within 2 kcal mol^{-1} error from the reference density matrix renormalization group (DMRG) energy by extrapolating the spawning threshold to zero. These recent developments improve the accuracy and efficiency of the PCI and extend the applicability to more complicated systems.

3.1 Introduction

In principle, the full configuration interaction (FCI) method can provide accurate energies and wave functions by an exact diagonalization of the Hamiltonian including

all the determinants in the Hilbert space.[1] However, this method is prohibitively expensive even for moderate size chemical systems as the total number of determinants grows combinatorially with respect to the number of electrons and basis functions.[2] One straightforward approach to reducing the cost of FCI is to exploit the sparsity of the FCI Hamiltonian or wave function.

Selected configuration interaction (SCI) methods[3–36] seek to find important subsets of determinants that can represent the wave functions within acceptable error. Such important determinant subspaces are usually generated iteratively by growing the space of determinants according to an importance criterion. A variety of criteria have been reported, such as perturbative analysis,[12] energy lowering to the current subspace[21,22] and expected coefficient magnitude.[7,13] However, because all the couplings between determinants (Hamiltonian matrix elements) in the selected subset need to be evaluated, the diagonalization step becomes the bottleneck for spaces containing more than 10^7 determinants.[37]

In contrast to selected CI methods where all the couplings need to be evaluated, the FCIQMC method samples the determinant Hilbert space by walkers and the determinant couplings using the walker spawning process.[38–45] This method applies the linearized imaginary-time projector to an initial guess of the wave function,

$$|\Psi\rangle = \lim_{\beta\to\infty} \exp\left(-\beta(\hat{H} - E_0)\right)|\Omega\rangle \approx \lim_{k\to\infty} \left(1 - \tau(\hat{H} - E_0)\right)^k |\Omega\rangle\,, \tag{3.1}$$

where $|\Psi\rangle$ and $|\Omega\rangle$ are the result and initial guess of wave function, β is the imaginary time scale, $\hat{H}$ is the hamiltonian, E_0 is the ground state energy and τ is a imaginary time step. In the FCIQMC method, only one determinant coupling need to be evaluated for each walker at each step, which significantly reduced the computational cost to diagonalize the Hilbert space. However, to accurately represent the wave function, a large numbers of walkers and iterations are required to overcome the "sign problem" and decrease statistical errors. Besides, the linearized imaginary-time projector in the FCIQMC converges slowly, in that a small imaginary time step is required to control

the energy fluctuation.

The success in the application of path filtering to evaluate path integral suggest that high accuracy can be achieved with path integral through only the most important paths.[46–49] The FCIQMC method can be also interpreted as a path-integral over imaginary-time, where the paths (determinant couplings) are sampled rather than selected deterministically.

Inspired by FCIQMC and path filtering, in a recently published paper, we introduced a projector CI (PCI) method.[50] The PCI can be interpreted as a deterministic alternative to the FCIQMC, with two major modifications: 1) stochastic propagation is replaced by a deterministic path-filtering projection scheme, and 2) imaginary-time propagation is replaced by a much faster polynomial projection scheme.

In PCI, path filtering significantly reduces the cost of deterministic projection by considering only the most important subset of determinant couplings in the imaginary time propagator. In order to evaluate the importance of a determinant coupling, the probability formula for walker spawning in FCIQMC is adapted to a deterministic criterion, which also coincides the criteria for important determinants in the Heat-Bath CI method.[17] However, as we will show, this criterion spoils the Hermitian character of the approximated Hamiltonian in both the original PCI and initiator FCIQMC methods, which potentially decreases the accuracy of the resulting wave functions and energies.

This non-Hermitian property also prevented us from applying the standard Hermitian matrix diagonalization algorithm, Davidson–Liu method[51,52] to the PCI method. To overcome the slow convergence of the linearized imaginary-time projection scheme in FCIQMC, we created the wall-Chebyshev polynomial projection approach.[50] Although this type of projector is proven to converge significantly faster than a linear propagation, PCI is still a linear convergent method. The convergence is even slower when the first excitation energy of the system is small.

This chapter is organized in this way: In the theory section, we first introduce the concept of determinant coupling space. The PCI algorithm is then reviewed. Next, we analyze the error in the PCI energy and propose a Hermitian version of PCI algorithm. What follows is an implementation section on the details of Davidson–Liu algorithm in PCI. In the result and discussion section, we begin with showing the improved accuracy of Hermitian PCI by computing the N_2 dissociation curve. It is followed by a convergence comparison between the Davidson–Liu and the polynomial projection methods. We then demonstrate that PCI is more efficient than the selected CI methods. Finally, we benchmark the PCI on the Cr_2 ground state energy with threshold extrapolation.

3.2 Theory

3.2.1 Introducing determinant coupling space

Configuration interaction methods are based on representing the wave function as a linear combination of a set of determinants,

$$|\Omega\rangle = \sum_{\Phi_J \in S} C_J \, |\Phi_J\rangle \,, \tag{3.2}$$

where $|\Omega\rangle$ is an arbitrary normalized wave function, S is a space containing a set of determinants, and $|\Phi_J\rangle$ and C_J are a Slater determinant and its corresponding coefficient.

In order to solve for the coefficients $\{C_J\}$, a Hamiltonian matrix $\mathbf{H}$ can be constructed with element $H_{IJ} = \langle \Phi_I | \, \hat{H} \, | \Phi_J \rangle$, where Φ_I and Φ_J are determinants in S. The corresponding eigenvector of the lowest eigenvalue is the best approximation to the ground state wave function within CI space S.

In order to minimize the number of determinants in S without introducing large error to the results, selected CI methods seeks to include only the most important

determinants in the CI space. Here, we can define the determinant efficiency as:

$$\mathrm{Eff}_S = \frac{E_{\mathrm{corr},S}}{E_{\mathrm{corr,FCI}}} / \frac{|S|}{|S_{\mathrm{FCI}}|}, \tag{3.3}$$

where $E_{\mathrm{corr},S}$ and $E_{\mathrm{corr,FCI}}$ are the correlation energy recovered by CI space S and the full CI, and $|S|$ and $|S_{\mathrm{FCI}}|$ are the number of determinants in S and full CI space S_{FCI}. A selected CI method is more determinantally efficient if it can recover more correlation energy with the same number of determinants.

However, in order to compute the eigen wave function, the most computation cost goes to compute the σ vectors from a trial wave function:

$$\sigma = \hat{H}_S \mathbf{C}, \tag{3.4}$$

or for each $\Phi_I \in S$,

$$\sigma_I = \sum_{\Phi_J \in S} \langle \Phi_I | \hat{H} | \Phi_J \rangle C_J, \tag{3.5}$$

where all the non-zero couplings ($\langle \Phi_I | \hat{H} | \Phi_J \rangle$) between distinct determinants in S need to be computed. Since the contribution $\Phi_I \leftarrow \Phi_J$ and $\Phi_J \leftarrow \Phi_I$ are generally computed separetely, we can define a *determinant coupling space* X containing all the directed couplings $\Phi_I \leftarrow \Phi_J$ ($\Phi_I \neq \Phi_J$) that must be evaluated. In a directed coupling $\Phi_I \leftarrow \Phi_J$, we call the left-hand side Φ_I is the determinant "coupled to" and right-hand side Φ_J is the one "coupled from". For any coupling space X, there exist a corresponding Hamiltonian $\hat{H}_X$ with elements

$$\hat{H}_X = \{H_{X,IJ}\} = \begin{cases} H_{IJ} & I = J \text{ or } \Phi_I \leftarrow \Phi_J \in X \\ 0 & \Phi_I \leftarrow \Phi_J \notin X, \end{cases} \tag{3.6}$$

so that the computational time of one Hamiltonian application $t_{\hat{H}_X}$ is proportional to the size of the coupling space,

$$t_{\hat{H}_X} \propto |X|, \tag{3.7}$$

where $|X|$ is the number of determinant couplings in X. Note here that the time for diagonal contributions $\Phi_J \leftarrow \Phi_J$ is ignored in Eq. (3.7) since $|X| \gg |S|$.

The Hamiltonian $\hat{H}_X$ generated by a coupling space X may not be symmetric if the directed couplings $\Phi_I \leftarrow \Phi_J$ and $\Phi_J \leftarrow \Phi_I$ do not exist in X simultaneously. Thus, we say that a directed coupling $\Phi_I \leftarrow \Phi_J$ is paired in coupling space X if $\Phi_J \leftarrow \Phi_I \in X$ and $\Phi_I \leftarrow \Phi_J \in X$. And a coupling space is symmetric if all the couplings in the space are paired.

In selected CI methods,[7] a CI space S determines a symmetric coupling space X,

$$X_S = \{\Phi_I \leftarrow \Phi_J \ : \ \Phi_I, \Phi_J \in S\}, \tag{3.8}$$

where all the non-trivial couplings between determinants in S are included. By non-trivial we mean that the coupling is not apparently zero because of the determinants are differed by more than two spin orbitals or are in different symmetry. Note here that conditions $\Phi_I \neq \Phi_J$ is natural to the definition of coupling space, so to be brief will not appear in the description of coupling space in this paper.

Conversely, we can define two determinant spaces out of a coupling space X. We define the function LDETS (short for left determinant space),

$$\mathrm{LDETS}(X) = \{\Phi_I \ : \ ^{\exists}\Phi_I \leftarrow \Phi_J \in X\}, \tag{3.9}$$

to generate a determinant space containing all the determinants that is "coupled to" appear in X. Meanwhile, we also define the function RDETS (short for right determinant space),

$$\mathrm{RDETS}(X) = \{\Phi_J \ : \ ^{\exists}\Phi_I \leftarrow \Phi_J \in X\}, \tag{3.10}$$

which generates a determinant space containing all elements "coupled from" X. Obviously, $\mathrm{LDETS}(X) = \mathrm{RDETS}(X)$ if X is symmetric. We refer to $S_X = \mathrm{LDETS}(X)$ as the corresponding determinant space of X, which is the determinant space generated by applying $\hat{H}_X$ to any trial wave function.

However, the X does not necessarily contain all the couplings between determinants in S_X. This gives rise to a property that, in general, the lowest eigenvalue of the Hamiltonian $\hat{H}_X$ generated according to coupling space X is not variational.

Since the lowest eigenstate $|\Psi_{X,0}\rangle$ of $\hat{H}_X$ is still a linear combination of determinants in S_X,

$$|\Psi_{X,0}\rangle = \sum_{\Phi_J \in S_X} C_{X,J} |\Phi_J\rangle , \tag{3.11}$$

we can define the eigen energy $E_{\text{eig},X}$ of determinant space X,

$$E_{\text{eig},X} = \text{eig}(\hat{H}_X) = \langle \Psi_{X,0}| \hat{H}_X |\Psi_{X,0}\rangle \tag{3.12}$$

We can also define the variational energy of X as

$$E_{\text{var},X} = \langle \Psi_{X,0}| \hat{H} |\Psi_{X,0}\rangle . \tag{3.13}$$

Note here that $\hat{H}$ is the bare Hamiltonian without any truncation or approximation. Further more, we can define determinant space energy of X as

$$E_{\text{det},X} = \text{eig}(\hat{H}_{S_X}) = \langle \Psi_{S_X,0}| \hat{H} |\Psi_{S_X,0}\rangle , \tag{3.14}$$

where $\hat{H}_{S_X}$ spans the determinant space generated from coupling space X, and $|\Psi_{S_X,0}\rangle$ is the lowest eigenstate of $\hat{H}_{S_X}$.

Now we are ready to define coupling efficiency as:

$$\text{Eff}_X = \frac{E_{\text{var,corr},X}}{E_{\text{corr,FCI}}} \Big/ \frac{|X|}{|X_{\text{FCI}}|}, \tag{3.15}$$

where $|X|$ and $|X_{\text{FCI}}|$ are the number of determinant couplings in X and full CI coupling space X_{FCI}, and $E_{\text{var,corr},X}$ is the correlation energy computed with variational energy, because variational energy is an indicator of wave function accuracy due to variational principle.

This implies that the most determinant efficient algorithm may not be the most coupling efficient one, in other words, not the algorithm with the lowest computational cost. It is possible to recover more electron correlation with a different coupling space that has the same size as the one determined by selected CI space.

3.2.2 Review of PCI

The PCI method is described in detail in ref 50. Here we revisit the PCI theory with the concept of coupling space we just defined.

The PCI method can be interpreted as a deterministic version of the FCIQMC method, where the sampled propagation of walkers on determinants is replaced by a path-integral formalism, and the imaginary propagation is accelerated by a polynomial projection approach.

In the PCI, the projector $\hat{P}_0$ is defined as an operator projecting a trial wave function $|\Omega\rangle$ onto the ground state $|\Psi_0\rangle$,

$$|\Psi_0\rangle = N_P \hat{P}_0 |\Omega\rangle , \tag{3.16}$$

where N_P is a normalization factor, and $|\Omega\rangle$ is not orthogonal to $|\Psi_0\rangle$. Although such a projector $\hat{P}_0$ cannot be directly formulated unless the ground state wave function is explicitly known, it can be achieved as an infinite power of a function of Hamiltonian $g(\hat{H})$

$$\hat{P}_0 = \lim_{k\to\infty} g^k(\hat{H}), \tag{3.17}$$

where the corresponding scalar function $g(\lambda)$ satisfies

$$|g(E_0)| = \sup(|g(\lambda)|) \tag{3.18}$$

in the domain of $[E_0, E_{\max}]$, where E_0 and $E_{\max}$ are the lowest and highest eigenvalue of $\hat{H}$. The function $g(\hat{H})$ is called a projector generator. In order to generate the effect of a projector, when $g(\hat{H})$ is successively applied to the trial wave function, $g(\hat{H})$ is designed to amplify the component of ground state eigenvector and eliminate all the excited ones. For example, the imaginary-time propagator, or the linear generator

$$g_{\text{linear}}(\hat{H}) = 1 - \tau(\hat{H} - S) \tag{3.19}$$

is the simplest and the most widely used generator, where S is a shift and τ is the imaginary-time interval.

In principle, the exact propagation results in a prohibitive computational cost similar to full CI if the exact Hamiltonian is applied in the projector generator. To reduce the computational cost, a path-filtering scheme is introduced in PCI to significantly reduce the cost.

Use linear imaginary-time projector generator as an example. Consider at the n-th iteration of PCI, where the intermediate wave function in the corresponding PCI subspace $S^{(n)}$ can be represented by a linear combination of Slater determinants,

$$|\Omega^{(n)}\rangle = \sum_{\Phi_J \in S^{(n)}} C_J^{(n)} |\Phi_J\rangle , \tag{3.20}$$

where $C_J^{(n)}$ is the normalized coefficient of determinant $|\Phi_J\rangle$.

When we apply $1-\tau(\hat{H}-E_0)$ onto the current intermediate wave function $|\Omega^{(n)}\rangle$ with path filtering, only significant couplings $\Phi_I \leftarrow \Phi_J$ with contribution $|H_{IJ}C_J^{(n)}|$ greater than a threshold η is included in the computation. The path-filtering scheme actually defines an important asymmetric determinant coupling space,

$$X^{(n)}(\eta) = \{\Phi_I \leftarrow \Phi_J \ : \ \Phi_J \in S^{(n)}, \ |H_{IJ}C_J^{(n)}| \geq \eta\}, \tag{3.21}$$

and correspondingly according to Eq. (3.6), an approximated Hamiltonian $\widetilde{H}^{(n)}(\eta)$ with

$$\widetilde{H}_{IJ}^{(n)}(\eta) = \begin{cases} H_{IJ} & \text{if } I=J \text{ or } |H_{IJ}C_J^{(n)}| \geq \eta \\ 0 & \text{otherwise,} \end{cases} \tag{3.22}$$

where η is called the spawning threshold specified by the user controlling the accuracy of PCI calculations. The approximated Hamiltonian is used to generate the next intermediate wave function by

$$|\tilde{\Omega}^{(n+1)}\rangle = \left[1-\tau\left(\widetilde{H}^{(n)}(\eta)-E_0\right)\right]|\Omega^{(n)}\rangle , \tag{3.23}$$

where $|\tilde{\Omega}^{(n+1)}\rangle$ is the next unnormalized intermediate wave function, or explicitly

$$\tilde{C}_I^{(n+1)} = \sum_{\Phi_J \in S^{(n)}} \left[\delta_{IJ}-\tau\left(\widetilde{H}_{IJ}^{(n)}(\eta)-E_0\delta_{IJ}\right)\right] C_J^{(n)}, \tag{3.24}$$

or

$$\tilde{C}_I^{(n+1)} = \left[1 - \tau \left(H_{II} - E_0\right)\right] C_I^{(n)} - \tau \sum_{\Phi_I \leftarrow \Phi_J \in X^{(n)}(\eta)} H_{IJ} C_J^{(n)}, \tag{3.25}$$

where $\tilde{C}_I^{(n+1)}$ is the unnormalized coefficient of determinant $|\Phi_I\rangle$ in the $(n+1)$-th intermediate wave function and δ_{IJ} is the Kronecker delta function. In this way, without a major compromise to the accuracy of results, the computational cost is reduced dramatically by computing only important couplings in the coupling space defined at each step by the spawning threshold η.

In general, begin with an initial guess of wave function, usually just a single Hartree–Fock determinant $|\Omega^{(0)}\rangle = |\Phi_{\text{HF}}\rangle$ or the result of a small (selected) CISD wave function, the PCI wave function is obtained iteratively until converge. Conceptually at n-th step with current wave function $|\Omega^{(n)}\rangle$, the algorithm of PCI is equivalently in terms of determinant coupling space:

1. Generate a determinant coupling space $X^{(n)}$ according to Eq. (3.21).
2. Generate an approximate Hamiltonian $H_X^{(n)}$ from $X^{(n)}$ according to Eq. (3.6).
3. Apply the generator $g(H_X^{(n)})$ to wave function $|\Omega^{(n)}\rangle$ to give $|\tilde{\Omega}^{(n+1)}\rangle = g(H_X^{(n)})\,|\Omega^{(n)}\rangle$.
4. Normalize $|\tilde{\Omega}^{(n+1)}\rangle$ to give $|\Omega^{(n+1)}\rangle$
5. Check convergence.

3.2.3 Improving the Approximate Hamiltonian

As explained in Ref. 50, there are two sources of error in the PCI: truncation error and path-filtering error,

$$\epsilon_{\text{total}} = \epsilon_{\text{tr}} + \epsilon_{\text{pf}}, \tag{3.26}$$

where ϵ_{total} is the total energy error, ϵ_{tr} is the truncation error and ϵ_{pf} is the path-filtering error.

It has been justified that the PCI method is equivalent to a power method diagonalizing an approximated Hamiltonian as shown in Eq. (3.22). Thus, the result accuracy of the PCI method is connected with the accuracy of the approximated Hamiltonian. In order to analyze the error, we can write the exact Hamiltonian as

$$H = \begin{pmatrix} H_{PP} & H_{PQ} \\ H_{QP} & H_{QQ} \end{pmatrix} = \underbrace{\begin{pmatrix} \tilde{H}_{PP} & 0 \\ 0 & D_{QQ} \end{pmatrix}}_{H^{(0)}} + \underbrace{\begin{pmatrix} \delta H_{PP} & H_{PQ} \\ H_{QP} & N_{QQ} \end{pmatrix}}_{H^{(1)}}, \tag{3.27}$$

where P denotes determinants in the current PCI subspace, Q denotes unincluded determinants, D_{QQ} and N_{QQ} are the diagonal and non-diagonal parts of H_{QQ}, respectively, and

$$\delta H_{PP} = H_{PP} - \tilde{H}_{PP}. \tag{3.28}$$

In the PCI we solve

$$\tilde{H}_{PP}\tilde{c}_P = \tilde{E}_P\tilde{c}_P, \tag{3.29}$$

and are interested in estimating the contribution from the part of the Hamiltonian neglected [$H^{(1)}$]. If we expand the exact eigenvalue and eigenvector of H as the power series:

$$E = E^{(0)} + \lambda E^{(1)} + \lambda^2 E^{(2)} + \dots \tag{3.30}$$

$$c = c^{(0)} + \lambda c^{(1)} + \lambda^2 c^{(2)} + \dots \tag{3.31}$$

we can identify the zeroth-order quantities in the following way

$$E^{(0)} = \tilde{E} \tag{3.32}$$

$$c^{(0)} = \begin{pmatrix} \tilde{c}_P \\ 0 \end{pmatrix}. \tag{3.33}$$

Applying Löwdin's perturbation theory to the PCI Hamiltonian we can estimate the truncation and path filtering error. To first order in λ, the only correction to the energy comes from path filtering and can be expressed as the expectation value of δH_{PP} with respect to the PCI wave function:

$$E^{(1)} = \tilde{c}_P^\dagger \delta H_{PP} \tilde{c}_P := \epsilon_{\text{pf}}^{(1)}. \tag{3.34}$$

Note that the variational energy of the PCI wave function is correct up to first order:

$$\tilde{c}_P^\dagger H \tilde{c}_P = \tilde{c}_P^\dagger \tilde{H} \tilde{c}_P + \tilde{c}_P^\dagger \delta H_{PP} \tilde{c}_P = E^{(0)} + E^{(1)}. \tag{3.35}$$

To second order in λ, there are two contributions to the energy correction. The first one is due to path filtering

$$\epsilon_{\mathrm{pf}}^{(2)} = \tilde{c}_P^\dagger \delta H_{PP} P' (\tilde{E} - \tilde{H}_{PP})^{-1} P' \delta H_{PP} \tilde{c}_P, \tag{3.36}$$

where $P' = 1 - \tilde{c}_P \tilde{c}_P^\dagger$ is the projector onto the eigenvectors of $\tilde{H}_{PP}$ complementary to $\tilde{c}_P$. Resolving P' in the spectral basis of $\tilde{H}_{PP}$ we can write the second-order error from path filtering as:

$$\epsilon_{\mathrm{pf}}^{(2)} = \sum_{i=1} \frac{|\tilde{c}_0^\dagger \delta H_{PP} \tilde{c}_i|^2}{\tilde{E}_0 - \tilde{E}_i}, \tag{3.37}$$

from which we can derive an upper bound to $|\epsilon_{\mathrm{pf}}^{(2)}|$:

$$|\epsilon_{\mathrm{pf}}^{(2)}| \leq \frac{1}{\tilde{E}_0 - \tilde{E}_1} \left[\tilde{c}_0^\dagger \delta H_{PP} (1 - \tilde{c}_0 \tilde{c}_0^\dagger) \delta H_{PP} \tilde{c}_0 \right]. \tag{3.38}$$

The second-order error due to truncation of FCI space is given by

$$\epsilon_{\mathrm{tr}}^{(2)} = \tilde{c}_P H_{PQ} c_Q^{(1)} = \sum_q \frac{|\sum_p \tilde{c}_p^\dagger H_{pq}|^2}{\tilde{E} - E_q}. \tag{3.39}$$

Interestingly, up to second order in λ the two sources of error are not coupled.

According to the above analysis, we cannot reduce the truncation error unless more determinants are introduced into the PCI subspace. However, the path-filtering error can be reduced if we make δH_{PP} smaller, i.e. $\tilde{H}_{PP}$ more accurate.

Consider a pair of determinant coupling ($I \neq J$),

$$\begin{cases} \Phi_I \leftarrow \Phi_J & \text{significant if } |H_{IJ} C_J^{(n)}| \geq \eta \\ \Phi_J \leftarrow \Phi_I & \text{significant if } |H_{IJ} C_I^{(n)}| \geq \eta. \end{cases} \tag{3.40}$$

They may not be both significant since in general $C_I^{(n)} \neq C_J^{(n)}$, which equivalently means the approximate Hamiltonian, $\widetilde{H}^{(n)}(\eta)$, corresponding to $C^{(n)}$ is not symmetric ($\widetilde{H}_{IJ}^{(n)}(\eta) \neq \widetilde{H}_{JI}^{(n)}(\eta)$).

In this situation, although one of the couplings is not considered important in the original PCI, due to the Hermiticity of full Hamiltonian, both matrix elements $H_{IJ} = H_{IJ}^{\dagger}$ are known when one of them is computed. It is straightforward to take both couplings in to account without increasing the computational cost.

Thus, we can modify the definition of coupling space and approximated Hamiltonian in Eqs. (3.21) and (3.22) to

$$X_{\text{symm}}^{(n)}(\eta) = \{\Phi_I \leftarrow \Phi_J \ : \ \Phi_J \in S^{(n)}, \ \max(|H_{IJ}C_J^{(n)}|, |H_{JI}C_I^{(n)}|) \geq \eta\}, \tag{3.41}$$

and

$$\widetilde{H}_{IJ,\text{symm}}^{(n)}(\eta) = \begin{cases} H_{IJ} & \text{if } I = J \text{ or } \max(|H_{IJ}C_J^{(n)}|, |H_{JI}C_I^{(n)}|) \geq \eta \\ 0 & \text{otherwise,} \end{cases} \tag{3.42}$$

which means that both couplings in eq. (3.40) are considered important if one of them is.

Since more determinant couplings are taken into account, δH_{PP} is smaller and path-filtering error is reduced in this way. Meanwhile, $\widetilde{H}_{\text{symm}}^{(n)}(\eta)$ is a Hermitian matrix that agrees better with the physical property of Hamiltonian. This improvement also enabled the application of standard Hermitian matrix diagonalization algorithms in PCI. Unless otherwise noted, in this paper, PCI refers to the Hermitian PCI method.

3.3 Implementation

The new PCI algorithm is implemented based on the original version in Forte,[53] a suite of multireference electronic structure methods written as a plugin to the open-source quantum chemistry package Psi4.[54]

3.3.1 Davidson–Liu diagonalization schemes

In PCI, we had accelerated the projection by utilizing the wall-Chebyshev generator, which can be seen as an accelerated power method for the eigenvalue problem. Nevertheless, there are many other, faster-converging eigenvalue solving methods such

as Lanczos and Davidson–Liu (DL) methods.[1,51,52] If we change from projector generator to a diagonalization scheme, a faster convergence to the final energy and wave function is expected.

An Davidson–Liu solver already exist in FORTE for the adaptive configuration interaction (ACI) method.[21,22] All we need to do is create a PCI version of σ vector generator for computing

$$\sigma = \widetilde{H}^{(n)}_{\text{symm}}(\eta)\mathbf{b}, \tag{3.43}$$

where σ and $\mathbf{b}$ are vectors in the DL algorithm.

The differences between computing Eq. (3.43) in the DL algorithm and $\widetilde{H}^{(n)}_{\text{symm}}(\eta)\mathbf{C}^{(n)}$ in the imaginary-time propagator are 1) $\mathbf{C}^{(n)}$ is always normalized, but $\mathbf{b}$ may not be, and 2) the latter need to be computed only once in each iteration, but the $\widetilde{H}^{(n)}_{\text{symm}}(\eta)$ for DL are reused multiple times with different $\mathbf{b}$ vector.

Thus, we need to keep the coefficient vector $\mathbf{C}^{(n)}$ at each iteration as a reference for $\widetilde{H}^{(n)}_{\text{symm}}(\eta)$ defined in Eq. (3.42). We require the determinants are sorted by decending absolute coefficient value so that $|C^{(n)}_I| \geq |C^{(n)}_J|$ if $I < J$. We also prepare in the beginning of PCI computation a sorted list (L) of tuples $(p, q, r, s, \langle pq\|rs\rangle)$ by $|\langle pq\|rs\rangle|$ in decending order, where we only keep unrepeating entries by requiring that $p < q$, $r < s$ and $(p, q) < (r, s)$. Assuming $\widetilde{H}^{(n)}_{\text{symm}}(\eta)$ real symmetric, when computing the σ vector,

$$\sigma_I = \sum_{\Phi_I \leftarrow \Phi_J \in X^{(n)}_{\text{symm}}} H_{IJ} b_J, \tag{3.44}$$

we loop over J and follow the procedure as in Algorithm 2.

The double excitation part of the algorithm is adapted from the efficient double excitation algorithm in Ref. 17, where only important determinant couplings are computed. Meanwhile, in our algorithm, since the determinants are sorted by coefficients, couplings $\Phi_I \leftarrow \Phi_J$ and $\Phi_J \leftarrow \Phi_I$ are always computed at the same time so that the Hamiltonian matrix element H_{IJ} is computed only once, and we do not need to check

Algorithm 2 Computing sigma vector according to Eq. (3.44).

for all $\Phi_J \in S^{(n)}$ **do**
  Diagonal contribution is computed $\sigma_J \leftarrow H_{JJ} b_J$;
  for all singly excited determinants Φ_I **do**
    if $\Phi_I \notin S^{(n)}$ **or** $I > J$ **then**
      Compute H_{IJ};
      if $|H_{IJ} C_J^{(n)}| \geq \eta$ **then**
        $\sigma_I \leftarrow H_{IJ} b_J$;
        $\sigma_J \leftarrow H_{IJ} b_I$;
      end if
    end if
  end for
  for $(p, q, r, s, \langle pq \| rs \rangle)$ in L **until** $| \langle pq \| rs \rangle C_J^{(n)}| < \eta$ **do**
    if p,q are occupied and r,s are unoccupied in Φ_J **or** vice versa **then**
      Determine the doubly excited determinant Φ_I according to p,q and r,s;
      if $\Phi_I \notin S^{(n)}$ **or** $I > J$ **then**
        Determine sign s_{IJ};
        $\sigma_I \leftarrow s_{IJ} \langle pq \| rs \rangle b_J$;
        $\sigma_J \leftarrow s_{IJ} \langle pq \| rs \rangle b_I$;
      end if
    end if
  end for
end for

the value of $|H_{IJ}C_J^{(n)}|$ for $\max(|H_{IJ}C_J^{(n)}|, |H_{IJ}C_I^{(n)}|) \geq \eta$ because $|C_I^{(n)}| \geq |C_J^{(n)}|$ always holds.

3.4 Results and Discussion

3.4.1 Accuracy improvements in Hermitian PCI

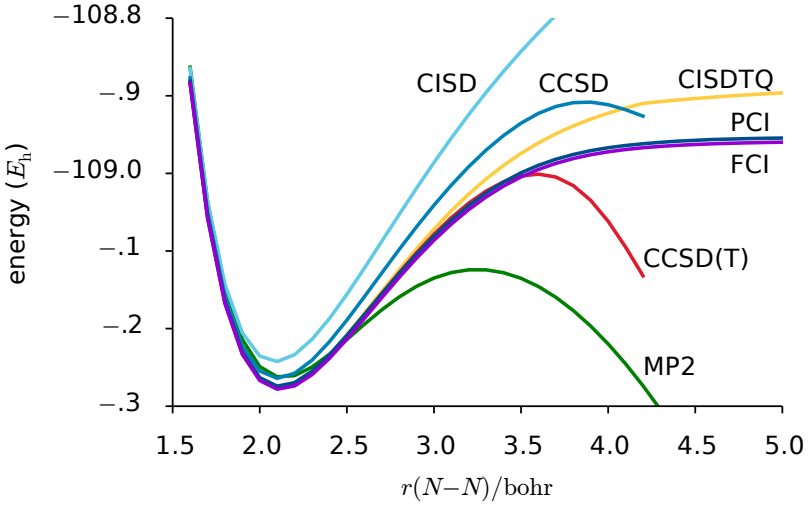

Figure 3.1 The dissociation potential energy curve computed with full CI, PCI(1×10^{-4}), CISD, CISDTQ, CCSD and CCSD(T). All computations used canonical Hartree–Fock orbitals and the cc-pVDZ basis set. The 1s-like orbitals of nitrogen were excluded from computations of the correlation energy.

Due to the triple bond in N_2, the dissociation potential energy curve is a challenging benchmark for quantum chemistry methods. The FCI reference energy, PCI variational energy along with energies from many other standard quantum chemistry methods are plotted in Fig. 3.1.

Stretched N_2 molecule is a typical strongly correlated system, where perturbation theory and coupled-cluster methods give qualitatively incorrect results and the latter could not converge at bond length $r > 4.2$ bohr. Truncated single reference configuration interaction methods also fail to recover the correlation energy at stretched geometries. In contrast, PCI with a moderate spawning threshold can provide en-

ergy almost indistinguishable from the FCI reference energy. In this benchmark, PCI shows its capability of computing strongly correlated systems accurately.

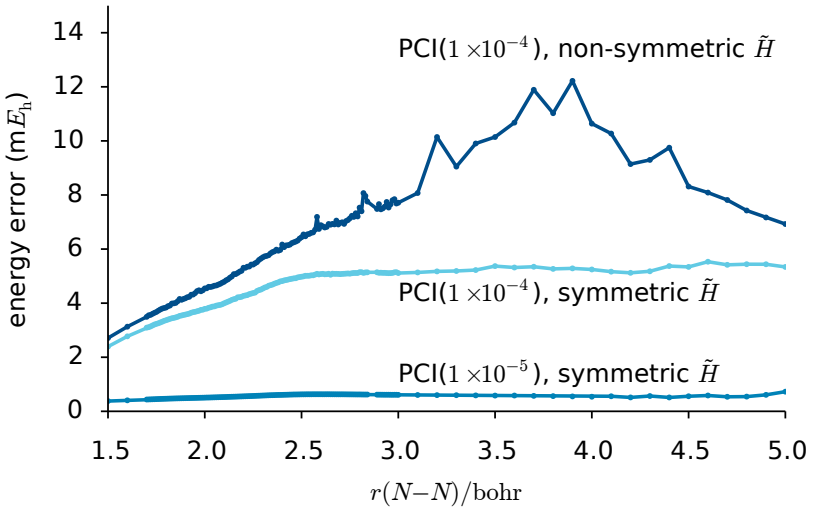

Figure 3.2 Error to full CI reference energy computed with non-symmetric PCI(1×10^{-4}) and real symmetric PCI(1×10^{-4}), PCI(1×10^{-5}). The non-symmetric PCI used 5^{th} order wall-Chebyshev generator scheme and real symmetric cases used Davidson–Liu method. All computations used canonical Hartree–Fock orbitals and the cc-pVDZ basis set. The 1s-like orbitals of nitrogen were excluded from computations of the correlation energy.

We also plot the error to FCI reference energy in Fig. 3.2 computed with different PCI schemes and thresholds. It is shown that the real symmetric approximate Hamiltonian results in a smaller energy error compared to the non-symmetric one. The real symmetric approximate Hamiltonian also shows significantly smaller non-parallelism error and a much smoother energy curve. The energy error and the curve smoothness can be further improved by applying a smaller spawning threshold. When the spawning threshold is decreased 10 times from 1×10^{-4} to 1×10^{-5}, the energy error also decreases 10 times from around 5 mE_h to 0.5 mE_h.

3.4.2 Comparison of the convergence rate

We use the equilibrium geometry of N_2 as an example to show the convergence speed of different algorithms including the conventional 5^{th} order wall-Chebyshev generator, the higher 10^{th} order wall-Chebyshev generator, the Lanczos method and

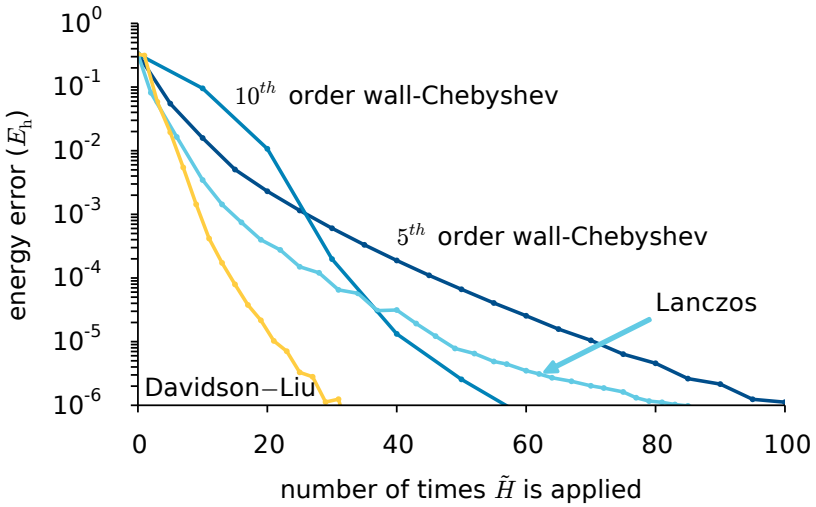

Figure 3.3 Ground state of N_2 at the equilibrium geometry ($r = 2.118$ bohr) computed with the PCI using a spawning threshold $\eta = 1 \times 10^{-5}$. Various algorithms are compared. This plot shows the difference between the energy at each iteration and the converged energy as a function of the number of times the Hamiltonian is applied. All computations used canonical Hartree–Fock orbitals and the cc-pVDZ basis set. The 1s-like orbitals of nitrogen were excluded from computations of the correlation energy.

the Davidson–Liu method. The convergence of the energy for each method is plotted in Fig. 3.3.

As shown in Fig. 3.3, both increasing the order of wall-Chebyshev polynomial and changing the diagonalization scheme accelerated the convergence of PCI. The Davidson–Liu method converged the fastest as expected. Benefitting from an efficient preconditioner, Davidson–Liu applies $\widetilde{H}$ only around 30 times to converge the energy to an error less than 1 μE_h, which is a three-fold speed-up compared to the 5^{th} order wall-Chebyshev generator scheme.

The Lanczos method accelerated the convergence especially at the beginning of computation. It slows down later on because when the wave function gradually converges, the growth of the Krylov subspace ($K = \{C, \widetilde{H}C, \widetilde{H}^2C, \ldots, \}$) immediately becomes numerically linearly dependent. When this linear dependency issue arises after several iterations, the Lanczos method is limited to a Krylov subspace of only two to three vectors and cannot efficiently optimize the wave function. Consequently,

there is not a dramatic speed up upon the 5^{th} order wall-Chebyshev generator scheme.

The algorithm in Sec. 3.3.1 also enabled the stable application of high order wall-Chebyshev generator. As shown in Fig. 3.3, the 10^{th} order wall-Chebyshev generator takes around half of the number of $\widetilde{H}$ application to converge to μE_{h} level of accuracy. However, at the beginning of iteration it converges slowly because the reference wave function is updated after every 10 **HC** product, which introduced the limitation that the PCI determinant subspace can grow only once every 10 micro iterations. It means that beginning with the Hartree–Fock determinant, the result PCI space of after first 10 iterations is a subspace of CISD, the end of 20 iterations is a subspace of CISDTQ, etc. Thus, high order wall-Chebyshev generator wasted many applications of $\widetilde{H}$ at the beginning of the computation.

In practice, the Davidson–Liu algorithm seems to give the best performance. To this point, the only weakness of the Davidson–Liu algorithm is that all the vectors of the same length of PCI determinant space in Krylov subspace need to be stored, which costs more memory than the wall-Chebyshev generator scheme. Since the high order wall-Chebyshev generator also provides fast convergence, it can be a useful alternative if memory is limited. Importantly, the resulting energy is invariant to the applied algorithm, because the same spawning threshold results in wave functions that are all the converged eigenvectors of the same determinant coupling space and approximate Hamiltonian (with neglectable error). Thus, a PCI computation with a spawning threshold η is labelled as PCI(η), because the spawning threshold is the only parameter determining the accuracy of the result. Unless otherwise noted, the results in the following sections are computed with Davidson–Liu algorithm.

3.4.3 Connection to the Heat-bath CI method

PCI uses a determinant coupling filtering criterion similar to the one in Heat-bath CI (HCI) method. In order to investigate the relationship between HCI and PCI, we

performed PCI computation on diatomic systems using the same threshold value as reported by Sharma and co-workers.[18]

As shown in Table 3.1, the determinant space energy E_{det} as defined in Sec. 3.2.1 are almost identical to the HCI variational energy. Their number of determinants included in the computation are also similar to each other. It shows that due to the same criteria, although the determinant space is not diagonalized exactly, the PCI is still able to choose similar determinant space as the HCI method.

The number of determinant couplings in the HCI method can be estimated by the size of the coupling space generated by the determinants in PCI. As a comparison, the number of determinant couplings needs to span the similar determinant space as HCI is only 1/40 of the full coupling space in cc-pVDZ basis and 1/100 in cc-pVTZ basis. Thus, if we want to select the important determinants as in HCI, the task can be done 40 to 100 times more efficient by the PCI algorithm. Please note that we are not proposing PCI as an alternative way to select important determinants. Although the PCI variational energy is less accurate than HCI with the same threshold, we will show that accurate wave function is available with a number of couplings less than selected CI methods.

On average, only 3 to 4 determinants are importantly connected with a determinant. Thus, in PCI, we exploit more the sparsity of the Hamiltonian than in selected CI methods.

3.4.4 Efficiency in computing the wave function

In order to show that more accurate wave function can be obtained with lower computational cost by filtering the most important determinant couplings. We plot the number of determinant couplings in X required for $E_{\text{var},X}$ to reach a certain accuracy in Fig. 3.4. Meanwhile, we also plot the corresponding total number of determinant couplings between all determinants in PCI determinant space S_X with

Table 3.1 PCI variational energy and energy obtained from diagonalizing the PCI determinant space. PCI results are computed with the same spawning threshold η value as the threshold ϵ_1 in Heat-bath CI(HCI). The 1s-like orbitals were excluded from computations of the correlation energy. HCI values are copied from Ref. 18.

molecule	basis	sym	η / ϵ_1 (E_h)	PCI					HCI	
				N_det	$\lvert X\rvert$	$E_\mathrm{var}/E_\mathrm{h}$	$\lvert X_S\rvert$	$E_\mathrm{det}/E_\mathrm{h}$	N_det	$E_\mathrm{var}/E_\mathrm{h}$
C_2	cc-pVDZ	$^1A_{1g}$	5×10^{-4}	29,131	118,682	−75.7139	4,873,796	−75.7217	28,566	−75.7217
C_2	cc-pVTZ	$^1A_{1g}$	3×10^{-4}	146,601	489,400	−75.7633	54,046,748	−75.77**40**	142,467	−75.77**38**
N_2	cc-pVDZ	$^1A_{1g}$	5×10^{-4}	39,860	150,818	−109.2622	5,959,810	−109.269**5**	37,593	−109.269**2**
N_2	cc-pVTZ	$^1A_{1g}$	3×10^{-4}	201,403	628,144	−109.3511	62,497,422	−109.36**12**	189,080	−109.36**08**
O_2	cc-pVDZ	$^1B_{1g}$	5×10^{-4}	56,502	223,306	−149.9724	8,417,008	−149.979**6**	52,907	−149.979**3**
O_2	cc-pVTZ	$^1B_{1g}$	3×10^{-4}	317,704	986,068	−150.1030	99,243,014	−150.113**6**	290,980	−150.113**0**
F_2	cc-pVDZ	$^1A_{1g}$	5×10^{-4}	72,333	266,722	−199.0869	9,570,478	−199.091**5**	68,994	−199.091**3**
F_2	cc-pVTZ	$^1A_{1g}$	3×10^{-4}	427,697	1,276,462	−199.2697	115,893,094	−199.278**8**	395,744	−199.278**2**

respect to the error of $E_{\mathrm{det},X}$.

Although the error of $E_{\mathrm{det},X}$ is always smaller than the error of $E_{\mathrm{var},X}$ for the same X, to reach the same accuracy, the number of determinant couplings required for PCI is still an order of magnitude smaller than a selected CI method. Consequently, although with a smaller spawning threshold, PCI can compute more accurate reference wave functions with lower computational cost than selected CI methods.

3.4.5 Ground state energy of Cr_2

Another challenging strongly correlated system is Cr_2 because of many near-degenerate 3d electrons and a formal hextuple bond. In order to get an accurate result, both the static (strong) and the dynamic (weak) correlation have to be treated equally well.[17,55]

In this case, we performed three PCI computations with spawning thresholds $\eta = 4\times10^{-5}$, 2×10^{-5} and 1×10^{-5} which we use to quadratically extrapolate to $\eta = 0$. The extrapolated energy -2086.418 E_h is within 3 mE_h from the reference extrapolated DMRG energy. In this series of computations, the PCI(2×10^{-5}) gives similar energy as CCSD(T), and PCI(1×10^{-5}) outperforms CCSDTQ.

The converged PCI(1×10^{-5}) result shows that the Hartree–Fock reference deter-

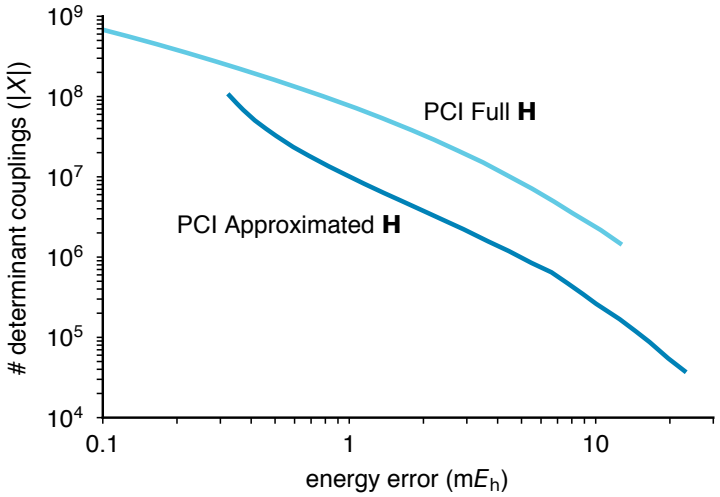

Figure 3.4 The number of determinant couplings in the PCI computation of C_2 with respect to the result absolute energy error to FCI. The approximated Hamiltonian is the Hamiltonian applied to propagate PCI wave function, and the full Hamiltonian is used to compute the variational energy. $|X|$ is the number of determinant couplings in the Hamiltonian matrix. All results are computed using the cc-pVDZ basis with the 1s-like orbitals of carbon excluded from computations of the correlation energy.

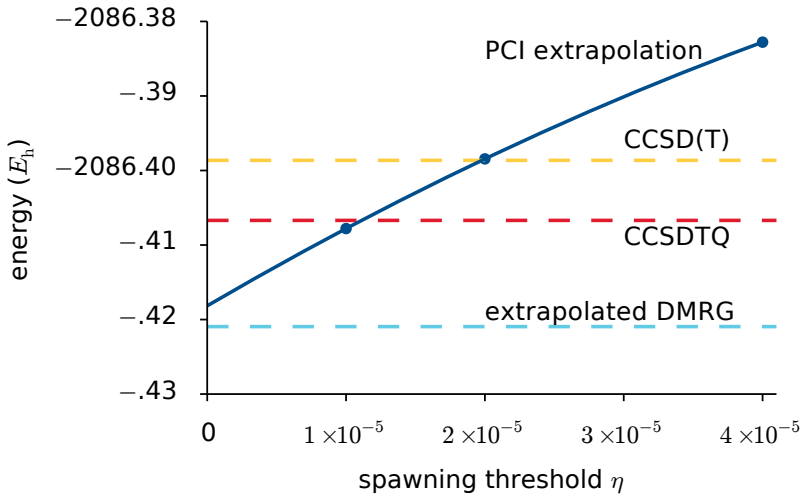

Figure 3.5 Cr_2 single point ground state energy computations at bond length $r = 1.5$ Å. All PCI computations used canonical Hartree–Fock orbitals and the Ahlrichs VDZ basis set in a (24e, 30o) active space. Extrapolation is done by a quadratic fitting of PCI energies with spawning thresholds $\eta = 4\times10^{-5}$, 2×10^{-5} and 1×10^{-5}. CCSD(T), CCSDTQ and extrapolated DMRG energy in the same basis set and active space are taken from Ref. 55.

minant only contributes 58% of the wave function. Meanwhile, no other determinant contributes more than 3% of the wave function. This shows that Cr_2 is a system in which both static (strong) and dynamic (weak) correlations are important, and PCI can treat them equally well.

3.5 Conclusion and Future work

In this report, we introduce recent developments in the PCI method. We first modified the filtering algorithm so that the path-filtering error is reduced and the approximated Hamiltonian is Hermitian. The benchmark on N_2 dissociation shows that the Hermitian version of PCI provides much smoother PES with half the non-parallelism error.

The Hermiticity in new PCI scheme enables integration of Davidson–Liu algorithm into PCI to converge the wave function onto the ground state wave function with fewer applications of the Hamiltonian. Convergence analysis shows that for N_2 at equilibrium geometry, the Davidson–Liu method converges three times faster than the conventional 5^{th} order wall-Chebyshev generator scheme. We also point out that when memory is not sufficient, a high order wall-Chebyshev generator scheme can be an alternative to the Davidson–Liu method since the former requires less memory.

We then show that PCI is able to efficiently select a similar determinant space as in HCI with the same threshold. If we exactly diagonalize the PCI determinant space, we get determinant space energy identical to the HCI variational energy. Our analysis also shows that to get a wave function of the same quality, the number of determinant couplings need to be evaluated is around one magnitude order less than a selected CI method.

Finally, we tried to compute Cr_2 ground state energy by spawning threshold extrapolation. Since the accuracy of PCI is controlled by a single parameter, we show that the optimal result is obtained by computing a series of energies with different

spawning threshold and extrapolating to $\eta \to 0$. The extrapolated energy is within 3 mE_h to the DMRG reference value.

Despite the demonstrated success of solving strongly correlated systems, we found that the bottleneck of PCI is that computing the variational energy requires a full determinant coupling space. Unfortunately, we have not found a more efficient way to compute the variational energy. Thus we seek to find applications where requires high-quality wave function but do not require the variational energy.

Acknowledgments

This work was supported by Emory University startup funds and by a Research Fellowship of the Alfred P. Sloan Foundation.

Bibliography

[1] Sherrill, C. D.; Schaefer, H. F. *Adv. Quant. Chem.* **1999**, *34*, 143–269.

[2] Rossi, E.; Bendazzoli, G. L.; Evangelisti, S.; Maynau, D. *Chem. Phys. Lett.* **1999**, *310*, 530–536.

[3] Bender, C. F.; Davidson, E. R. *Phys. Rev.* **1969**, *183*, 23–30.

[4] Buenker, R. J.; Peyerimhoff, S. D. *Theoret. Chim. Acta* **1974**, *35*, 33–58.

[5] Buenker, R. J.; Peyerimhoff, S. D. *Theoret. Chim. Acta* **1975**, *39*, 217–228.

[6] Burton, P. G.; Buenker, R. J.; Bruna, P. J.; Peyerimhoff, S. D. *Chem. Phys. Lett.* **1983**, *95*, 379–385.

[7] Huron, B.; Malrieu, J. P.; Rancurel, P. *J. Chem. Phys.* **2003**, *58*, 5745–5759.

[8] Evangelisti, S.; Daudey, J.-P.; Malrieu, J.-P. *Chem. Phys.* **1983**, *75*, 91–102.

[9] (a) Angeli, C.; Cimiraglia, R.; Persico, M.; Toniolo, A. *Theor. Chem. Acc.* **1997**, *98*, 57–63.

[10] Cimiraglia, R. *J. Chem. Phys.* **1985**, *83*, 1746–1749.

[11] Giner, E.; Scemama, A.; Caffarel, M. *J. Chem. Phys.* **2015**, *142*, 044115.

[12] Harrison, R. J. *J. Chem. Phys.* **1991**, *94*, 5021–5031.

[13] Greer, J. C. *J. Chem. Phys.* **1995**, *103*, 1821–1828.

[14] Greer, J. C. *J. Comput. Phys.* **1998**, *146*, 181–202.

[15] Győrffy, W.; Bartlett, R. J.; Greer, J. C. *J. Chem. Phys.* **2008**, *129*, 064103.

[16] Tubman, N. M.; Lee, J.; Takeshita, T. Y.; Head-Gordon, M.; Whaley, K. B. *J. Chem. Phys.* **2016**, *145*, 044112.

[17] Holmes, A. A.; Tubman, N. M.; Umrigar, C. J. *J. Chem. Theory Comput.* **2016**, *12*, 3674–3680.

[18] Sharma, S.; Holmes, A. A.; Jeanmairet, G.; Alavi, A.; Umrigar, C. J. *J. Chem. Theory Comput.* **2017**, *13*, 1595–1604.

[19] Smith, J. E. T.; Mussard, B.; Holmes, A. A.; Sharma, S. *J. Chem. Theory Comput.* **2017**, *13*, 5468–5478.

[20] Evangelista, F. A. *J. Chem. Phys.* **2014**, *140*, 124114.

[21] Schriber, J. B.; Evangelista, F. A. *J. Chem. Phys.* **2016**, *144*, 161106.

[22] Schriber, J. B.; Evangelista, F. A. *J. Chem. Theory Comput.* **2017**, *13*, 5354–5366.

[23] (a) Knowles, P. J.; Handy, N. C. *Comput. Phys. Commun.* **1989**, *54*, 75–83.

[24] Meller, J.; Heully, J. L.; Malrieu, J. P. *Chem. Phys. Lett.* **1994**, *218*, 276–282.

[25] Sambataro, M.; Gambacurta, D.; Lo Monaco, L. *Phys. Rev. B* **2011**, *83*, 045102.

[26] Bytautas, L.; Ruedenberg, K. *Chem. Phys.* **2009**, *356*, 64–75.

[27] Ivanic, J.; Ruedenberg, K. *Theor. Chem. Acc.* **2001**, *106*, 339–351.

[28] Miralles, J.; Castell, O.; Caballol, R.; Malrieu, J.-P. *Chem. Phys.* **1993**, *172*, 33–43.

[29] Cave, R. J.; Xantheas, S. S.; Feller, D. *Theoret. Chim. Acta* **1992**, *83*, 31–55.

[30] Mitrushenkov, A. O.; Dmitriev, Y. Y. **1995**, *235*, 410–413.

[31] Bunge, C. F. *J. Chem. Phys.* **2006**, *125*, 014107.

[32] Knowles, P. J. *Mol. Phys.* **2015**, *113*, 1655–1660.

[33] Ben Amor, N.; Bessac, F.; Hoyau, S.; Maynau, D. *J. Chem. Phys.* **2011**, *135*, 014101.

[34] Bories, B.; Maynau, D.; Bonnet, M.-L. *J. Comput. Chem.* **2006**, *28*, 632–643.

[35] (a) Hanrath, M.; Engels, B. *Chem. Phys.* **1997**, *225*, 197–202.

[36] Neese, F. *J. Chem. Phys.* **2003**, *119*, 9428–9443.

[37] Stampfuß, P.; Wenzel, W. *J. Chem. Phys.* **2005**, *122*, 024110–024116.

[38] Booth, G. H.; Thom, A. J. W.; Alavi, A. *J. Chem. Phys.* **2009**, *131*, 054106–054110.

[39] Cleland, D.; Booth, G. H.; Alavi, A. *J. Chem. Phys.* **2010**, *132*, 041103–041104.

[40] (a) Booth, G. H.; Cleland, D.; Thom, A. J. W.; Alavi, A. *J. Chem. Phys.* **2011**, *135*, 084104–084115.

[41] Thomas, R. E.; Overy, C.; Booth, G. H.; Alavi, A. *J. Chem. Theory Comput.* **2014**, *10*, 1915–1922.

[42] Booth, G. H.; Smart, S. D.; Alavi, A. *Mol. Phys.* **2014**, *112*, 1855–1869.

[43] Thomas, R. E.; Booth, G. H.; Alavi, A. *Phys. Rev. Lett.* **2015**, *114*, 033001.

[44] Petruzielo, F. R.; Holmes, A. A.; Changlani, H. J.; Nightingale, M. P.; Umrigar, C. J. *Phys. Rev. Lett.* **2012**, *109*, 230201–230205.

[45] Blunt, N. S.; Smart, S. D.; Kersten, J. A. F.; Spencer, J. S.; Booth, G. H.; Alavi, A. *J. Chem. Phys.* **2015**, *142*, 184107–184110.

[46] Sim, E.; Makri, N. *Comput. Phys. Commun.* **1997**, *99*, 335–354.

[47] Sim, E.; Makri, N. *J. Phys. Chem. B* **1997**, *101*, 5446–5458.

[48] Makri, N. *Annu. Rev. Phys. Chem.* **1999**, *50*, 167–191.

[49] Lambert, R.; Makri, N. *J. Chem. Phys.* **2012**, *137*, 22A553–12.

[50] Zhang, T.; Evangelista, F. A. *J. Chem. Theory Comput.* **2016**, *12*, 4326–4337.

[51] Davidson, E. R. *J. Comput. Phys.* **1975**, *17*, 87–94.

[52] Liu, B. *Technical Report LBL-8158* **1978**, Lawrence Berkeley Laboratory, University of California, Berkeley.

[53] Forte, a suite of quantum chemistry methods for strongly correlated electrons. For current version see https://github.com/evangelistalab/forte, 2019.

[54] (a) Parrish, R. M. et al. *J. Chem. Theory Comput.* **2017**, *13*, 3185–3197; (b) Smith, D. G. A. et al. *J. Chem. Theory Comput.* **2018**, *14*, 3504–3511.

[55] Olivares-Amaya, R.; Hu, W.; Nakatani, N.; Sharma, S.; Yang, J.; Chan, G. K.-L. *J. Chem. Phys.* **2015**, *142*, 034102.

Chapter 4 Improving the efficiency of the multireference driven similarity renormalization group via sequential transformation, density fitting, and the non-interacting virtual orbital approximation

Chapter Abstract

This study examines several techniques to improve the efficiency of the linearized multireference driven similarity renormalization group truncated to one- and two-body operators [MR-LDSRG(2)]. We propose a sequential MR-LDSRG(2) [sq-MR-LDSRG(2)] approach, in which one-body rotations are folded exactly into the Hamiltonian. This new approach is combined with density fitting (DF) to reduce the storage cost of two-electron integrals. To further avoid the storage of large four-index intermediates, we propose a non-interacting virtual orbit (NIVO) approximation in which tensor blocks labeled by three and four virtual indices are neglected. The NIVO approximation reduces the computational cost prefactor of the MR-LDSRG(2) bringing it closer to that of coupled cluster with singles and doubles (CCSD). We test the effect of the DF and NIVO approximations on the MR-LDSRG(2) and sq-MR-LDSRG(2) methods by computing properties of eight diatomic molecules. The diatomic constants obtained by DF-sq-MR-LDSRG(2)+NIVO are found to be as accurate as those from the original MR-LDSRG(2) and coupled cluster theory with singles, doubles, and perturbative triples. Finally, we demonstrate that the DF-sq-MR-LDSRG(2)+NIVO scheme can be applied to chemical systems with more than 550 basis functions by computing the automerization energy of cyclobutadiene with a quintuple-ζ basis set. The predicted automerization energy is found similar to the

values computed with Mukherjee's state-specific multireference coupled cluster theory with singles and doubles.

4.1 Introduction

The failure of conventional many-body methods to describe near-degenerate electronic states has motivated the development of many efficient and practical multireference approaches, including perturbation theories (MRPTs)[1–6] and multireference configuration interaction (MRCI) schemes.[7–11] Considerable efforts have been dedicate to the development of multireference coupled cluster (MRCC) methods,[12–27] with the goal of creating nonperturbative theories that are both size extensive and systematically improvable. Analogous many-body methods based on unitary transformations have received considerably less attention.[27–34] Unitary theories have, in principle, two advantages over traditional coupled cluster approaches: 1) the energy satisfies the variational principle, and 2) the transformed Hamiltonian is Hermitian. The latter property is an important advantage in new applications of unitary methods to quantum computing, both in quantum algorithms[35–46] and downfolding approaches aimed at reducing the number of orbitals in quantum computations.[47]

One of the main obstacles in the formulation of both single- and multi-reference unitary coupled cluster theories is that they lead to nonterminating equations. The central quantity evaluated in these approaches is the similarity transformed Hamiltonian ($\bar{H}$) defined as

$$\hat{H} \rightarrow \bar{H} = \hat{U}^{\dagger}\hat{H}\hat{U} = e^{-\hat{A}}\hat{H}e^{\hat{A}} \tag{4.1}$$

where ($\hat{H}$) is the bare Hamiltonian and $\hat{U}$ is a unitary operator. In writing this transformation, we have expressed $\hat{U}$ as the exponential of the anti-Hermitian operator $\hat{A}$ ($\hat{A}^{\dagger} = -\hat{A}$), which is commonly written in terms of the coupled cluster excitation operator $\hat{T}$ as $\hat{A} = \hat{T} - \hat{T}^{\dagger}$. Using the Baker–Campbell–Hausdorff (BCH) identity,[29,31,33]

the transformed Hamiltonian may be computed as the following commutator series

$$\bar{H} = \hat{H} + [\hat{H}, \hat{A}] + \frac{1}{2!}[[\hat{H}, \hat{A}], \hat{A}] + \frac{1}{3!}[[[\hat{H}, \hat{A}], \hat{A}], \hat{A}] \ldots . \tag{4.2}$$

Since the operator $\hat{A}$ contains both excitations and de-excitations, contractions are possible among components of $\hat{A}$, and as a consequence, the BCH series given in Eq. (4.2) is nonterminating.

Various approximations have been proposed to evaluate the unitarily transformed Hamiltonian. Perhaps the simplest way to approximate the nonterminating unitary series is to truncate the BCH expansion after a certain number of commutators.[48,49] Proof-of-principle studies on unitary coupled cluster (CC) theory[48] suggest that for a a series containing up to n-nested commutators, the error decays as 10^{-n}, and about four commutators are necessary to achieve sub-milliHartree accuracy. Taube and Bartlett[33] have suggested tractable approximations to unitary CC theory based on the Zassenhaus expansion that are exact for a given number of electrons. A common way to truncate the unitary BCH series is to use a recursive approximation of the commutator $[\,\cdot\,, \hat{A}]$, as suggested by Yanai and Chan.[50] In their linear truncation scheme, these authors proposed to approximate each single commutator $[\,\cdot\,, \hat{A}]$ with its scalar and one- and two-body components, which we indicate as $[\,\cdot\,, \hat{A}]_{0,1,2}$. Since in this truncation scheme the commutator $[\,\cdot\,, \hat{A}]_{0,1,2}$ preserves the many-body rank (number of creation and annihilation operators) of the Hamiltonian, the full BCH series can then be evaluated via a recursive relation. An advantage of this approach is that closed-form expressions for terms like $[\hat{O}, \hat{A}]_{0,1,2}$, where $\hat{O}$ is an operator containing up to two-body terms can be easily derived. This truncation scheme has been employed in canonical transformation (CT) theory[50] and has been used to truncate normal-ordered equations in the flow renormalization group of Wegner.[51,52]

We have recently developed a multireference driven similarity renormalization group (MR-DSRG)[53–57] approach that avoids the multiple-parentage problem[20,23,58–61] and numerical instabilities[60–66] encountered in other nonperturbative

multireference methods. In the MR-DSRG, we perform a unitary transformation of the Hamiltonian controlled by a flow parameter, which determines to which extend the resulting effective Hamiltonian is band diagonal.[54,57] The simplest non-perturbative approximation, the linearized MR-DSRG truncated to two-body operators [MR-LDSRG(2)],[55] assumes that $\hat{A}$ contains up to two-body operators (singles and doubles) and employs the linear commutator approximation of Yanai and Chan. Preliminary benchmarks indicate that the MR-LDSRG(2) method is more accurate than CCSD around equilibrium geometries, and that this accuracy is preserved along potential energy curves, especially for single-bond breaking processes.[67] The cost to evaluate a single commutator in the MR-LDSRG(2) scales as $\mathcal{O}(N_{\mathbf{C}}^2 N_{\mathbf{V}}^2 N^2) = \mathcal{O}(N_{\mathbf{C}}^2 N_{\mathbf{V}}^4 + N_{\mathbf{C}}^3 N_{\mathbf{V}}^3 + \ldots)$ where $N_{\mathbf{C}}$, $N_{\mathbf{V}}$, and N are the numbers of core, virtual, and total orbitals, respectively. This scaling is identical to that of CC with singles and doubles (CCSD) [$\mathcal{O}(N_{\mathbf{C}}^2 N_{\mathbf{V}}^4)$]. However, while in CCSD the most expensive term is evaluated only once, in the MR-LDSRG(2) the same term must be evaluated for each nested commutator. Consequently, if the BCH series is truncated after $n+1$ terms, the computational cost of the MR-LDSRG(2) is roughly n times that of CCSD, where approximately ten or more terms are usually required to convergence the energy error in the BCH series to 10^{-12} E_h.[55] A second reason is that computing the BCH series requires storing large intermediate tensors with memory costs that scale as $\mathcal{O}(N^4)$. When these intermediates are stored in memory, practical computations are limited to 200–300 basis functions on a single computer node.

In this work, we combine a series of improvements and approximations to reduce the computational and memory requirements of the MR-LDSRG(2) down to a small multiple of the cost of CCSD. To begin, we consider an alternative ansatz for the MR-DSRG based on a sequential similarity transformation.[68] This sequential ansatz reduces the complexity of the MR-DSRG equations and, when combined with integral factorization techniques, reduces significantly the cost to evaluate sin-

gles contributions. Second, we apply density fitting (DF)[69–71] to reduce the memory requirements and the I/O cost by avoiding the storage of of two-electron repulsion integrals. Together with Cholesky decomposition (CD)[72–76] and other tensor decomposition schemes,[77] these techniques have been crucial in enabling computations with 1000 or more basis functions and found application in numerous electronic structure methods,[78–89] including coupled cluster methods.[90–94] Third, we reduce the cost of MR-LDSRG(2) computations by neglecting operators that involve three or more virtual electrons. We term this truncation scheme the non-interacting virtual orbital (NIVO) approximation. A perturbative analysis of the NIVO approximation shows that the errors introduced appear at third order. To the best of our knowledge, such approximation has not been introduced in multireference theories, but it is analogous to other truncation schemes used in CCSD in which certain diagrams are have modified coefficients[95–98] or are completely removed.[99,100]

This paper is organized in the following way. In Sec. 4.2 we present an overview of the MR-DSRG theory, discuss the sequential MR-DSRG, and introduced the NIVO approximation. Details of the implementation together with a discussion of timings are given in Sec. 4.3. In Sec. 4.4 we assess the accuracy of several MR-LDSRG(2) schemes on a benchmark set of several diatomic molecules and determine the automerization barrier of cyclobutadiene. Finally, in Sec. 4.5 we conclude this work with a discussion of the main results.

4.2 Theory

We first define the orbital labeling convention employed in this work. The set of molecular spin orbitals $\mathbf{G} \equiv \{\phi^p, p = 1, 2, \ldots, N\}$ is partitioned into core ($\mathbf{C}$), active ($\mathbf{A}$), and virtual ($\mathbf{V}$) components of sizes $N_{\mathbf{C}}$, $N_{\mathbf{A}}$, and $N_{\mathbf{V}}$, respectively. We use indices m, n to label core orbitals, u, v, x, y to label active orbitals, and e, f, g, h to label virtual orbitals. For convenience, we also define the set of hole ($\mathbf{H} = \mathbf{C} \cup \mathbf{A}$) and

particle ($\mathbf{P} = \mathbf{A} \cup \mathbf{V}$) orbitals with dimensions $N_{\mathbf{H}} = N_{\mathbf{C}} + N_{\mathbf{A}}$ and $N_{\mathbf{P}} = N_{\mathbf{A}} + N_{\mathbf{V}}$, respectively. Hole orbitals are denoted by indices i, j, k, l and those of particle by indices a, b, c, d. General orbitals are labeled by indices p, q, r, s.

The MR-DSRG assumes a multideterminantal reference wave function (Φ):

$$|\Phi\rangle = \sum_{\mu=1}^{d} c_\mu \, |\Phi^\mu\rangle \, . \tag{4.3}$$

In this work, the set of determinants $\{\Phi^\mu; \mu = 1, 2, \ldots, d\}$ in Eq. (4.3) is assumed to form a complete active space (CAS) and the corresponding coefficients $\{c_\mu; \mu = 1, 2, \ldots, d\}$ are obtained from a CAS self-consistent field (CASSCF) computation.[101] All operators are then normal ordered with respect to Φ according to the scheme of Mukherjee and Kutzelnigg.[102,103] For example, the bare Hamiltonian is expressed as

$$\hat{H} = E_0 + \sum_{pq} f^q_p \{\hat{a}^p_q\} + \frac{1}{4} \sum_{pqrs} v^{rs}_{pq} \{\hat{a}^{pq}_{rs}\}, \tag{4.4}$$

where $E_0 = \langle \Phi | \hat{H} | \Phi \rangle$ is the reference energy and $\{\hat{a}^{pq\cdots}_{rs\cdots}\} = \{\hat{a}^p \hat{a}^q \ldots \hat{a}_s \hat{a}_r\}$ is a product of creation ($\hat{a}^p \equiv \hat{a}^\dagger_p$) and annihilation ($\hat{a}_p$) operators in its normal-ordered form, as indicated by the curly braces. The generalized Fock matrix (f^q_p) introduced in Eq. (4.4) is defined as

$$f^q_p = h^q_p + \sum_{rs} v^{qs}_{pr} \gamma^r_s, \tag{4.5}$$

where $h^q_p = \langle \phi_p | \hat{h} | \phi^q \rangle$ and $v^{rs}_{pq} = \langle \phi_p \phi_q \| \phi^r \phi^s \rangle$ are the one-electron and anti-symmetrized two-electron integrals, respectively. Here, we have also used the one-particle reduced density matrix (1-RDM) defined as $\gamma^p_q = \langle \Phi | \hat{a}^p_q | \Phi \rangle$.

4.2.1 Review of the MR-DSRG method

The MR-DSRG performs a parametric unitary transformation of the bare Hamiltonian analogous to Eq. (4.1), whereby the anti-Hermitian operator $\hat{A}(s)$ depends on the so-called flow parameter, a real number s defined in the range of $[0, \infty)$. The resulting transformed Hamiltonian $[\bar{H}(s)]$ is a function of s defined as

$$\bar{H}(s) = e^{-\hat{A}(s)} \hat{H} e^{\hat{A}(s)}. \tag{4.6}$$

The operator $\hat{A}(s)$ is a sum of many-body operators with rank ranging from one up to the total number of electrons (n),

$$\hat{A}(s) = \sum_{k=1}^{n} \hat{A}_k(s), \tag{4.7}$$

where $\hat{A}_k(s)$ is the k-body component of $\hat{A}(s)$. In the DSRG the operators $\hat{A}_k(s)$ are written as $\hat{A}_k(s) = \hat{T}_k(s) - \hat{T}_k^\dagger(s)$, where $\hat{T}_k(s)$ is an s-dependent cluster operator defined as

$$\hat{T}_k(s) = \frac{1}{(k!)^2} \sum_{ij\cdots}^{\mathbf{H}} \sum_{ab\cdots}^{\mathbf{P}} t_{ab\cdots}^{ij\cdots}(s) \{\hat{a}_{ij\cdots}^{ab\cdots}\}. \tag{4.8}$$

Note that the cluster amplitudes $t_{ab\cdots}^{ij\cdots}(s)$ exclude internal excitations, which are labeled only with active orbital indices. The DSRG transformed Hamiltonian has a many-body expansion similar to Eq. (4.4),

$$\bar{H}(s) = \bar{E}_0(s) + \sum_{pq} \bar{H}_q^p(s) \{\hat{a}_p^q\} + \frac{1}{4} \sum_{pqrs} \bar{H}_{rs}^{pq}(s) \{\hat{a}_{pq}^{rs}\} + \cdots, \tag{4.9}$$

where,

$$\bar{E}_0(s) = \langle \Phi | \bar{H}(s) | \Phi \rangle, \tag{4.10}$$

is the DSRG energy and the tensors $\bar{H}_{rs\cdots}^{pq\cdots}(s)$ are analogous to one- and two-electron integrals but dressed with dynamical correlation effects.

The goal of the DSRG transformation is to decouple the interactions between the reference wave function (Φ) and its excited configurations. Such interactions are the couplings between hole and particle orbitals represented by generalized excitation $[\bar{H}_{ab\cdots}^{ij\cdots}(s)\{\hat{a}_{ij\cdots}^{ab\cdots}\}]$ and de-excitation $[\bar{H}_{ij\cdots}^{ab\cdots}(s)\{\hat{a}_{ab\cdots}^{ij\cdots}\}]$ operators, where $ij\cdots \in \mathbf{H}$ and $ab\cdots \in \mathbf{P}$, excluding cases where all the indices are active orbitals. These terms of $\bar{H}(s)$ that the DSRG transformation aims to suppress are called the off-diagonal components and will be denoted as $\bar{H}_{\mathrm{od}}(s)$. Instead of achieving a full decoupling of the off-diagonal components [i.e., $\bar{H}_{\mathrm{od}}(s) = 0$], we demand that the DSRG transformation achieves a partial decoupling, avoiding the components of $\bar{H}_{\mathrm{od}}(s)$ with small

or vanishing Møller–Plesset energy denominators. This condition is imposed via the DSRG flow equation, a nonlinear implicit equation of the form

$$\bar{H}_{\mathrm{od}}(s) = \hat{R}(s), \tag{4.11}$$

where the *source operator* $\hat{R}(s)$ is Hermitian and continuous in s. The role of the source operator in the DSRG flow equation is to drive the off-diagonal elements of $\bar{H}(s)$ to zero, a goal achieved by an appropriate parameterization of $\hat{R}(s)$.[53]

In the linearized MR-DSRG approximation [MR-LDSRG(2)], the BCH series [Eq. (4.2)] is evaluated by keeping up to two-body normal-ordered operators of each commutator. The transformed Hamiltonian can then be evaluated by the following recursive equations

$$\begin{cases} \hat{C}^{(k+1)}(s) = \dfrac{1}{k+1}[\hat{C}^{(k)}_{1,2}(s), \hat{A}(s)]_{0,1,2}, \\ \bar{H}^{(k+1)}(s) = \bar{H}^{(k)}(s) + \hat{C}^{(k+1)}(s), \end{cases} \tag{4.12}$$

starting from $\hat{C}^{(0)}(s) = \bar{H}^{(0)} = \hat{H}$ and iterating until the norm of $\hat{C}^{(k+1)}_{1,2}(s)$ is less than a given convergence threshold.

The solution of Eq. (4.11) yields a set of amplitudes $t^{ij\cdots}_{ab\cdots}(s)$ that define the operator $\hat{A}(s)$ and the DSRG transformed Hamiltonian $\bar{H}(s)$. From this latter quantity, the MR-DSRG electronic energy is computed as the expectation value with respect to the reference

$$\bar{E}_0(s) = \langle \Phi | \bar{H}(s) | \Phi \rangle \,. \tag{4.13}$$

We refer the energy computed using Eq. (4.13) as the *unrelaxed* energy since the reference coefficients are not optimized. To include reference relaxation effects, we require that Φ is an eigenstate of $\bar{H}(s)$ within the space of reference determinants, a condition that is equivalent to solving the eigenvalue problem

$$\sum_{\mu=1}^{d} \langle \Phi_\nu | \bar{H}(s) | \Phi^\mu \rangle \, c'_\mu = E(s) c'_\nu. \tag{4.14}$$

Equation (4.14) defines a new reference Φ' with expansion coefficients c'_μ. This new reference may be used as a starting point for a subsequent MR-DSRG transformation and this procedure can be repeated until convergence and such converged energy is referred as *fully relaxed* energy. For the nonperturbative MR-DSRG schemes discussed in this work, we use the fully relaxed energy by default, unless otherwise noted.

4.2.2 Simplifying the MR-DSRG equations: Sequential transformation

Our first modification to the MR-DSRG approach is an alternative way to transform the bare Hamiltonian via a sequence of unitary operators with increasing particle rank

$$\bar{H}(s) = e^{-\hat{A}_n(s)} \cdots e^{-\hat{A}_2(s)} e^{-\hat{A}_1(s)} \hat{H} e^{\hat{A}_1(s)} e^{\hat{A}_2(s)} \cdots e^{\hat{A}_n(s)}. \tag{4.15}$$

We term the MR-DSRG approach based on Eq. (4.15) the *sequential* MR-DSRG (sq-MR-DSRG), while we refer to the original formalism based on Eq. (4.6) as the *traditional* MR-DSRG. Note that in the limit of $s \to \infty$ and no truncation of $\hat{A}(s)$, both the traditional and sequential MR-DSRG can approach the full configuration interaction limit.[68] However, these schemes are not equivalent for truncated $\hat{A}(s)$ [for example, $n = 2$ in Eqs. (4.7) and (4.15)] due to the fact that operators of different particle rank do not commute, that is, $[\hat{A}_i(s), \hat{A}_j(s)] \neq 0$ for $i \neq j$.

An advantage of the sq-MR-DSRG approach is that $\hat{A}_1(s)$ can be exactly folded into the Hamiltonian via a unitary transformation. The resulting $\hat{A}_1(s)$-dressed Hamiltonian $[\tilde{H}(s)]$,

$$\tilde{H}(s) = e^{-\hat{A}_1(s)} \hat{H} e^{\hat{A}_1(s)}, \tag{4.16}$$

preserves the particle rank of the bare Hamiltonian [Eq. (4.4)]. The corresponding scalar and tensor components of $\tilde{H}(s)$ can be obtained by a simple unitary transformation of the one- and two-electron integrals (f_p^q and v_{pq}^{rs}) and update of the scalar energy. As will be discussed in Sec. 4.3.1, the $\hat{A}_1(s)$-dressed Hamiltonian can be com-

puted very efficiently when the two-electron integrals are approximated with DF or CD.

The transformed Hamiltonian for the sq-MR-DSRG truncated to one- and two-body operators is given by

$$\bar{H}(s) = e^{-\hat{A}_2(s)} \tilde{H}(s) e^{\hat{A}_2(s)}. \tag{4.17}$$

In the linear approximation, the evaluation of Eq. (4.17) is simpler than in the traditional MR-LDSRG(2) since the total number of tensor contractions is reduced from 39 to 30.[55] Another advantage of the sequential approach is that $\hat{A}_1(s)$ is treated exactly, while in the traditional scheme some contractions involving singles are neglected. To appreciate this point, consider all the contributions to the double-commutator term in the MR-LDSRG(2) that depend on $\hat{A}_1(s)$

$$\begin{aligned} [[\hat{H}, \hat{A}(s)]_{1,2}, \hat{A}(s)]_{0,1,2} \leftarrow \quad & [[\hat{H}, \hat{A}_1(s)]_{1,2}, \hat{A}_1(s)]_{0,1,2} \\ & + [[\hat{H}, \hat{A}_1(s)]_{1,2}, \hat{A}_2(s)]_{0,1,2} \\ & + [[\hat{H}, \hat{A}_2(s)]_{1,2}, \hat{A}_1(s)]_{0,1,2}. \end{aligned} \tag{4.18}$$

The first term on the r.h.s. of Eq. (4.18) is treated exactly in the MR-LDSRG(2). However, since contractions involving $\hat{A}_2(s)$ generate three-body terms (truncated in the linearized approximation), the contribution of $\hat{A}_1(s)$ in the second and third terms are not included exactly in the MR-LDSRG(2) transformed Hamiltonian. In the sequential approach, all contributions from $\hat{A}_1(s)$ are treated by forming the operator $\tilde{H}(s)$, and since the BCH expansion for such transformation does not generate intermediates with rank greater than two, all terms involving $\hat{A}_1(s)$ are treated exactly in the linearized approximation.

4.2.3 Alleviating the memory bottleneck: The non-interacting virtual orbital (NIVO) approximation

In both the traditional and sequential MR-DSRG approaches, the DF approximation reduces the cost to store both the bare and $\hat{A}_1(s)$-dressed Hamiltonian from

$\mathcal{O}(N^4)$ to $\mathcal{O}(N^2M)$. However, in the evaluation of the recursive commutator approximation of $\bar{H}(s)$, two-body operators are generated during the evaluation of each intermediate commutator $[\hat{C}^{(k)}(s)]$ and $\bar{H}(s)$. These quantities have $\mathcal{O}(N^4)$ storage cost and, thus, reintroduce the bottleneck avoided with DF.

In order to reduce the cost to store $\bar{H}_2(s)$ and $\hat{C}_2^{(k)}(s)$, we shall neglect certain tensor blocks of these operators. By partitioning of orbitals into core (**C**), active (**A**) and virtual (**V**) spaces, each general 4-index tensor may be subdivided into 81 blocks according to the combination of orbital indices, for example **CCCC**, **AAVV**, **CAVA**, etc. We propose a non-interacting virtual orbital (NIVO) approximation, which neglects the operator components of $\hat{C}_2^{(k+1)}(s) = [\hat{C}_{1,2}^{(k)}(s), \hat{A}(s)]_2$, $k \geq 0$, with three or more virtual orbital indices (**VVVV**, **VCVV**, **VVVA**, etc.) in the recursive definition of the linearized BCH series. Neglecting these blocks, the number of elements in each NIVO-approximated tensor is reduced from $\mathcal{O}(N^4)$ to $\mathcal{O}(N^2N_{\mathbf{H}}^2)$, a size comparable to that of the $\hat{A}_2(s)$ tensor. For instance, in the cyclobutadiene computation using a quintuple-ζ basis set reported in Sec. 4.4.2, the memory requirements of $\bar{H}_2(s)$ or $\hat{C}_2^{(k)}(s)$ are reduced from 2.7 TB to 6.8 GB by the NIVO approximation.

To justify the NIVO approximation we analyze its effect on the energy. The first term in the BCH series that is approximated in the sq-MR-LDSRG(2)+NIVO scheme is the commutator $\hat{C}_2^{(1)}(s) = [\tilde{H}(s), \hat{A}_2(s)]_2$. Indicating the terms neglected in NIVO as $\delta\hat{C}_2^{(1)}(s)$, we see that the first energy contribution affected by the NIVO approximation comes from the expectation value of the triple commutator term $[\delta\hat{C}_0^{(3)}(s)]$

$$\delta\hat{C}_0^{(3)}(s) = \frac{1}{6}[[\delta\hat{C}_2^{(1)}(s), \hat{A}_2(s)]_{1,2}, \hat{A}_2(s)]_0, \tag{4.19}$$

whose contributions are shown as diagrams in Fig. 4.1. From a perturbation theory perspective, these diagrams are of order four or higher [assuming $\hat{A}_2(s)$ to be of order one] and, therefore, are negligible compared to the leading error (third order) of the linearized commutator approximation.

Hereafter, we shall append "+NIVO" at the end of the method name to indicate

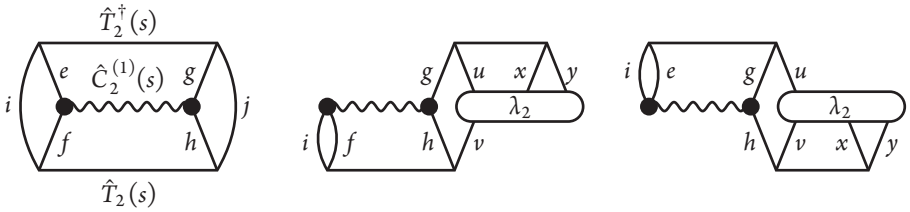

Figure 4.1 Diagrams that are neglected by the NIVO approximation in the evaluation of the term $\hat{C}_0^{(3)}(s)$ as in Eq. (4.19). The wiggly and horizontal solid lines indicate the effective interaction of $\hat{C}_2^{(1)}(s)$ and $\hat{A}_2(s)$, respectively. The two-body density cumulant is labeled by λ_2.

the use of NIVO approximation. For example, the density fitted MR-LDSRG(2) method in the sequential transformation ansatz with NIVO approximation is termed "DF-sq-MR-LDSRG(2)+NIVO".

4.3 Implementation

The sq-MR-LDSRG(2) method combined with DF and the NIVO approximation was implemented in Forte,[104] an open-source suite of multireference theories for molecular computations. This implementation reuses several components of our previous MR-LDSRG(2) code based on conventional four-index two-electron integrals.[55] The DSRG equations were implemented as tensor contractions using the Ambit tensor library,[105] while integrals were generated using the Psi4 package.[106] In the following, we provide the details of our implementation of the sequential ansatz in combination with DF.[107]

4.3.1 Sequential transformation

The $\hat{A}_1(s)$-dressed Hamiltonian [$\tilde{H}(s)$, Eq. (4.16)] can be obtained by a unitary transformation of $\hat{H}$ via the operator $\hat{U}(s) = \exp[\hat{A}_1(s)]$. For clarity, we shall drop the label "(s)" for all s-dependent quantities [$\tilde{H}(s), \hat{A}_1(s)$, and $\hat{U}(s)$] in this section.

The one- and two-body components of $\tilde{H}$ ($\tilde{h}^{q'}_{p'}$ and $\tilde{v}^{r's'}_{p'q'}$) are given by

$$\tilde{h}^{q'}_{p'} = \sum_{pq} U^{q}_{q'}\, h^{q}_{p}\, U^{p'}_{p}, \tag{4.20}$$

$$\tilde{v}^{r's'}_{p'q'} = \sum_{pqrs} U^{r'}_{r}\, U^{s'}_{s}\, v^{rs}_{pq}\, U^{p}_{p'}\, U^{q}_{q'}. \tag{4.21}$$

Here, the unitary matrix $U^{p'}_{p} = (\mathbb{U})_{p'p}$ and its inverse $U^{p}_{p'} = (\mathbb{U})^{*}_{p'p}$ are given by $\mathbb{U} = e^{\mathbb{A}}$, where the matrix $\mathbb{A}$ is composed of elements of the $\hat{A}_1$ tensor, $(\mathbb{A})_{ia} = t^{i}_{a}$ and $(\mathbb{A})_{ai} = -t^{i}_{a}$. Note that we use primed indices only as a way to distinguish labels, yet these indices by no means imply a new set of orbitals.

The $\hat{A}_1$-dressed Hamiltonian written in normal ordered form with respect to Φ is given by

$$\tilde{H} = \tilde{E}_0 + \sum_{pq} \tilde{f}^{q}_{p}\{\hat{a}^{p}_{q}\} + \frac{1}{4}\sum_{pqrs} \tilde{v}^{rs}_{pq}\{\hat{a}^{pq}_{rs}\}, \tag{4.22}$$

where the transformed energy ($\tilde{E}_0$) is given by

$$\tilde{E}_0 = \sum_{i'j'}^{\mathbf{H}} \tilde{h}^{j'}_{i'}\gamma^{i'}_{j'} + \frac{1}{4}\sum_{i'j'k'l'}^{\mathbf{H}} \tilde{v}^{k'l'}_{i'j'}\gamma^{i'j'}_{k'l'}, \tag{4.23}$$

and the Fock matrix elements ($\tilde{f}^{q'}_{p'}$) are defined as

$$\tilde{f}^{q'}_{p'} = \tilde{h}^{q'}_{p'} + \sum_{i'j'}^{\mathbf{H}} \tilde{v}^{q'j'}_{p'i'}\gamma^{i'}_{j'}. \tag{4.24}$$

Note that the quantities $\gamma^{i'}_{j'}$ and $\gamma^{i'j'}_{k'l'}$ in Eqs. (4.23) and (4.24) are the *untransformed* 1- and 2-RDMs of the reference $|\Phi\rangle$ defined as $\gamma^{p}_{q} = \langle\Phi|\hat{a}^{p}_{q}|\Phi\rangle$ and $\gamma^{pq}_{rs} = \langle\Phi|\hat{a}^{pq}_{rs}|\Phi\rangle$, respectively.

The two-electron integral transformation [Eq. (4.21)] has a noticeable cost [$\mathcal{O}(N^5)$] and must be repeated each time the $\hat{A}_1$ operator is updated. However, in the implementation based on DF integrals, this transformation may be performed in a significantly more efficient way. In DF, the four-index electron repulsion integral tensor as a contraction of a three-index auxiliary tensor (B^{Q}_{pq}),

$$\langle pq|rs\rangle \approx \sum_{Q}^{M} B^{Q}_{pr}B^{Q}_{qs}, \tag{4.25}$$

where M is the dimension of the fitting basis in DF. Using this decomposition, the unitary transformation may be directly applied to each auxiliary tensor,

$$\tilde{B}^{Q}_{p'q'} = \sum_{pq} B^{Q}_{pq}\, U^{p}_{p'}\, U^{q}_{q'}, \tag{4.26}$$

reducing the cost to evaluate $\tilde{H}$ down to $\mathcal{O}(N^3M)$.

Equations (4.22)–(4.23) specify the procedures to obtain $\tilde{H}$ as a unitary transformation of $\hat{H}$. Since $\tilde{H}$ retains the structure of $\hat{H}$, we can reuse most of our previous MR-LDSRG(2) code[55] to implement sq-MR-LDSRG(2) by employing $\tilde{H}$ (instead of $\hat{H}$) and removing terms involving $\hat{A}_1$.

As described in Ref. 55, we evaluate the commutator $\hat{C}^{(k+1)} = \frac{1}{k+1}[\hat{C}^{(k)}_{1,2}, \hat{A}]_{0,1,2}$ in Eq. (4.12) using the following recursive system of equations

since $[\hat{C}^{(k)}_{1,2}, \hat{T}^\dagger] = -[\hat{C}^{(k)}_{1,2}, \hat{T}]^\dagger$, computing the

$$\begin{cases} \hat{O}^{(k+1)} = \dfrac{1}{k+1}[\hat{C}^{(k)}_{1,2}, \hat{T}]_{0,1,2}, \\ \hat{C}^{(k+1)} = \hat{O}^{(k+1)} + [\hat{O}^{(k+1)}]^\dagger, \end{cases} \tag{4.27}$$

where $\hat{O}^{(k+1)}$ is an intermediate containing up to two-body components. The iteration starts from either $\hat{C}^{(0)} = \hat{H}$, in traditional MR-LDSRG(2), or $\hat{C}^{(0)} = \tilde{H}$ in the sequential version, optionally applying the NIVO approximation to the two-body intermediate tensors $\hat{O}^{(k)}_2$, $\hat{C}^{(k)}_2$ and $\bar{H}^{(k)}_2$ for $k \geq 1$.

4.3.2 Batched tensor contraction for the DF algorithm

Despite the storage cost reduction of the DF and NIVO approximations, another potential memory bottleneck is the size of the intermediate tensors generated during the evaluation of commutators. For example, consider the following contraction,

$$O^{ij}_{rs} \leftarrow \sum_{ab}^{\mathbf{P}} \langle rs \| ab \rangle\, t^{ij}_{ab} \quad \forall i,j \in \mathbf{H}, \forall r,s \in \mathbf{G}, \tag{4.28}$$

Algorithm 3 The batched algorithm to compute $C^{ij}_{rs} \leftarrow \sum_{ab}^{\mathbf{P}} \sum_{Q}^{M} B^{Q}_{ar} B^{Q}_{bs} t^{ij}_{ab}$.

1: Permute memory layout of C^{ij}_{rs} and B^{Q}_{ar} so that their r-subblocks $C^{ij}_{[r]s}$ and $B^{Q}_{a[r]}$ are contiguous in memory.
2: **for** each $r = 1, 2, \ldots, N_{\mathbf{G}}$ **do**
3: $\quad I_{abs} := \sum_{Q}^{M} B^{Q}_{a[r]} B^{Q}_{bs}$
4: $\quad C^{ij}_{[r]s} \leftarrow \sum_{ab}^{\mathbf{P}} I_{abs} t^{ij}_{ab} \quad i, j \in \mathbf{H}, r \in \mathbf{G}$
5: **end for**
6: Permute C^{ij}_{rs} back to the original memory layout.

which is also found in the CCSD equations. In the DF case, Eq. (4.28) is written as two contractions involving auxiliary tensors,

$$O^{ij}_{rs} \leftarrow \sum_{ab}^{\mathbf{P}} \sum_{Q}^{M} B^{Q}_{ar} B^{Q}_{bs} t^{ij}_{ab} - \sum_{ab}^{\mathbf{P}} \sum_{Q}^{M} B^{Q}_{as} B^{Q}_{br} t^{ij}_{ab}. \tag{4.29}$$

The most efficient way to evaluate the first term of Eq. (4.29) is to introduce the intermediate tensor $I_{arbs} = \sum_{Q}^{M} B^{Q}_{ar} B^{Q}_{bs}$ of size $\mathcal{O}(N^2 N^2_{\mathbf{P}})$. To avoid storage of these large intermediates, it is common to evaluate Eq. (4.29) using a batched algorithm, whereby a slice of the tensor I_{arbs} is computed and contracted on the fly with the amplitudes t^{ij}_{ab}. To automate this optimization of the tensor contraction we have coded a generic batching algorithm in the tensor library Ambit.[105] Whereas the Ambit code for the first term in Eq. (4.29) is written as

```
O["ijrs"] += B["Qar"] * B["Qbs"] * t["ijab"];
```

our new implementation allows batching over the index r by simply surrounding the contraction with the `batched()` function decorator

```
O["ijrs"] += batched("r", B["Qar"] * B["Qbs"] * t["ijab"]);
```

4.3.3 Computational cost reduction

Here we discuss timings for all the MR-LDSRG(2) variants introduced in this work. In MR-LDSRG(2) theory, the computational bottleneck is forming the DSRG transformed Hamiltonian $\bar{H}$. Timings for computing $\bar{H}$ in the case of cyclobutadiene

(see Sec. 4.4.2 for details) are summarized in Fig. 4.2. Detailed timings for the evaluation of $\bar{H}$ using all the combinations of the approximations considered here are reported in the Supplementary Material.

The total timing (t_{tot}) for computing the transformed Hamiltonian in n iterations is partitioned according to

$$t_{\text{tot}} = t_1 + t_2 + t_{\text{misc}}, \tag{4.30}$$

where t_1 and t_2 are the timings to evaluate the commutators involving $\hat{T}_1$ and $\hat{T}_2$, respectively. In the sequential transformation approach, t_1 is instead defined as the time for forming the $\hat{A}_1$-transformed Hamiltonian. The term t_{misc} accounts for the cost to sort and accumulate the results of contractions with $\hat{T}_1$ and $\hat{T}_2$, as shown in the second line of Eq. (4.27). Figure 4.2 shows that the timing for the conventional MR-LDSRG(2) is dominated by contractions involving $\hat{T}_1$ and $\hat{T}_2$. The cost of the singles contractions can be reduced significantly (3–5 times) by employing the sequentially transformed approach, even though at each iteration of the sq-MR-LDSRG(2) equations it is necessary to build the operator $\tilde{H}$.

Applying the NIVO approximation to the original MR-LDSRG(2) leads to a drastic reduction of the total computational time (×18 speedup). This reduction in timings is due to several contributing factors. First, the evaluation of the $\hat{T}_1$ contractions in NIVO is sped up by a factor of $\mathcal{O}(nN/N_{\mathbf{H}})$, where n is the number of commutators included in the BCH series. Second, the contributions due to doubles, $\hat{O}^{(k+1)} \leftarrow [\hat{C}^{(k)}, \hat{T}_2]$, have identical scaling for the first commutator, but for $k \geq 1$ they can be evaluated with a speedup of a factor of $\mathcal{O}(N^2/N_{\mathbf{H}}^2)$. Third, the NIVO approximation also reduces t_{misc} significantly because the tensors transpose and accumulation operations costs are reduced from $\mathcal{O}(N^4)$ to $\mathcal{O}(N^2 N_{\mathbf{H}}^2)$. For large $N/N_{\mathbf{H}}$ ratios, the cost to evaluate $\bar{H}$ in the NIVO approximation is dominated by the commutator $[\hat{H}, \hat{T}_2]$, with scaling identical to that of CCSD. For comparison, the similarity-transformed Hamiltonian can be evaluated in 24 s with Psi4's CCSD, in 121

s with our NIVO-MR-LDSRG(2) code, and 2208 s with the original MR-LDSRG(2) code (in both cases employing an unrestricted implementation and C_1 symmetry).

In general, we observe an increase in t_2 due to the extra cost to build two-body intermediates from the auxiliary tensors for methods combined with DF. The traditional and sequential approaches using the DF/NIVO approximations have similar costs, with the latter being slightly faster due to the efficient transformation of the auxiliary tensors [$\tilde{B}$, Eq. (4.26)] afforded by the DF approximation. For this example, the DF-sq-MR-LDSRG(2)+NIVO computation ran 12 times faster than the one using the original approach. As we will demonstrate in the next section, this method is as accurate as the MR-LDSRG(2) and, therefore, the method we recommend for large-scale computations.

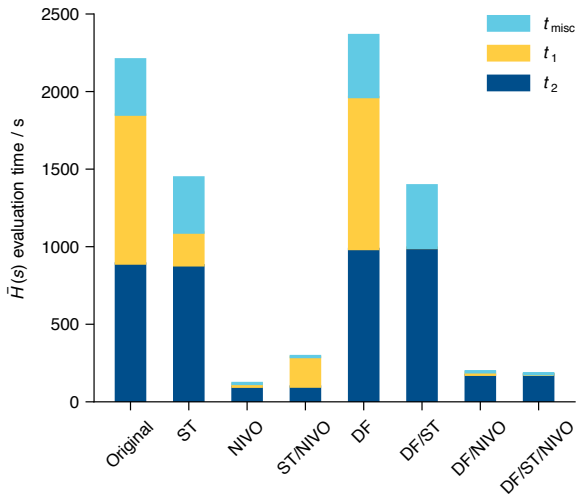

Figure 4.2 The time to evaluate the DSRG transformed Hamiltonian [$\bar{H}$] of the ground-state cyclobutadiene when different techniques are introduced to the MR-LDSRG(2) method. These techniques include: density fitting (DF), sequential transformation (ST), and the non-interacting virtual orbital (NIVO) approximation. The total time of computing [$\hat{C}^{(k)}, \hat{T}_1$] in MR-LDSRG(2) or $\tilde{H} = e^{-\hat{A}_1} \hat{H} e^{\hat{A}_1}$ in sq-MR-LDSRG(2) is labeled as t_1 in this plot. All computations employed the cc-pVTZ basis set and they were carried out on an Intel Xeon E5-2650 v2 processor using 8 threads.

4.4 Results and Discussion

4.4.1 First row diatomic molecules

We first benchmark the effect of DF and the NIVO approximation on the traditional and sequential versions of the MR-LDSRG(2). Our test set consists of eight diatomic molecules: BH, HF, LiF, BeO, CO, C_2, N_2, and F_2. Specifically, we computed equilibrium bond lengths (r_e), harmonic vibrational frequencies (ω_e), anharmonicity constants ($\omega_e x_e$), and dissociation energies (D_0) and compare those to experimental data taken from Ref. 108. The dissociation energy D_0 includes zero-point vibrational energy corrections that account for anharmonicity effects and is computed as $D_0 = D_e - \omega_e/2 + \omega_e x_e/4$ (in a.u.), where D_e is the dissociation energy with respect to the bottom of the potential.[109] Since our current implementation of the MR-DSRG cannot handle half-integer spin states, the energies of the atoms Li, B, C, N, O, and F were computed as half of the energy of the stretched homonuclear diatomic molecule at a distance of 15 Å. All spectroscopic constants were obtained via a polynomial fit of the energy using nine equally spaced points centered around the equilibrium bond length and separated by 0.2 Å. For all eight molecules, we adopted a full-valence active space where the 1s orbital of hydrogen, and the 2s and 2p orbitals of first-row elements are considered as active orbitals. No orbitals were frozen in the CASSCF optimization procedure. The flow parameter for all DSRG computations was set to $s = 0.5\ E_\mathrm{h}^{-2}$, as suggested by our previous work.[54] All computations utilized the cc-pVQZ basis set[110,111] and 1s-like orbitals of the first-row elements were frozen in the CC and MR-DSRG treatments of electron correlation. In DF computations, we employed a mixed flavor of the auxiliary basis sets. For CASSCF, the cc-pVQZ-JKFIT auxiliary basis set[81] was used for H, B, C, N, O and F atoms, and the def2-QZVPP-JKFIT basis set[112] was used for Li and Be atoms. The cc-pVQZ-RI basis set[113] was applied to all atoms in DSRG computations.

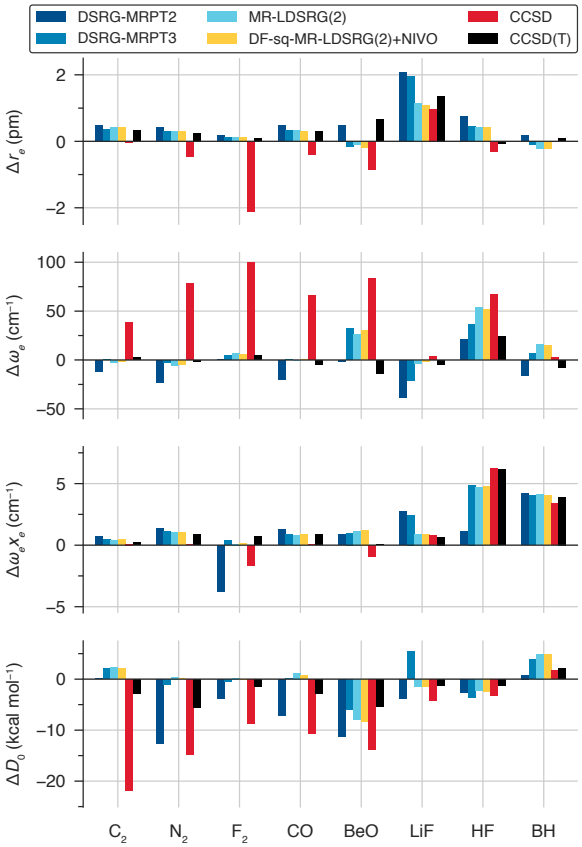

Figure 4.3 Comparison of second- and third-order MR-DSRG perturbation theory (DSRG-MRPT2, DSRG-MRPT3), MR-LDSRG(2), DF-sq-MR-LDSRG(2)+NIVO, and single reference coupled cluster methods on a test set composed of 8 diatomic molecules. Deviations of equilibrium bond lengths (r_e), harmonic vibrational frequencies (ω_e), anharmonicity constants ($\omega_e x_e$), and dissociation energies (D_0) with respect to experimental values.[108] All results were computed with cc-pVQZ basis, and core orbitals are frozen in MR-DSRG and coupled cluster computations.

Figure 4.3 and Table 4.1 report a comparison of second- and third-order DSRG multireference perturbation theory (DSRG-MRPT2/3), the original MR-LDSRG(2), DF-sq-LDSRG(2)+NIVO, CCSD, and CCSD(T). The mean absolute error (MAE) and standard deviation (SD) reported in Table 4.1 show that MR-LDSRG(2) method is as accurate as CCSD(T) in predicting r_e, $\omega_e x_e$ and D_0, while it predicts ω_e that are of accuracy between that of CCSD and CCSD(T).

The fact that the MR-LDSRG(2) results are more accurate than those from CCSD suggests that the full-valence treatment of static correlation leads to a more accurate treatment of correlation. It is also rewarding to see that in many instances the MR-

Table 4.1 Error statistics for the equilibrium bond lengths (r_e, in pm), harmonic vibrational frequencies (ω_e, in cm^{-1}), anharmonicity constants ($\omega_e x_e$, in cm^{-1}), and dissociation energies (D_0, in kcal mol^{-1}) of the eight diatomic molecules computed using various MR-DSRG schemes. All results were obtained using the cc-pVQZ basis and core orbitals were frozen in the MR-DSRG and CC computations. The statistical indices are: mean signed error (Mean), mean absolute error (MAE), standard deviation (SD), and maximum absolute error (Max).

		DSRG-MRPT		MR-LDSRG(2)			sq-MR-LDSRG(2)			DF-sq-MR-LDSRG(2)+NIVO			CCSD	CCSD(T)
		PT2	PT3	Conv.[a]	DF	DF+NIVO	Conv.[a]	DF	DF+NIVO	comm(2)	comm(3)	comm(4)		
r_e	Mean	0.63	0.41	0.30	0.30	0.30	0.28	0.28	0.28	0.28	0.28	0.28	−0.41	0.38
	MAE	0.63	0.48	0.39	0.39	0.38	0.39	0.39	0.39	0.40	0.38	0.39	0.65	0.40
	SD	0.85	0.74	0.49	0.50	0.49	0.48	0.48	0.48	0.49	0.48	0.48	0.92	0.57
	Max	2.07	1.96	1.15	1.15	1.15	1.10	1.10	1.10	1.11	1.10	1.09	2.13	1.36
ω_e	Mean	−11.2	7.2	11.2	11.1	11.1	11.8	11.9	11.8	13.0	11.9	11.9	54.9	−0.1
	MAE	16.5	13.1	14.3	14.2	14.3	13.8	13.9	13.9	16.0	13.8	13.9	54.9	7.9
	SD	20.0	19.0	22.0	21.9	22.0	21.9	22.1	22.1	26.3	21.6	22.2	64.5	10.7
	Max	38.3	36.1	53.2	52.8	53.7	51.2	51.8	51.9	64.5	50.3	52.3	99.3	24.5
$\omega_e x_e$	Mean	1.1	1.9	1.7	1.5	1.7	1.7	1.8	1.7	1.9	1.6	1.7	1.0	1.7
	MAE	2.0	1.9	1.7	1.5	1.7	1.7	1.8	1.7	1.9	1.6	1.7	1.6	1.7
	SD	2.4	2.5	2.3	2.1	2.3	2.3	2.6	2.3	2.6	2.2	2.3	2.6	2.6
	Max	4.2	4.9	4.7	4.1	4.8	4.8	5.7	4.7	5.9	4.4	4.8	6.2	6.2
D_0	Mean	−5.0	0.1	−0.3	−0.1	−0.0	−0.6	−0.3	−0.5	−1.0	−0.5	−0.3	−9.5	−2.4
	MAE	5.3	2.8	2.6	2.8	2.6	2.6	2.9	2.5	3.1	2.7	2.8	9.9	2.9
	SD	6.8	3.5	3.5	3.7	3.5	3.7	3.8	3.6	4.0	3.7	3.8	11.8	3.3
	Max	12.7	6.0	7.9	7.8	7.5	8.4	8.4	8.3	8.6	8.4	8.2	21.9	5.6

[a] Computed using conventional four-index two-electron integrals.

LDSRG(2) has an accuracy similar to that of CCSD(T), despite the fact that the former does not include triples corrections.

To analyze the impact of each approximation of the MR-LDSRG(2) method, in Table 4.2 we report the mean absolute difference between properties computed with and without each approximation. The use of a sequential ansatz has a modest effect on all properties, with the largest mean absolute differences observed for ω_e (1.6 cm^{-1}) and D_0 (0.3 kcal mol^{-1}). Nevertheless, the MAE with respect experimental results is nearly unchanged, if not slightly improving. The DF and NIVO approximations have an effect on molecular properties that is comparable in magnitude and smaller than the deviation introduced by the sequential ansatz. When these three approximations are combined together, the resulting method shows errors with respect to experimental values that are nearly identical to those from the conventional MR-LDSRG(2). The only noticeable deviations are found for ω_e (MAE 13.9 vs. 14.3 cm^{-1}) and D_0 (MAE 2.6 vs. 2.5 kcal mol^{-1}).

In this study, we also investigate the effect of combining the DF-sq-LDSRG(2)+NIVO method with truncation of the BCH expansion, i.e., terminating

Table 4.2 The mean absolute differences in predicting equilibrium bond lengths (r_e, in pm), harmonic vibrational frequencies (ω_e, in cm^{-1}), anharmonicity constants ($\omega_e x_e$, in cm^{-1}), and dissociation energies (D_0, in kcal mol^{-1}) of the eight diatomic molecules between method pairs that differ by only one technique introduced in this report. Techniques include: sequential transformation (ST), density fitting (DF), NIVO approximation, and commutator truncation of the BCH expansion [comm(k), $k = 2, 3, 4$]. All results were computed using the cc-pVQZ basis set and core orbitals were frozen in the MR-DSRG computations.

Technique	MR-LDSRG(2) method pair		Mean absolute difference			
			r_e	ω_e	$\omega_e x_e$	D_0
ST	Original	ST	0.03	1.6	0.0	0.3
	DF	DF/ST	0.03	1.5	0.3	0.2
DF	Original	DF	0.00	0.2	0.1	0.2
	ST	DF/ST	0.00	0.2	0.1	0.3
NIVO	DF	DF/NIVO	0.01	0.4	0.1	0.2
	DF/ST	DF/ST/NIVO	0.01	0.3	0.1	0.3
comm(4)	DF/ST/NIVO	DF/ST/NIVO/comm(4)	0.00	0.1	0.0	0.3
4$^{\text{th}}$ comm.	DF/ST/NIVO/comm(4)	DF/ST/NIVO/comm(3)	0.01	0.8	0.1	0.4
3$^{\text{rd}}$ comm.	DF/ST/NIVO/comm(3)	DF/ST/NIVO/comm(2)	0.04	4.3	0.3	0.6

$\bar{H}(s) = \tilde{H}(s) + \sum_{n=1}^{k} \frac{1}{n!} \hat{C}^{(n)}(s)$ at a given integer k. The recursive evaluation of $\bar{H}(s)$ via Eq. (4.12) usually requires 10–12. Truncation of the BCH series to a few terms may therefore introduce speedups of up to 3–4 times. In Table 4.1 and Table 4.2 we report statistics computed by approximating the BCH expansion up to 2, 3, and 4 commutators. The use of only two commutator introduces noticeable deviations with respect to experiments for ω_e and D_0. Compared to the full BCH series, this truncation level increases the MAE of ω_e and D_0 by 12.6 cm^{-1} and 0.5 kcal mol^{-1}, respectively. The inclusion of the triply-nested commutator significantly reduces these deviations to only 0.1 cm^{-1} and 0.2 kcal mol^{-1}, respectively. The four-fold commutator term yields r_e, ω_e, and $\omega_e x_e$ that are nearly identical to those from the untruncated BCH series, while the MAE of D_0 deviates only by 0.3 kcal mol^{-1}.

Since the error introduced by neglecting the four commutator term is smaller or comparable to the other approximations considered here, our results suggest that a BCH series truncated to three commutators may offer a good compromise between accuracy and speed.

4.4.2 Cyclobutadiene

Next, we consider the automerization reaction of cyclobutadiene (CBD, C_4H_4). We study the energy difference between the rectangular (D_{2h}) energy minimum and the square transition state (D_{4h}).[114] This reaction is a challenging chemistry problem for both experiment and theory.[114,115,115–120,120–126] Due to its instability, there are no direct measurements of the reaction barrier, and experiments performed on substituted cyclobutadienes suggest the barrier height falls in the range 1.6–10 kcal mol^{-1}.[115] In this work, we optimized the equilibrium and transition state geometries using finite differences of energies to compute the barrier height. Specifically, we compare both DF-MR-LDSRG(2)+NIVO and DF-sq-MR-LDSRG(2)+NIVO optimized geometries to those obtained from the state-specific MRCC of Mukherjee and co-workers (Mk-MRCC)[20,127–130] as implemented in Psi4.[131]

To reduce computational cost, all MR-DSRG calculations performed two steps of the reference relaxation procedure discussed in Sec. 4.2.1. A comparison of this procedure with full reference relaxation using the cc-pVDZ basis set shows errors of ca. 0.01 kcal mol^{-1} for absolute energies, 0.0001 Å for bond lengths, and 0.001° for bond angles. We applied a Tikhonov regularization denominator shift[132] of 1 mE_h in all Mk-MRCC calculations to guarantee convergence. The Mk-MRCC implementation used in this work neglects effective Hamiltonian couplings between reference determinants that differ by three or more spin orbitals, and therefore yield approximate results when applied to the CAS(4e,4o) reference considered here. All computations utilized the cc-pVXZ (X=D, T, Q, 5) basis set,[110,111] and the corresponding cc-pVXZ-JKFIT[81] and cc-pVXZ-RI[113] auxiliary basis sets for DF-CASSCF and DF-DSRG computations, respectively. The 1s core electrons of carbon atoms were frozen in all post-CASSCF methods. All results were computed using semi-canonical CASSCF orbitals.

Preliminary computations using the cc-pVDZ basis using the CAS(2e,2o) and CAS(4e,4o) active spaces revealed an interesting aspect of this system. As shown in

Fig. 4.4, the s-dependency of the automerization barrier displays significantly different behavior for these two active spaces. In both cases, the predicted activation energies change significantly for small values of s ($< 0.2\ E_\mathrm{h}^{-2}$), a normal trend observed for all DSRG computations and due to the increased recovery of dynamical correlation energy. Interestingly, while the CAS(4e,4o) curve flattens out for larger values of s, the CAS(2e,2o) curve shows a significant s-dependence in the range $s \in [0.5, 8]\ E_\mathrm{h}^{-2}$.

To understand the origin of this difference we analyze the double substitution amplitudes $[t_{ab}^{ij}(s)]$ as a function of s for both the equilibrium and transition state geometries, as shown in Fig. 4.5. In the CAS(2e,2o) case, we notice some abnormally large amplitudes (indicated in red), some of which are as large as 0.1. These amplitudes correspond to excitations within the four π orbitals of CBD, and suggests that the CAS(2e,2o) space is insufficient to capture all static correlation effects in CBD. The offending amplitudes converge at different rates as s increases, and introduce a strong s-dependence in the energy barrier. Note also that in the limit of $s \to \infty$ there is a significant difference in the barrier for the CAS(2e,2o) and CAS(4e,4o) spaces.

In contrast, in the CAS(4e,4o) computations all excitations within the π orbitals are included in the active space and the resulting DSRG amplitudes have absolute values less than 0.05. Diverging amplitudes in computations with CAS(4e,4o) reference wave functions, corresponding to intruder states, can also be seen in Fig. 4.5. Our results reported in Table 4.3 are all based on the flow parameter value $s = 1.0\ E_\mathrm{h}^{-2}$, which is significantly far from the region ($s > 5.0\ E_\mathrm{h}^{-2}$) where amplitudes begin to diverge, and at the same time leads to well converged absolute energies. We also performed computations using $s = 0.5\ E_\mathrm{h}^{-2}$ (reported in Table S4) to verify that the automerization energies computed with different values of the flow parameter are consistent. In general, the difference in automerization energies computed with $s = 0.5$ and $1.0\ E_\mathrm{h}^{-2}$ is of the order of 0.6–0.7 kcal mol^{-1}. Note that intruder states are also encountered in Mk-MRCCSD computations based on the CAS(4e,4o) reference, and

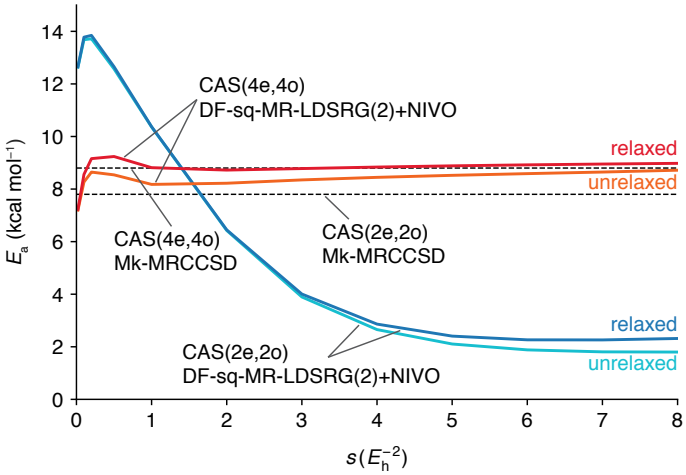

Figure 4.4 The automerization barrier (E_a) of cyclobutadiene computed using the DF-sq-MR-LDSRG(2)+NIVO theory with varying flow parameters. Results were obtained using the cc-pVDZ basis set. We also applied a Tikhonov regularization denominator shift[132] of 1 mE_h in all Mk-MRCC calculations to guarantee convergence.

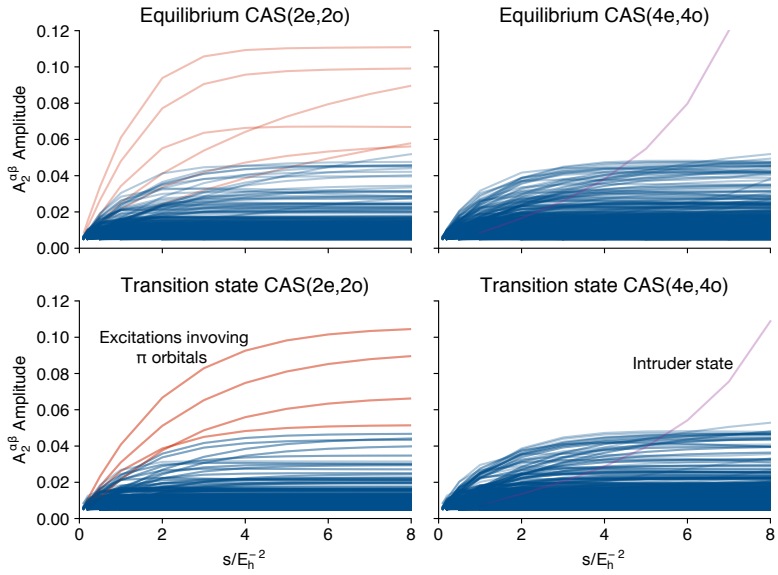

Figure 4.5 The unrelaxed DF-sq-MR-LDSRG(2)+NIVO/cc-pVDZ double substitution amplitudes involving both alpha and beta electrons ($A_2^{\alpha\beta}$) as a function of the flow parameter s for the rectangular equilibrium and the square transition state of cyclobutadiene.

Table 4.3 Automerization reaction barrier (E_a, in kcal mol^{-1}) and geometry parameters (bond lengths in Å, bond angles in degree) of cyclobutadiene. All DSRG computations used $s = 1.0\ E_\mathrm{h}^{-2}$. All computations employed the CAS(4e,4o) reference and core orbitals constructed from carbon 1s orbitals were frozen for MR-DSRG and MRCC computations. As such, $n_\mathbf{C} = 8$ and $n_\mathbf{A} = 4$, where $n_\mathbf{X} = N_\mathbf{X}/2$ ($\mathbf{X} \in \{\mathbf{C}, \mathbf{A}, \mathbf{V}, \mathbf{H}, \mathbf{P}, \mathbf{G}\}$) is the number molecular spacial orbitals for space $\mathbf{X}$.

Method	E_a	D_{2h}				D_{4h}	
		C−C[a]	C=C[a]	C−H	∠C−C−H[b]	C−C	C−H
cc-pVDZ ($n_\mathbf{V} = 60$)							
CASSCF	6.49	1.5502	1.3567	1.0790	134.87	1.4472	1.0779
DF-MR-LDSRG(2)+NIVO	8.56	1.5769	1.3660	1.0945	134.92	1.4624	1.0932
DF-sq-MR-LDSRG(2)+NIVO	8.62	1.5768	1.3659	1.0944	134.92	1.4623	1.0931
Mk-MRCCSD	8.80	1.5733	1.3623	1.0931	134.91	1.4585	1.0920
Mk-MRCCSD(T)	7.56	1.5772	1.3699	1.0951	134.92	1.4652	1.0941
cc-pVTZ ($n_\mathbf{V} = 160$)							
CASSCF	7.44	1.5475	1.3471	1.0694	134.83	1.4409	1.0683
DF-MR-LDSRG(2)+NIVO	9.87	1.5668	1.3488	1.0789	134.91	1.4483	1.0775
DF-sq-MR-LDSRG(2)+NIVO	9.93	1.5666	1.3487	1.0788	134.91	1.4481	1.0774
Mk-MRCCSD	10.09	1.5628	1.3452	1.0775	134.89	1.4442	1.0764
Mk-MRCCSD(T)	8.56	1.5671	1.3535	1.0797	134.90	1.4515	1.0786
cc-pVQZ ($n_\mathbf{V} = 324$)							
CASSCF	7.53	1.5467	1.3462	1.0689	134.84	1.4400	1.0678
DF-MR-LDSRG(2)+NIVO	10.16	1.5634	1.3452	1.0782	134.96	1.4447	1.0768
DF-sq-MR-LDSRG(2)+NIVO	10.21	1.5631	1.3451	1.0781	134.96	1.4446	1.0766
Mk-MRCCSD	10.28	1.5591	1.3417	1.0768	134.94	1.4406	1.0756
Mk-MRCCSD(T)	8.69	1.5634	1.3500	1.0791	134.95	1.4480	1.0779
cc-pV5Z ($n_\mathbf{V} = 568$)							
DF-MR-LDSRG(2)+NIVO[c]	10.26						
DF-sq-MR-LDSRG(2)+NIVO[c]	10.30						

[a] C−C and C=C refer to the longer and shorter carbon–carbon bonds, respectively.
[b] ∠C−C−H is the bond angle between the C−H bond and the longer C−C bond.
[c] Based on the corresponding cc-pVQZ optimized geometries.

lead to convergence issues that could be avoided only via Tikhonov regularization.

Geometric parameters for the optimized structures and energy barriers of CBD computed with the CAS(4e,4o) reference are reported in Table 4.3. A comparison the energy barrier computed at the CASSCF and correlated levels shows that dynamical correlation is important in this system as it increases is by about 1–3 kcal mol^{-1}. Our best estimate for the automerization barrier of CBD is 10.3 kcal mol^{-1} at the DF-sq-MR-LDSRG(2)+NIVO/cc-pV5Z level of theory. This value is likely to be slightly higher then the exact results since in the Mk-MRCC results perturbative triples corrections contribute to lowering the barrier by ca. 1.5 kcal mol^{-1}. In general, the MR-LDSRG(2) results are between those of Mk-MRCCSD and Mk-

MRCCSD(T), reinforcing the same observation we made in the benchmark of diatomic molecules. For instance, the MR-LDSRG(2) predicted C−C bond length at the D_{4h} geometry is 1.4446 Å, which is almost midway between the Mk-MRCCSD (1.4406 Å) and Mk-MRCCSD(T) (1.4480 Å) values. As expected, the differences between the conventional and sequentially transformed MR-DSRG(2) results are negligible. Our results in cc-pVDZ and cc-pVTZ bases also agree well with other reported theoretical values, especially those computed with multireference methods,[114,117,120,120–125] and the experimental range reported in Ref. 115. Using our new implementation, we were able to perform, for the first time, nonperturbative multireference computations on cyclobutadiene using the cc-pV5Z basis (580 correlated orbitals) on a single node with 128 GB of memory.

4.5 Conclusion

In this work, we describe a strategy to reduce the computational and memory costs of the multireference driven similarity renormalization group (MR-DSRG). We demonstrate that the cost of the linear MR-DSRG with singles and doubles [MR-LDSRG(2)] can be lowered substantially without compromising its accuracy by using a combination of: 1) a sequential unitary transformation, 2) density fitting (DF) of the two-electron integrals, and 3) the non-interacting virtual orbital (NIVO) operator approximation. The sequential MR-DSRG scheme introduced in this work [sq-MR-DSRG] reduces the cost of evaluating single-excitations and allows to treat them exactly. Like in the case of Brueckner coupled cluster theory,[133–135] this approach reduces the number of algebraic terms in the DSRG equations because there are no terms (diagrams) containing single excitations. The use of DF integrals reduces the memory requirements of the original MR-DSRG(2) from $\mathcal{O}(N^4)$ to $\mathcal{O}(N^2M)$, where N is the number of basis functions. Density fitting is particularly convenient when combined with the sequential approach because the contributions of singles can be

directly included in the DF auxiliary three-index integrals, reducing the integral transformation cost from $\mathcal{O}(N^5)$ to $\mathcal{O}(N^3M)$, where M is the number of auxiliary basis functions. The NIVO approximation neglects the operator components of a commutator with three or more virtual indices. A formal analysis of this approximation showed that the leading error is of fourth order in perturbation theory. In practice, NIVO is crucial to both avoiding the memory bottleneck of the MR-DSRG(2) and reducing the computational cost to evaluate the transformed Hamiltonian.

To benchmark the MR-LDSRG(2) and sq-MR-LDSRG(2) approaches and assess the impact of the DF and NIVO approximations, we computed the spectroscopic constants of eight diatomic molecules using the full-valence active space and the cc-pVQZ basis set. Compared to experimental data, both MR-DSRG methods yield results that are as accurate as those obtained with CCSD(T). Moreover, the DF-sq-MR-LDSRG(2)+NIVO results are almost identical to those computed without the NIVO approximation: the harmonic vibrational frequencies, anharmonicity constants, and dissociation energies only differ by, on average, 0.1 cm^{-1}, 0.1 cm^{-1}, and 0.2 kcal mol^{-1}, respectively. These results supports our claim that the speedup brought by the NIVO approximation does not sacrifice the accuracy of both variants of the MR-LDSRG(2).

Combining DF and the NIVO approximation, both the traditional and sequential MR-LDSRG(2) can be routinely applied to chemical systems with more than 500 basis function. We demonstrate this point by studying the automerization reaction of cyclobutadiene using a quintuple-ζ basis set (584 basis functions). Our best estimate of the reaction barrier from DF-sq-MR-LDSRG(2)+NIVO/cc-pV5Z is 10.3 kcal mol^{-1}. However, we expect that this result is likely overestimated due to the lack of three-body corrections in the MR-LDSRG(2) theory. Our results agree well with Mk-MRCCSD predictions and multireference coupled cluster reported in the literature.

In conclusion, we have shown that it is possible to significantly reduce the cost of MR-LDSRG(2) computations without reducing the accuracy of this approach. The sequential approach and NIVO approximations are general, and can be applied to improve the efficiency of other unitary nonperturbative methods (e.g., unitary coupled cluster theory) and downfolding schemes for classical-quantum hybrid algorithms.[47]

Acknowledgments

This work was supported by the U.S. Department of Energy under Award No. DE-SC0016004, a Research Fellowship of the Alfred P. Sloan Foundation, and a Camille Dreyfus Teacher-Scholar Award.

Bibliography

[1] (a) Andersson, K.; Malmqvist, P.-Å.; Roos, B. O.; Sadlej, A. J.; Wolinski, K. *J. Phys. Chem.* **1990**, *94*, 5483–5488; (b) Andersson, K.; Malmqvist, P.-Å.; Roos, B. O. *J. Chem. Phys.* **1992**, *96*, 1218–1226.

[2] Hirao, K. *Chem. Phys. Lett.* **1992**, *190*, 374–380.

[3] Nakano, H. *J. Chem. Phys.* **1993**, *99*, 7983–7992.

[4] Werner, H.-J. *Mol. Phys.* **1996**, *89*, 645–661.

[5] Mahapatra, U. S.; Datta, B.; Mukherjee, D. *J. Phys. Chem. A* **1999**, *103*, 1822–1830.

[6] (a) Angeli, C.; Cimiraglia, R.; Evangelisti, S.; Leininger, T.; Malrieu, J. P. *J. Chem. Phys.* **2001**, *114*, 10252–10264; (b) Angeli, C.; Pastore, M.; Cimiraglia, R. *Theor. Chem. Acc.* **2007**, *117*, 743–754.

[7] Liu, B. *J. Chem. Phys.* **1973**, *58*, 1925–1937.

[8] (a) Werner, H.-J.; Knowles, P. J. *J. Chem. Phys.* **1988**, *89*, 5803–5814; (b) Knowles, P. J.; Werner, H.-J. *Chem. Phys. Lett.* **1988**, *145*, 514–522.

[9] (a) Hanrath, M.; Engels, B. *Chem. Phys.* **1997**, *225*, 197–202.

[10] Szalay, P. G.; Müller, T.; Gidofalvi, G.; Lischka, H.; Shepard, R. *Chem. Rev.* **2012**, *112*, 108–181.

[11] Sivalingam, K.; Krupicka, M.; Auer, A. A.; Neese, F. *J. Chem. Phys.* **2016**, *145*, 054104.

[12] Čížek, J. *Adv. Chem. Phys.* **1969**, *14*, 35–89.

[13] Jeziorski, B.; Monkhorst, H. J. *Phys. Rev. A* **1981**, *24*, 1668–1681.

[14] Haque, M. A.; Mukherjee, D. *J. Chem. Phys.* **1984**, *80*, 5058–5069.

[15] Stolarczyk, L. Z.; Monkhorst, H. J. *Phys. Rev. A* **1985**, *32*, 725–742.

[16] Malrieu, J. P.; Durand, P.; Daudey, J. P. *J. Phys. A: Math. Gen.* **1985**, *18*, 809–826.

[17] Lindgren, I.; Mukherjee, D. *Phys. Rep.* **1987**, *151*, 93–127.

[18] (a) Piecuch, P.; Paldus, J. *Theor. Chim. Acta* **1992**, *83*, 69–103; (b) Paldus, J.; Piecuch, P.; Pylypow, L.; Jeziorski, B. *Phys. Rev. A* **1993**, *47*, 2738–2782.

[19] Mášik, J.; Hubač, I. *Adv. Quantum Chem.* **1998**, *31*, 75–104.

[20] Mahapatra, U. S.; Datta, B.; Bandyopadhyay, B.; Mukherjee, D. *Adv. Quantum Chem.* **1998**, *30*, 163–193.

[21] (a) Mahapatra, U. S.; Datta, B.; Mukherjee, D. *Mol. Phys.* **1998**, *94*, 157–171; (b) Mahapatra, U. S.; Datta, B.; Mukherjee, D. *J. Chem. Phys.* **1999**, *110*, 6171–6188.

[22] Li, S. *J. Chem. Phys.* **2004**, *120*, 5017–5026.

[23] Hanrath, M. *J. Chem. Phys.* **2005**, *123*, 084102.

[24] Evangelista, F. A.; Gauss, J. *J. Chem. Phys.* **2011**, *134*, 114102.

[25] Hanauer, M.; Köhn, A. *J. Chem. Phys.* **2011**, *134*, 204111.

[26] Datta, D.; Kong, L.; Nooijen, M. *J. Chem. Phys.* **2011**, *134*, 214116.

[27] Chen, Z.; Hoffmann, M. R. *J. Chem. Phys.* **2012**, *137*, 014108.

[28] Hoffmann, M. R.; Simons, J. *J. Chem. Phys.* **1988**, *88*, 993–1002.

[29] Bartlett, R. J.; Kucharski, S. A.; Noga, J. *Chem. Phys. Lett.* **1989**, *155*, 133–140.

[30] Watts, J. D.; Trucks, G. W.; Bartlett, R. J. *Chem. Phys. Lett.* **1989**, *157*, 359–366.

[31] Kutzelnigg, W. *Theor. Chim. Acta* **1991**, *80*, 349–386.

[32] Mertins, F.; Schirmer, J. *Phys. Rev. A* **1996**, *53*, 2140–2152.

[33] Taube, A. G.; Bartlett, R. J. *Int. J. Quantum Chem.* **2006**, *106*, 3393–3401.

[34] Harsha, G.; Shiozaki, T.; Scuseria, G. E. *J. Chem. Phys.* **2018**, *148*, 044107.

[35] Yung, M. H.; Casanova, J.; Mezzacapo, A.; McClean, J.; Lamata, L.; Aspuru-Guzik, A.; Solano, E. *Sci Rep* **2014**, *4*, 714.

[36] Peruzzo, A.; McClean, J.; Shadbolt, P.; Yung, M.-H.; Zhou, X.-Q.; Love, P. J.; Aspuru-Guzik, A.; O'Brien, J. L. *Nat Commun* **2014**, *5*, 36.

[37] O'Malley, P. J. J.; Babbush, R.; Kivlichan, I. D.; Romero, J.; McClean, J. R.; Barends, R.; Kelly, J.; Roushan, P.; Tranter, A.; Ding, N.; Campbell, B.; Chen, Y.; Chen, Z.; Chiaro, B.; Dunsworth, A.; Fowler, A. G.; Jeffrey, E.; Lucero, E.;

Megrant, A.; Mutus, J. Y.; Neeley, M.; Neill, C.; Quintana, C.; Sank, D.; Vainsencher, A.; Wenner, J.; White, T. C.; Coveney, P. V.; Love, P. J.; Neven, H.; Aspuru-Guzik, A.; Martinis, J. M. *Phys. Rev. X* **2016**, *6*, 361.

[38] Shen, Y.; Zhang, X.; Zhang, S.; Zhang, J.-N.; Yung, M.-H.; Kim, K. *Phys. Rev. A* **2017**, *95*, 020501.

[39] Dumitrescu, E. F.; McCaskey, A. J.; Hagen, G.; Jansen, G. R.; Morris, T. D.; Papenbrock, T.; Pooser, R. C.; Dean, D. J.; Lougovski, P. *Phys. Rev. Lett.* **2018**, *120*, 210501.

[40] Ryabinkin, I. G.; Yen, T.-C.; Genin, S. N.; Izmaylov, A. F. *J. Chem. Theory Comput.* **2018**, *14*, 6317–6326.

[41] Hempel, C.; Maier, C.; Romero, J.; McClean, J.; Monz, T.; Shen, H.; Jurcevic, P.; Lanyon, B. P.; Love, P.; Babbush, R.; Aspuru-Guzik, A.; Blatt, R.; Roos, C. F. *Phys. Rev. X* **2018**, *8*, 031022.

[42] Romero, J.; Babbush, R.; McClean, J. R.; Hempel, C.; Love, P. J.; Aspuru-Guzik, A. *Quantum Sci. Technol.* **2019**, *4*, 014008.

[43] Lee, J.; Huggins, W. J.; Head-Gordon, M.; Whaley, K. B. *J. Chem. Theory Comput.* **2018**, *15*, 311–324.

[44] Li, Y.; Hu, J.; Zhang, X. M.; Song, Z.; Yung, M.-H. *Adv. Theory Simul.* **2019**, *309*, 1800182.

[45] Kühn, M.; Zanker, S.; Deglmann, P.; Marthaler, M.; Weiß, H. `arXiv:1812.06814 [quant-ph]` **2018**,

[46] Nam, Y.; Chen, J.-S.; Pisenti, N. C.; Wright, K.; Delaney, C.; Maslov, D.; Brown, K. R.; Allen, S.; Amini, J. M.; Apisdorf, J.; Beck, K. M.; Blinov, A.; Chaplin, V.; Chmielewski, M.; Collins, C.; Debnath, S.; Ducore, A. M.; Hudek, K. M.;

Keesan, M.; Kreikemeier, S. M.; Mizrahi, J.; Solomon, P.; Williams, M.; Wong-Campos, J. D.; Monroe, C.; Kim, J. `arXiv:1902.10171v2 [quant-ph]` **2019**,

[47] Bauman, N. P.; Bylaska, E. J.; Krishnamoorthy, S.; Low, G. H.; Wiebe, N.; Kowalski, K. `arXiv:1902.01553v2 [quant-ph]` **2019**,

[48] Evangelista, F. A. *J. Chem. Phys.* **2011**, *134*, 224102.

[49] Hanauer, M.; Köhn, A. *J. Chem. Phys.* **2012**, *136*, 204107.

[50] (a) Yanai, T.; Chan, G. K.-L. *J. Chem. Phys.* **2006**, *124*, 194106; (b) Yanai, T.; Chan, G. K.-L. *J. Chem. Phys.* **2007**, *127*, 104107.

[51] Wegner, F. *Ann. Phys.* **1994**, *506*, 77–91.

[52] Kehrein, S. *The Flow Equation Approach to Many-Particle Systems*; Springer Berlin Heidelberg, 2006.

[53] Evangelista, F. A. *J. Chem. Phys.* **2014**, *141*, 054109.

[54] Li, C.; Evangelista, F. A. *J. Chem. Theory Comput.* **2015**, *11*, 2097–2108.

[55] (a) Li, C.; Evangelista, F. A. *J. Chem. Phys.* **2016**, *144*, 164114; (b) Li, C.; Evangelista, F. A. *J. Chem. Phys.* **2018**, *148*, 079903.

[56] Li, C.; Evangelista, F. A. *J. Chem. Phys.* **2018**, *148*, 124106.

[57] Li, C.; Evangelista, F. A. *Annu. Rev. Phys. Chem.* **2019**, *70*, 275–303.

[58] Meller, J.; Malrieu, J. P.; Caballol, R. *J. Chem. Phys.* **1996**, *104*, 4068–4076.

[59] Köhn, A.; Hanauer, M.; Mück, L. A.; Jagau, T.-C.; Gauss, J. *Wiley Interdiscip. Rev.: Comput. Mol. Sci.* **2013**, *3*, 176–197.

[60] Lyakh, D. I.; Musiał, M.; Lotrich, V. F.; Bartlett, R. J. *Chem. Rev.* **2012**, *112*, 182–243.

[61] Evangelista, F. A. *J. Chem. Phys.* **2018**, *149*, 030901.

[62] (a) Schucan, T. H.; Weidenmüller, H. A. *Ann. Phys.* **1972**, *73*, 108–135; (b) Schucan, T. H.; Weidenmüller, H. A. *Ann. Phys.* **1973**, *76*, 483–509.

[63] Salomonson, S.; Lindgren, I.; Mårtensson, A.-M. *Phys. Scr.* **1980**, *21*, 351–356.

[64] Evangelisti, S.; Daudey, J. P.; Malrieu, J. P. *Phys. Rev. A* **1987**, *35*, 4930–4941.

[65] Zarrabian, S.; Laidig, W. D.; Bartlett, R. J. *Phys. Rev. A* **1990**, *41*, 4711–4720.

[66] (a) Kowalski, K.; Piecuch, P. *Phys. Rev. A* **2000**, *61*, 052506; (b) Kowalski, K.; Piecuch, P. *Int. J. Quantum Chem.* **2000**, *80*, 757–781.

[67] (a) Li, C.; Evangelista, F. A. *J. Chem. Phys.* **2017**, *146*, 124132; (b) Li, C.; Evangelista, F. A. *J. Chem. Phys.* **2018**, *148*, 079902.

[68] Evangelista, F. A.; Hanauer, M.; Köhn, A.; Gauss, J. *J. Chem. Phys.* **2012**, *136*, 204108.

[69] Whitten, J. L. *J. Chem. Phys.* **1973**, *58*, 4496–4501.

[70] Dunlap, B. I.; Connolly, J. W. D.; Sabin, J. R. *J. Chem. Phys.* **1979**, *71*, 3396–3402.

[71] Kendall, R. A.; Fruchtl, H. A. *Theor. Chem. Acc.* **1997**, *97*, 158–163.

[72] Beebe, N. H. F.; Linderberg, J. *Int. J. Quantum Chem.* **1977**, *12*, 683–705.

[73] Røeggen, I.; Wisløff-Nilssen, E. *Chem. Phys. Lett.* **1986**, *132*, 154–160.

[74] Koch, H.; Sánchez de Merás, A.; Pedersen, T. B. *J. Chem. Phys.* **2003**, *118*, 9481–9484.

[75] Boman, L.; Koch, H.; de Merás, A. S. *J. Chem. Phys.* **2008**, *129*, 134107.

[76] Aquilante, F.; Gagliardi, L.; Pedersen, T. B.; Lindh, R. *J. Chem. Phys.* **2009**, *130*, 154107.

[77] Parrish, R. M.; Sherrill, C. D.; Hohenstein, E. G.; Kokkila, S. I. L.; Martínez, T. J. *J. Chem. Phys.* **2014**, *140*, 181102.

[78] Vahtras, O.; Almlöf, J.; Feyereisen, M. W. *Chem. Phys. Lett.* **1993**, *213*, 514–518.

[79] Aquilante, F.; Pedersen, T. B.; Lindh, R. *J. Chem. Phys.* **2007**, *126*, 194106.

[80] Feyereisen, M.; Fitzgerald, G.; Komormicki, A. *Chem. Phys. Lett.* **1993**, *208*, 359–363.

[81] Weigend, F. *Phys. Chem. Chem. Phys.* **2002**, *4*, 4285–4291.

[82] Werner, H.-J.; Manby, F. R.; Knowles, P. J. *J. Chem. Phys.* **2003**, *118*, 8149–8160.

[83] Aquilante, F.; Malmqvist, P.-Å.; Pedersen, T. B.; Ghosh, A.; Roos, B. O. *J. Chem. Theory Comput.* **2008**, *4*, 694–702.

[84] Boström, J.; Delcey, M. G.; Aquilante, F.; Serrano-Andrés, L.; Pedersen, T. B.; Lindh, R. *J. Chem. Theory Comput.* **2010**, *6*, 747–754.

[85] Győrffy, W.; Shiozaki, T.; Knizia, G.; Werner, H.-J. *J. Chem. Phys.* **2013**, *138*, 104104.

[86] Hannon, K. P.; Li, C.; Evangelista, F. A. *J. Chem. Phys.* **2016**, *144*, 204111.

[87] Freitag, L.; Knecht, S.; Angeli, C.; Reiher, M. *J. Chem. Theory Comput.* **2017**, *13*, 451–459.

[88] Hättig, C.; Weigend, F. *J. Chem. Phys.* **2000**, *113*, 5154–5161.

[89] Pedersen, T. B.; de Merás, A. M. J. S.; Koch, H. *J. Chem. Phys.* **2004**, *120*, 8887–8897.

[90] Rendell, A. P.; Lee, T. J. *J. Chem. Phys.* **1994**, *101*, 400–408.

[91] Boström, J.; Pitoňák, M.; Aquilante, F.; Neograd y, P.; Pedersen, T. B.; Lindh, R. *J. Chem. Theory Comput.* **2012**, *8*, 1921–1928.

[92] DePrince, A. E.; Sherrill, C. D. *J. Chem. Theory Comput.* **2013**, *9*, 2687–2696.

[93] Epifanovsky, E.; Zuev, D.; Feng, X.; Khistyaev, K.; Shao, Y.; Krylov, A. I. *J. Chem. Phys.* **2013**, *139*, 134105.

[94] Qiu, Y.; Henderson, T. M.; Zhao, J.; Scuseria, G. E. *J. Chem. Phys.* **2017**, *147*, 064111.

[95] Huntington, L. M. J.; Nooijen, M. *J. Chem. Phys.* **2010**, *133*, 184109.

[96] Evangelista, F. A.; Gauss, J. *Chem. Phys.* **2012**, *401*, 27–35.

[97] (a) Kats, D.; Manby, F. R. *J. Chem. Phys.* **2013**, *139*, 021102; (b) Kats, D. *J. Chem. Phys.* **2014**, *141*, 061101.

[98] Rishi, V.; Perera, A.; Nooijen, M.; Bartlett, R. J. *J. Chem. Phys.* **2017**, *146*, 144104.

[99] Koch, S.; Kutzelnigg, W. *Theor. Chim. Acta* **1981**, *59*, 387–411.

[100] Bartlett, R. J.; Musiał, M. *J. Chem. Phys.* **2006**, *125*, 204105.

[101] Roos, B. O.; Taylor, P. R.; Siegbahn, P. E. M. *Chem. Phys.* **1980**, *48*, 157–173.

[102] (a) Mukherjee, D. *Chem. Phys. Lett.* **1997**, *274*, 561–566; (b) Kutzelnigg, W.; Mukherjee, D. *J. Chem. Phys.* **1997**, *107*, 432–449; (c) Kutzelnigg, W.; Shamasundar, K. R.; Mukherjee, D. *Mol. Phys.* **2010**, *108*, 433–451; (d) Kong, L.; Nooijen, M.; Mukherjee, D. *J. Chem. Phys.* **2010**, *132*, 234107.

[103] Sinha, D.; Maitra, R.; Mukherjee, D. *Comput. Theor. Chem.* **2013**, *1003*, 62–70.

[104] Forte, a suite of quantum chemistry methods for strongly correlated electrons. For current version see https://github.com/evangelistalab/forte, 2019.

[105] Ambit, a C++ library for the implementation of tensor product calculations through a clean, concise user interface. For current version see https://github.com/jturney/ambit, 2018.

[106] (a) Parrish, R. M.; Burns, L. A.; Smith, D. G. A.; Simmonett, A. C.; DePrince, A. E.; Hohenstein, E. G.; Bozkaya, U.; Sokolov, A. Y.; Di Remigio, R.; Richard, R. M.; Gonthier, J. F.; James, A. M.; McAlexander, H. R.; Kumar, A.; Saitow, M.; Wang, X.; Pritchard, B. P.; Verma, P.; Schaefer, H. F.; Patkowski, K.; King, R. A.; Valeev, E. F.; Evangelista, F. A.; Turney, J. M.; Crawford, T. D.; Sherrill, C. D. *J. Chem. Theory Comput.* **2017**, *13*, 3185–3197; (b) Smith, D. G. A.; Burns, L. A.; Sirianni, D. A.; Nascimento, D. R.; Kumar, A.; James, A. M.; Schriber, J. B.; Zhang, T.; Zhang, B.; Abbott, A. S.; Berquist, E. J.; Lechner, M. H.; Cunha, L. A.; Heide, A. G.; Waldrop, J. M.; Takeshita, T. Y.; Alenaizan, A.; Neuhauser, D.; King, R. A.; Simmonett, A. C.; Turney, J. M.; Schaefer, H. F.; Evangelista, F. A.; DePrince, A. E.; Crawford, T. D.; Patkowski, K.; Sherrill, C. D. *J. Chem. Theory Comput.* **2018**, *14*, 3504–3511.

[107] Hohenstein, E. G.; Parrish, R. M.; Martínez, T. J. *J. Chem. Phys.* **2012**, *137*, 044103.

[108] Huber, K. P.; Herzberg, G. *Molecular Spectra and Molecular Structure*; Springer: Boston, MA, 1979.

[109] Irikura, K. K. *J. Phys. Chem. Ref. Data* **2007**, *36*, 389–397.

[110] Dunning Jr, T. H. *J. Chem. Phys.* **1989**, *90*, 1007–1018.

[111] Woon, D. E.; Dunning, T. H. *J. Chem. Phys.* **1994**, *100*, 2975.

[112] (a) Weigend, F.; Ahlrichs, R. *Phys. Chem. Chem. Phys.* **2005**, *7*, 3297–3305; (b) Weigend, F. *J. Comput. Chem.* **2008**, *29*, 167–175.

[113] (a) Weigend, F.; Köhn, A.; Hättig, C. *J. Chem. Phys.* **2002**, *116*, 3175–3183; (b) Hättig, C. *Phys. Chem. Chem. Phys.* **2005**, *7*, 59–66.

[114] Shen, J.; Piecuch, P. *J. Chem. Phys.* **2012**, *136*, 144104.

[115] Whitman, D. W.; Carpenter, B. K. *J. Am. Chem. Soc.* **1982**, *104*, 6473–6474.

[116] Nakamura, K.; Osamura, Y.; Iwata, S. *Chem. Phys.* **1989**, *136*, 67–77.

[117] Balková, A.; Bartlett, R. J. *J. Chem. Phys.* **1998**, *101*, 8972–8987.

[118] Sancho-García, J. C.; Pittner, J.; Čársky, P.; Hubač, I. *J. Chem. Phys.* **2000**, *112*, 8785–8788.

[119] Levchenko, S. V.; Krylov, A. I. *J. Chem. Phys.* **2003**, *120*, 175–185.

[120] Eckert-Maksić, M.; Vazdar, M.; Barbatti, M.; Lischka, H.; Maksić, Z. B. *J. Chem. Phys.* **2006**, *125*, 064310.

[121] Lyakh, D. I.; Lotrich, V. F.; Bartlett, R. J. *Chem. Phys. Lett.* **2011**, *501*, 166–171.

[122] Shen, J.; Fang, T.; Li, S.; Jiang, Y. *J. Phys. Chem. A* **2008**, *112*, 12518–12525.

[123] Li, X.; Paldus, J. *J. Chem. Phys.* **2009**, *131*, 114103.

[124] Bhaskaran-Nair, K.; Demel, O.; Pittner, J. *J. Chem. Phys.* **2008**, *129*, 184105.

[125] Demel, O.; Shamasundar, K. R.; Kong, L.; Nooijen, M. *J. Phys. Chem. A* **2008**, *112*, 11895–11902.

[126] Wu, J. I.-C.; Mo, Y.; Evangelista, F. A.; Schleyer, P. v. R. *Chem. Commun.* **2012**, *48*, 8437–8439.

[127] Mahapatra, U. S.; Datta, B.; Mukherjee, D. *J. Phys. Chem. A* **1999**, *103*, 1822–1830.

[128] Chattopadhyay, S.; Mahapatra, U. S.; Mukherjee, D. *J. Chem. Phys.* **2000**, *112*, 7939–7952.

[129] Chattopadhyay, S.; Pahari, D.; Mukherjee, D.; Mahapatra, U. S. *J. Chem. Phys.* **2004**, *120*, 5968–5986.

[130] Pahari, D.; Chattopadhyay, S.; Deb, A.; Mukherjee, D. *Chem. Phys. Lett.* **2004**, *386*, 307–312.

[131] (a) Evangelista, F. A.; Allen, W. D.; Schaefer, H. F. *J. Chem. Phys.* **2006**, *125*, 154113; (b) Evangelista, F. A.; Simmonett, A. C.; Allen, W. D.; Schaefer, H. F.; Gauss, J. *J. Chem. Phys.* **2008**, *128*, 124104; (c) Evangelista, F. A.; Prochnow, E.; Gauss, J.; Schaefer, H. F. *J. Chem. Phys.* **2010**, *132*, 074107.

[132] Taube, A. G.; Bartlett, R. J. *J. Chem. Phys.* **2009**, *130*, 144112.

[133] Chiles, R. A.; Dykstra, C. E. *J. Chem. Phys.* **1981**, *74*, 4544–4556.

[134] Handy, N. C.; Pople, J. A.; Head-Gordon, M.; Raghavachari, K.; Trucks, G. W. *Chem. Phys. Lett.* **1989**, *164*, 185–192.

[135] Stanton, J. F.; Gauss, J.; Bartlett, R. J. *J. Chem. Phys.* **1998**, *97*, 5554–5559.

Chapter 5 Concluding remarks and outlook

In this dissertation, we have presented several efficient methods for both static and dynamical correlation. Their improvements upon existing methods pushed the limit on the treatable size of strongly correlated systems.

In the initial stage of our research, we tried to convert the full configuration interaction quantum Monte Carlo (FCIQMC) method into an efficient deterministic method. We introduced a general projector diagonalization approach and combined it with path filtering to create a novel projector configuration interaction (PCI) method. In PCI, we apply path filtering with a user-provided *spawning threshold* (η), the determinant space is expanded but only include the most important determinants. The path filtering algorithm distinguishes PCI from selected CI algorithms by the fact that the Hamiltonian diagonalization is also approximated, which dramatically decreased the computational cost. We reported computations with large CI space containing over 10^8 determinants. The benchmarks show chemical accuracy can be achieved using only a small fraction of the Hilbert space of determinants.

Efforts then devoted to further improve the accuracy and efficiency of the PCI method. To improve accuracy, we implemented a Hermitian version of PCI without significantly increasing the computational cost. Computation on an N_2 potential energy curve showed half the non-parallelism error. As for efficiency, with the approximated Hamiltonian being Hermitian, we introduced the Davidson–Liu algorithm that converges three times faster than the 5^{th} order wall-Chebyshev generator. We also show that if the PCI determinant space is exactly diagonalized, the result energy is almost identical to the Heat-bath CI (HCI) energy computed with the same threshold. Meanwhile, with the same theoretical computational cost, PCI is able to compute more accurate wave function than selected CI methods.

However, we realized the bottleneck of PCI is the computation of the variational energy, in which the Hamiltonian matrix cannot be approximated so the computational cost is the same as selected CI methods. Although we have not figured out a solution for efficiently variational energy, but recent developments[1] in the field provides potential application of PCI where accurate wave function is needed, but not the variational energy. Furthermore, there are still many open questions in the PCI theory. To better understand PCI, we need further research on how to target a give accuracy like in adaptive CI[2] and how to perturbatively correct the PCI results. These problems should be investigated in future projects.

In the last part of this dissertation, we focused on the MR-DSRG methods. We reduce the cost of the linear MR-DSRG with singles and doubles [MR-LDSRG(2)] without compromising its accuracy by using a combination of 1) a sequential unitary transformation, 2) density fitting (DF) of the two-electron integrals, and 3) the non-interacting virtual orbital (NIVO) operator approximation. These techniques reduced the memory requirement from $\mathcal{O}(N^4)$ to $\mathcal{O}(N^2M + N^2N_{\mathbf{H}}^2)$, where N is the number of basis functions, M is the number of auxiliary basis functions and $N_{\mathbf{H}}$ is the number of hole orbitals. The computational time is also reduced by one order of magnitude in our benchmarks. These cost reductions enabled the study of the cyclobutadiene automerization reaction using basis sets as large as quintuple-ζ.

This dissertation establishes the PCI as a CI method more efficient than general selected CI methods and provides a low-cost alternative to the original MR-LDSRG(2) method. A straightforward future project is to combine these two methods for accurate description of large strongly correlated chemical systems. Similar research has been published in our group that the combination of adaptive CI with the DSRG-MRPT2 method (ACI-DSRG-MRPT2)[3] is able to predict properties of acene series on an active space of 30 electrons in 30 orbitals with more than 1000 correlated basis functions. We expect the combination of PCI and DSRG methods shows similar or

even better results in the future.

Bibliography

[1] (a) Deustua, J. E.; Shen, J.; Piecuch, P. *Phys. Rev. Lett.* **2017**, *119*, 223003; (b) Deustua, J. E.; Magoulas, I.; Shen, J.; Piecuch, P. *J. Chem. Phys.* **2018**, *149*, 151101.

[2] Schriber, J. B.; Evangelista, F. A. *J. Chem. Phys.* **2016**, *144*, 161106.

[3] Schriber, J. B.; Hannon, K. P.; Li, C.; Evangelista, F. A. *J. Chem. Theory Comput.* **2018**, *14*, 6295–6305.